

Politecnico di Torino (POLITO)
Institut supérieur de mécanique de Paris (SUPMECA)
Master degree in Mechanical engineering

Non-linear dynamic analysis of cycloidal reducers

Laboratory Quartz (SUPMECA)



Supervisors:

Prof. Alessandro Fasana (POLITO)

Prof. Jean-Luc Dion (SUPMECA)

Prof. Nicolas Peyret (SUPMECA)

Student:

Vittorio Chianca (239841)

September 2018

To my parents, to my family, to my grandmother

Contents

Abstract	V
Abstract (Italian version)	VII
Acknowledgements	IX
Acknowledgements(Italian version)	XI
1 Introduction to cycloidal reducers	1
1.1 Constructive elements and main features of the reducer	1
1.2 Planetary representations and Gear ratio	5
1.3 Literature context on cycloidal reducer	8
1.4 Technological variants and applications	9
2 Geometrical characterization and design of the cycloidal plate	13
2.1 Analytical determination of the cycloidal geometry (theoretical and working profile)	13
2.2 Theoretical and working curvature radius of the cycloidal profile . . .	22
2.3 Distinctive meshing angles	24
2.4 Parametric analysis on cycloidal plate	26
3 Kinematic and dynamic analysis: rigid model bodies	30
3.1 Kinematic analysis	30
3.2 Distribution of forces	35
3.3 Torques distribution	38
3.4 Main dynamic equations derived from analytical mechanics	40
3.5 Main dynamic equations derived from Newton method	47
4 Experimentation on dynamic behaviour and on performances	50
4.1 Test Bench	50
4.2 Methodology and results	55
4.3 Processing of experimental data	56
4.4 Simulations coming from rigid bodies model	58

4.5	Conclusions	61
5	Optimization of the machine's main parameters with rigid bodies model	63
5.1	Main vibration problems of cycloidal reducers	63
5.2	Influence of the profile modification coefficient	65
5.3	Influence of the pins radius	65
5.4	Influence of the teeth number	66
5.5	Influence of the output rollers number	67
5.6	Influence of friction coefficient	68
5.7	Optimizing the gearbox's performance	69
6	Linear and non-linear stiffness model of the cycloidal disk	72
6.1	Motivations in adding an elastic mobility	73
6.2	Dynamic equations with elastic properties	73
6.3	Dynamic equations with elastic properties (Newton's method)	80
6.4	Mathematical formulation of dynamic problem	82
6.5	Linear stiffness model: research of the experimental stiffness coefficient	83
6.6	Linear stiffness model: comparison between experimentation and simulations	85
6.7	Non-linear stiffness model: motivations	86
6.8	Non-linear stiffness model: research of the shape factors	88
6.9	Non-linear stiffness model: comparison between experimentation and simulations	89
7	Conclusions	92
A	Kennedy theorem	94
B	General models for kinetic friction	96
C	Reference to Hertz theory of contact and Palmgren formula	98
D	Basic phenomenology of simple non-linear spring-mass system	100
E	Introduction to Simulink to resolve the main dynamic equation of non linear stiffness model	102
	Bibliography	104

Nomenclature

μ_E	Bearing friction coefficient
μ_p	Housing pins friction coefficient
μ_s	Output rollers friction coefficient
ψ	Angular position of output shaft
φ	Angular position of input shaft
C_s	Output constant load (torque)
C_{X_i}, C_{Y_i}	Components of the forces exchanged between disk and pins
e	Eccentricity
i	Gearbox ratio
K_c	Amplitude factor of forces exchanged between output rollers and disk
K_s	Amplitude factor of forces exchanged between housing pins and disk
k_{cy}	Linear/Non-linear stiffness constant
M_{C_i}	Net torque exchanged between disk and pins
m_{cy}	Cycloidal disc mass
M_{S_j}	Net torque exchanged between disk and rollers
N_c	Number of output rollers
p	Exponent of non-linearity
r_1	Primitive radius
r_2	Pins distribution radius
r_c	Housing pins radius

r_c	Output rollers radius
R_s	Roller distribution radius
S_{X_j}, S_{Y_j}	Components of the forces exchanged between disk and rollers
x	Correction coefficient
z_1	Number of teeth of cycloidal plate
z_2	Number of housing pins

Abstract

The main aim of the following work is to underline the essential keys to figure the cycloidal reducer's dynamic behaviour out. In order to make an useful and meaningful contribution, the research work should be divided in two pivotal parts: the experimental one and the computational and modelling one. The experimental measurements on the dynamics of the reducer were performed by the researchers of Lodz's polytechnic University (Lodz, Poland), while the modelling work was accomplished by the author of this thesis with the fundamental guide of the prof. Jean-Luc Dion and the prof. Nicolas Peyret (SUPMECA, Saint Ouen, Ile-de-Paris). The fruit-full collaboration between the two researcher institutes (SUPMECA and Lodz) lead to an important contribution to the topic and, at the end, this allows us to publish a scientific article (Mechanism and Machine Theory, Elsevier).

The personal contribution- given to the topic of dynamic analysis of the cycloidal reducer- consists in finding out a mathematical model able to fit the experimental efficiency. The modelling work has the following pivotal points:

- Analysing the experimentation obtained through the test bench in Lodz and comparison with PSA's experimentation (one of the starting point was the experimentation done at PSA). All these let to understand fully the particularities of the dynamic behaviour of the machine and it allows to start thinking about the kinematic and dynamic analysis;
- Writing the kinematic and dynamic equations for the rigid bodies of the reducer. Moreover, a particular focus is given to the geometric features of the cycloidal disc;
- Comparing the efficiency coming from the rigid bodies model with the experimental efficiency. The rigid bodies model permits to get a first optimization process of the main features of the machine and to describe effectively the dynamics of the exchanged forces;
- Because of the lack of correspondence between experimental data and theoretical previsions with the rigid bodies model, some elastic dynamic effects has to be kept into account (linear stiffness model and non-linear stiffness

model). The best suiting model lets to have a dynamic optimization of the main features of the machine.

The sequence of the chapters follows with minutia the path followed by the candidate in addressing the issue. Moreover, the aforesaid sequence aims to guide the reader to what were the main reasons that justified the most important choices of the thesis work.

Abstract (Italian version)

L'obiettivo principale del seguente lavoro di tesi è quello di individuare le chiavi essenziali di interpretazione della dinamica del riduttore cicloidale. Questa macchina presenta caratteristiche tecnologicamente interessanti: ridotto ingombro con elevato rapporto di riduzione, -se ben progettata- a regime livello di vibrazione minimo. Per rendere il lavoro incisivo ed efficace, si reputa necessario riferirsi a due metodi di indagine: quello sperimentale e quello computazionale e modellistico. Il lavoro di indagine sperimentale -sebbene in parte compiuto dal SUPMECA (Institut Supérieur de Mécanique de Paris)- è quello che fa riferimento a quanto ottenuto dai colleghi del Politecnico di Lodz (Lodz University of Technology), con i cui ricercatori c'è stata un'importante collaborazione per la stesura di un articolo che riguarda in parte le tematiche affrontate in questo lavoro di tesi. La parte modellistica e computazionale è stata invece svolta dal candidato sotto la supervisione del prof. Jean-Luc Dion e dal prof. Nicolas Peyret. La proficua e piena collaborazione tra i due istituti di ricerca (SUPMECA e Lodz) ha consentito di dare un importante contributo al tema. Il contributo personale -dato al tema dell'analisi dinamica del riduttore cicloidale- consiste nell'aver posto le basi di un modello matematico in grado di giustificare gli andamenti sperimentali dell'efficienza. Il lavoro di modellazione ha i seguenti punti cardine:

- Analisi dei risultati ottenuti dalla sperimentazione proveniente da Lodz, confrontando con i risultati ottenuti in un banco prova analogo al centro ricerca PSA. Questo confronto ha consentito di comprendere appieno le peculiarità della dinamica della macchina in questione, ponendo le basi per la scrittura delle equazioni cardine;
- Scrittura delle equazioni cinematiche e dinamiche per corpi più rilevanti del riduttore (considerandoli perfettamente rigidi). Inoltre, una particolare attenzione merita il disco cicloidale e la sua peculiare geometria;
- Confronto dei risultati esiti dalla sperimentazione e quelli provenienti dalle simulazioni. Il modello a corpi rigidi (rigid bodies model) permette di ottenere un primo processo di ottimizzazione dei parametri geometrici principali della macchina. A causa della mancanza di corrispondenza tra dati sperimentali

e previsioni teoriche con il modello a corpi rigidi, vengono introdotti effetti elastici dinamici, prima lineari (linear stiffness model) e poi non lineari (non-linear stiffness model). Quest'ultima introduzione consente di ottenere una significativa corrispondenza fra sperimentazione e previsioni teoriche.

La scansione dei capitoli segue con minuziosità il percorso seguito dal candidato nell'affrontare la questione. Inoltre, la suddetta scansione vuole guidare il lettore a quale siano state le principali motivazioni che hanno giustificato le scelte più rilevanti che contraddistinguono il lavoro di tesi in questione.

Acknowledgements

I would like to thank my supervisors at SUPMECA, prof. Jean-Luc Dion and prof. Nicolas Peyret, for guiding and supporting me during all the works of thesis, for the pivotal speeches that we have had during the months I stayed at SUPMECA. Moreover, I am very grateful to them because from the beginning they gave me a lot of confidence, as well as essential advice to achieve an excellent result. You have set an example of excellence as a researcher, mentor and instructor.

I am very grateful for the welcome given by all the researchers of the department of the Laboratory Quartz, at the beginnings I felt myself out of the place but they were very kind and welcoming.

I would especially thank my home-university supervisor prof. Alessandro Fasana for guiding me in the last fundamental steps of the thesis's preparations and of the final dissertation speech.

I would especially like to thank my amazing family for the love, support, and constant encouragement I have got over the years. In particular, I would like to thank my parents, my brother, my sisters. They are the most important reason of life in my eyes. You are the salt of the earth, and I undoubtedly could not have done this without you. I should like to thank also my grandmother and my grandfathers to be an example of life for me and to my uncle Giovanni for being always presents with my family.

I would like to thank and dedicate this thesis to my grandmother, whose grace failed some years ago. It was you who originally generated my self-confidence. Although it has been years since you have passed, I still take your life lessons with me, every day.

Finally, I should thank my friends, they are one of the most relevant and important gift received since I arrived in Turin. During all these years they were with me in the most troubling and hardest steps. I should remind of Raffaele for the unconditional support given and for his constant presence, of Giuseppe for having always had respect for me and for making always me laugh, of Saverio for happiness brought with his smile, of Matteo for having taught and shared the passion for mechanics, of Emidia for making me feel at home from the beginning of this experience in Turin,

of Laura and Caterina for always wanting to be loved and having always been close to me, of Chiara for the beautiful and joyful moments shared together, of Donatella for always having been side by side with affection since I met her and, last but not least, of my friends "arianesi" because seeing them lets me breath the air of my beloved home-town. All they are becoming for me a kind of family, when my real family is far, I fell at home if they are with me.

Furthermore, during the university lectures, I have met two fellow students that I hope we would keep in contact for all my life, Maria Teresa and Espedito: they were fundamental to pass all the most difficult and hardest moments of my studies, I have had with them the most enjoyable time in my university years. I can certainly affirm that I would have learnt less without the continuously comparison with them. Certainly, I must considered myself to be lucky enough because of having met two real friends between the university benches.

I should thank my friends from Collegio Einaudi, undoubtedly living there lets me understand better myself and the others, I have met pleasant people and I can remind of incredible and wonderful time passed with them.

I would like to acknowledge who have provided any support to me in some way, who have given an important contribute to my academic and personal development.

The last acknowledgements is dedicated to my last experience in Paris and to all people I have had enjoyable time with- I should remind of Marco, Joao, Agnese and Alice: meeting new people, living in a international contest must have allowed me to get a resourceful and international mind-set. I have learnt to know better myself, to challenge myself, to broaden my personal limits. This experience- according to my thoughts- must be considered as formative and educational as the previous years of studies.

Acknowledgements (Italian version)

Ci terrei particolarmente a ringraziare i miei relatori francesi al SUPMECA, il prof. Jean Luc Dion e il prof. Nicolas Peyret, per avermi guidato e supportato durante il lavoro di tesi, per i colloqui e i meeting risolutivi che abbiamo avuto nei mesi di permanenza al SUPMECA. Inoltre, gli sono molto grato perché, sin dall'inizio, hanno manifestato nei miei confronti una forte e convinta stima e fiducia, mi hanno elargito consigli essenziali per raggiungere un ottimo risultato. Sono stati ai miei occhi esempi di eccellenza come ricercatori, mentori e docenti.

Vorrei inoltre aggiungere un sentito ringraziamento ai dottorandi del dipartimento del Quartz Laboratory (SUPMECA) per l'accoglienza mostratami: in principio mi sentivo fuori posto, ma sono stati decisivi nel farmi sentire parte di un team di lavoro.

Ringrazio soprattutto la mia università di origine (Politecnico di Torino) e il mio relatore quivi, il prof. Alessandro Fasana, per avermi guidato negli ultimi passaggi decisivi del lavoro di tesi includendo la stesura della tesi e la preparazione della discussione finale.

Ringraziamento particolarmente sentito va alla mia straordinaria famiglia per l'amore, il sostegno morale ed economico e il costante incoraggiamento che non mi hanno mai fatto mancare. La mia famiglia è tutto per me, partendo dai miei genitori e finendo con mio fratello e le mie sorelle. Sono per me la ragione più importante di vita. Un sentito ringraziamento va anche ai miei nonni paterni e a mio nonno materno per essere ai miei occhi dei modelli di vita da ammirare e da seguire. Per non dimenticare in ultimo, il ringraziamento a mio zio Giovanni per la costante presenza e il sostegno alla mia famiglia.

Un ringraziamento molto importante va a mia nonna venuta a mancare qualche anno fa: è stata fondamentale per la mia crescita, mi ha accompagnato nei passi più importanti dei miei primi anni universitari. Ricordo ancora le sue lezioni di vita che porterò sempre con me. A lei dedico questo lavoro di tesi, proprio perché rappresenta un modello di vita di grande autorevolezza morale.

Ciò detto, il mio percorso universitario -di cui questa tesi è il momento ultimo- si è potuto realizzare grazie alla costante presenza degli amici, il più importante regalo ricevuto durante questi anni a Torino. Ognuno di loro è stato indispensabile per me, ricordo dell'incondizionato sostegno e della costante presenza di Raffaele V., della stima mostratami e della bella compagnia di Giuseppe D., della condivisione della passione per la meccanica di Matteo B.; dovrei inoltre ringraziare Emidia V. per avermi fatto sentire a casa sin dall'inizio, e le amiche sempre presenti Laura G. e Caterina L. per aver condiviso bellissimi momenti insieme e per avermi sempre compreso. Per non dimenticare Chiara M. con cui ho passato ore spensierate e festose e Donatella V. per la costante rassicurante presenza durante questi anni. Va inoltre aggiunto un ringraziamento ai miei amici "arianesi", vedere loro a Torino mi permette di percepire l'aria e l'atmosfera della mia città nonostante i chilometri di lontananza.

Fra i banchi universitari ho incontrato due colleghi che sono diventati due amici veri, con loro ho condiviso i momenti più belli e più difficoltosi del percorso universitario. Trattasi di Maria Teresa C. ed Espedito C.: aver incontrato loro è stata una grande fortuna poiché, senza il costante confronto avuto con loro, avrei certamente imparato meno. Devo a loro molto anche e soprattutto per i bei momenti passati per festeggiare prove o esami ben riusciti. Sono sicuro che sarà l'inizio di una lunga e duratura amicizia.

Gli ultimi ringraziamenti sono dedicati a tutte le persone incontrate nell'esperienza a Parigi, con loro ho trascorso momenti memorabili- ricordo di Marco B., Agnese P., Alice G. e Joao G.- vivere in un contesto internazionale mi ha reso maggiormente intraprendete. Ho imparato a conoscere meglio me stesso e a mettermi alla prova ampliando i miei orizzonti e limiti personali. Questa esperienza è stata tanto formativa, quanto gli studi conseguiti al Politecnico di Torino.

Chapter 1

Introduction to cycloidal reducers

In this first chapter, the industrial and technological context - that motivates the profitable work about the cycloidal reducers- will be introduced. To fully understand the operating principles of the reducer, some information about history, technological context, main constructive elements are presented. Moreover, we are going to estimate the gear ratio and the parameters that have impact on it, because of knowing that one of the best properties of the cycloidal gearbox consists exactly in high speed ratio in a small size. The background presented in this chapter allows to get a general overview of the basic features of the reducer.

1.1 Constructive elements and main features of the reducer

Cycloidal speed reducers belong to the newest generation of mechanical gears. The good performances encourage increasingly applications in modern engineering. The contexts, where the cycloidal gearbox could replace the traditional gearboxes, are robust system, robots and all the applications that require high speed and high gear ratio in a small size. The high speed ratio is provided by the peculiarities of the structure that is summarised (without the housing) in figure 1.1.

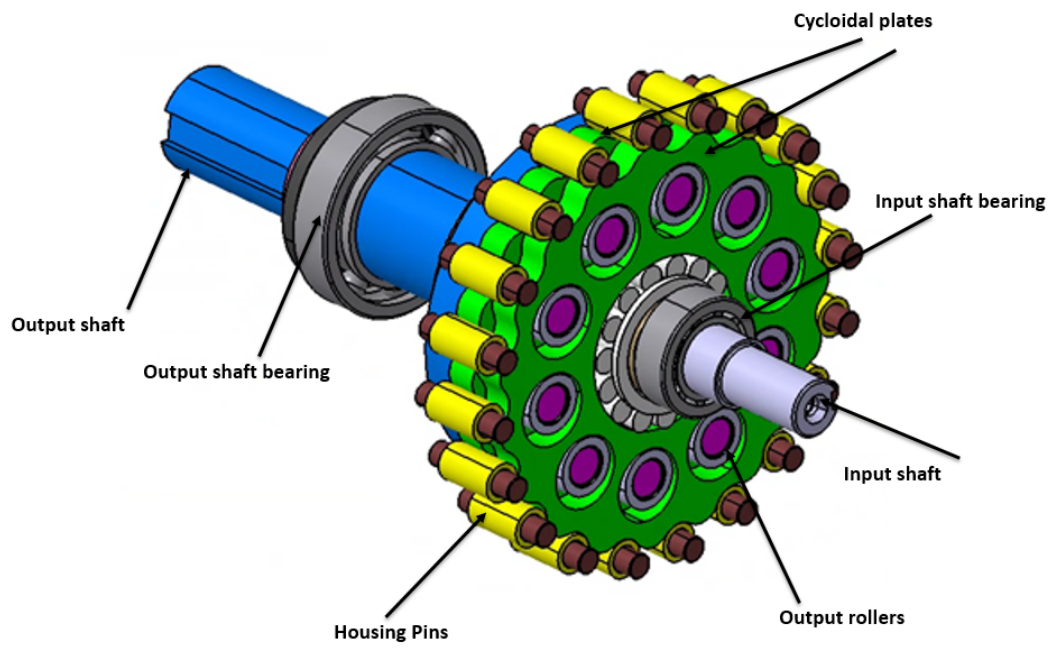


Figure 1.1: Cycloidal reducer with the main elements highlighted (Lodz's machine)

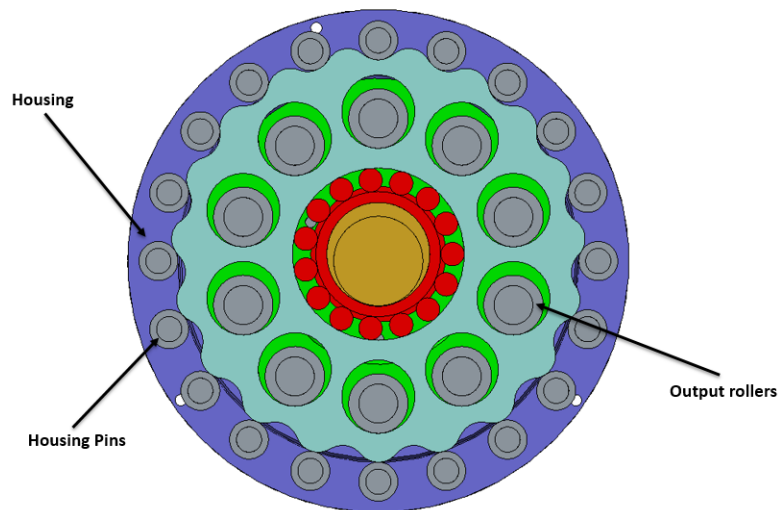


Figure 1.2: Cycloidal reducer: front view (Lodz's machine)

Then- with regard to the tested machine- we have all the mechanical parts represented in the figure 1.3.

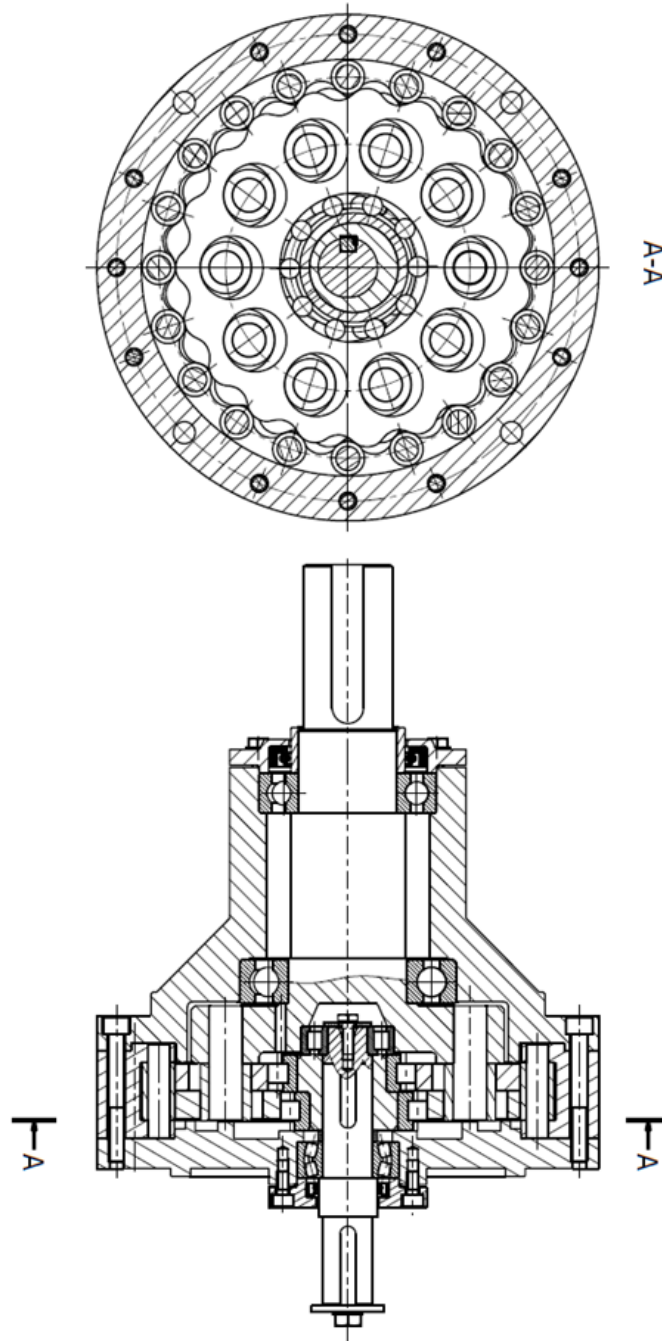


Figure 1.3: Cycloidal reducer: technical draws of Lodz's machine

The cycloidal gearbox consists in four main elements:

1. Input shaft: it involves the lower torque and the higher speed and it is coupled directly with the cycloidal plates. Moreover, the input shaft has two eccentric rollers bearings - as figure 1.3 shows-;
2. Cycloidal plates: there is the possibility of adding more than one plate, in order to reduce the strains on the cycloidal plates themselves- especially for high loads-. However, the disks must be mounted in such way to decrease vibrations. Due to the introduction of the eccentric bearing, there is an eccentricity between the axes of the input shaft and the cycloidal plate, which are mounted out-of-phase. This eccentricity lets the disks centres rotate in the housing, making the engagement possible. The cycloidal wheels are equipped with teeth whose number is lower than the housing pins, causing the reverse orbit rotation within the housing itself;
3. Housing with internal pins: the pins (that stay in fixed state) mesh with the teeth of the cycloidal disks;
4. Output shaft with rollers: the rollers are coupled with the cycloidal disks through the internal lobes which makes possible to transfer the motion from the plates to the output shaft. Furthermore, the output shaft involves the higher torque and the lower speed.

Then, the high-speed shaft is linked to the cycloidal plates through a key connection, this rigid connection causes the eccentric cycloid gear rotation. This lets the disks roll over the ring gear pins (housing pins). The junction between the output rollers and the plates by the internal holes makes the rotation of the output shaft possible. These holes are bigger than the dimension of the output rollers and this allows the rollers to rotate around the holes themselves. All these engagements explain why the rotation of the output shaft has the same direction of the rotation of the input shaft. Analysing these main features, it appears clear that the cycloidal gearboxes in comparison with the traditional ones have a more complex structure, with the adding of new kind of elements to replace the gears. Moreover, it is possible to get high gear ratio with a single stage, which affects the overall dimensions of the gearbox. In some applications, the dimension could be one of the most restrictive design and in-service condition.

Between the traditional gearboxes and the cycloidal drive, the precision needed in the applications will become one of benchmarks for the design choice. If backlash and positioning accuracy are crucial, then cycloidal gearboxes offer the best choice. In ratios from 3 : 1 to 100 : 1, planetary gearboxes offer the best torque density, weight and precision. Anyways, if the required ratio goes beyond 100 : 1, cycloidal gearboxes hold advantages because stacking stages are unnecessary, so the gearbox

can be shorter and less expensive.

Conversely, cycloidal reducers are larger in diameter for the same torque but are not as long. The compound reduction cycloidal gear train handles all ratios within the same package size, so higher-ratio cycloidal gear boxes become even shorter than planetary versions with the same ratios.

Backlash, ratio, and size provide engineers with a preliminary gearbox selection. But choosing the right gearbox also involves bearing capacity, torsional stiffness, shock loads, environmental conditions, duty cycle and life.

Both cycloidal and planetary reducers are appropriate in any industry that uses servos or stepper motors. And although both are epicyclical reducers, the differences between most planetary gearboxes consist more in gear geometry and manufacturing processes rather than in principles of operation.

To summarise all the discussions, we can enumerate the benefits of planetary gearboxes:

1. High torque density (especially for lower loads);
2. Load distribution and sharing between planet gears;
3. High efficiency;
4. Low input inertia;
5. Low backlash;
6. Low cost.

In opposition, for the cycloidal gearboxes we have as benefits:

1. Zero or very-low backlash stays relatively constant during life of the application;
2. Rolling instead of sliding contact;
3. Shock-load capacity;
4. Ratios exceeding 200 : 1 in a compact size;
5. Quiet operation.

1.2 Planetary representations and Gear ratio

The first step before analysing the experimentation and setting the mathematical model able to describe the dynamic behaviour of the cycloidal reducer, consists in

achieving the overall gear ratio. This goal will be got through the analogy with the epicyclical gearing.

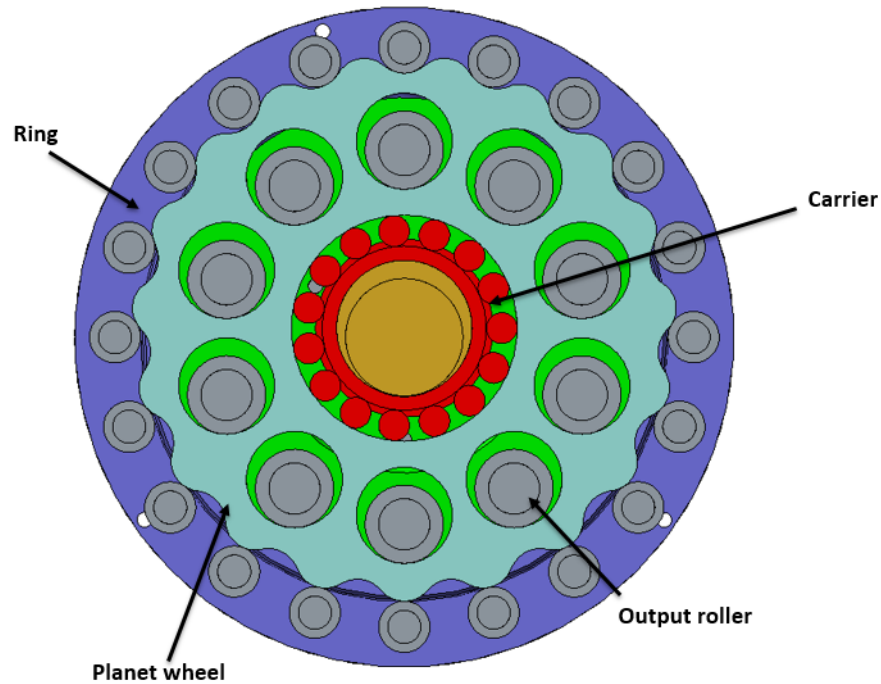


Figure 1.4: Cycloidal reducer whose elements are presented in analogy with epicyclical gearing

Referring to figure 1.4, we may compare analogous elements:

1. the housing with its fixed pins plays the role of the ring;
2. the output rollers with the low-speed shaft and the cycloidal plate -all these elements are moving at the same speed due to the homo-kinetic of the coupling between the rollers and the internal holes- stay for the planet wheels;
3. the input shaft, instead, has the role of the carrier.

Anyways, we can describe the motion referring to the carrier - as Willis formula's approach suggests-:

$$\frac{\omega_S - \omega_C}{\omega_R - \omega_C} = \frac{z_1}{z_2} \quad (1.1)$$

where:

1. ω_R is the rotational speed of the housing as analogous to the ring;
2. ω_C is the rotational speed of the input shaft as analogous to the carrier;
3. ω_S is the rotational speed of the cycloidal plate(s) as analogous to the planet wheels;
4. z_1 is the number of teeth of the cycloidal plate;
5. z_2 is the number of housing pins;

The most common working condition has the housing in a fixed state, then:

$$\omega_R = 0 \tag{1.2}$$

$$1 - \frac{\omega_S}{\omega_C} = \frac{z_1}{z_2} \tag{1.3}$$

$$i = \frac{\omega_C}{\omega_S} = \frac{z_1}{z_2 - z_1} \tag{1.4}$$

Where i indicates the gearbox ratio. As demonstrated, the gearbox ratio depends only on the number of the teeth of the cycloidal plate and of the number of housing pins.

The number of disks mounted does not affect the kinematic of the transmission: if we did again all the passages on the system shown in the figure 1.5 (with two plates in series), we would obtain that the overall gearbox ratio is the same of a single stage of the gearbox. In other words, the adding of more than one disk lets to reduce both the vibration level and mechanical stress for each disk, but it does not affect the overall gearbox ratio.

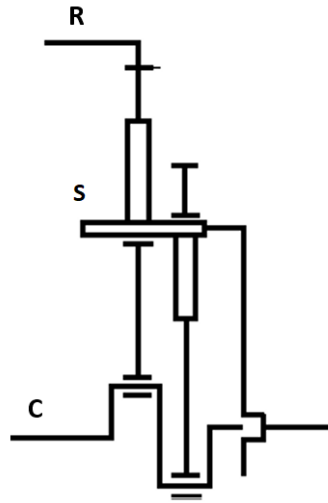


Figure 1.5: Cycloid gear kinematic: R stands for the ring/housing pins, S for planetary wheels/cycloidal plate and C for the carrier/input shaft

1.3 Literature context on cycloidal reducer

This study has been performed with the support of PSA Automotive in the technical context of electric car developments. Compactness, high speed ratio are important benefits of this technology. In this work, we highlight some possible ways to optimise the efficiency of the cycloidal drive. The cycloidal drive -through the important experimentation made during the last years and the new interest in applications - has shown relevant operating properties: long and reliable working life, large range of gear ratio in comparison with the traditional gearboxes, if it is well designed minimal vibrations and low noise, high overload capacity, reverse applications as a reducer, high efficiency with increasing load, compact design with small size. All these reasons encourage both the experimentation and the computational work with the main purpose to find the pivotal features to raise up the efficiency. The first achievement is that a new design has to take account of the experimental data analysis. T. Mackic et al.([1]) investigated the influence of geometrical parameters on the cycloid drive efficiency. They summarized that the optimum choice of design parameters has a significant impact on its efficiency. M. Blagojevic et al.([8]) developed a model of cycloid drive which takes into account only the friction in contact of the cycloid disc and housing rollers, while occurrence of friction in other locations was neglected. They noticed that the appearance of friction has a significant impact on the core strength parameter of the cycloidal speed reducer. In another paper M. Blagojevic et al. ([2]) introduce a dynamic model of the cycloid drive which takes

into consideration the elastic connection with stiffness and dumping between: input shaft with eccentric cam – cycloid gear, cycloid gear – housing roller and cycloid gear – output shaft pin. The simulation shows that the biggest influence on dynamic operating of the cycloid drive comes from the coefficient of the damping during the contact between the cycloid gear tooth and the central gear roller as well as from its stiffness. For the main geometric modelling of the cycloidal disk the main approach is highly inspired by the classical one ([4],[5],[10],[5], [17]). Moreover, the basic of kinematic analysis has as starting point the work of J.H. Shin and S.M. Kwon ([7]) whose great intuition is to apply the Kennedy theorem on the cycloidal disc and to introduce an mathematical analysis on cycloidal disc’s kinematic. In order to understand fully the technological context of applications, some fundamental lectures are [13], [?] and [14].

1.4 Technological variants and applications

The name *Cyclo* derives from *Kyklos*- the Greek word for circle and refers to the cycloidal disk, whose outer profile describes a cycloidal curve. The unique operating principle was invented in 1931 by the German engineer Lorenz Braren (1886-1953) - that was a German designer, entrepreneur and genealogist- and the ingenious design has continued its progressive development up to the present day. In order to realise the path-breaking extent of the cycloidal drive in applications, we should make a summary of the main differences between the cycloidal gearboxes and the traditional one -as the following table shows-.

Table 1.1: Difference between cycloidal gearboxes and traditional ones

Cycloidal drive	Planetary gearbox
Four main components: input shaft, cycloidal disc, housing with pins and output shaft	Three main members: sun gear, multiple satellite or planet gears and an internal ring gear
Cycloidal Gears are very good for extremely heavy loads	Planetary Gears may run at higher speeds
Cycloidal Gears work at higher ratio’s allowing them to be driven with less power	Planetary Gears will work with very low ratios
Cycloidal Gears are best in applications for high positioning accuracy and when a minimum lost motion is required	Planetary Gears are good if positioning accuracy and lost motion are not a concern

Every times we should choose- for a particular application- whether to resort or not to the cycloidal drive, it is compulsory keeping into account the following issues:

1. Environmental conditions (operating temperature, dust, ...);

2. Physical size, generally, any shape or space requirements;

3. Maintenance and lubrication access;

4. Torsional rigidity of the main elements of the reducer itself.

5. Kind of duty cycle.

According to the aforementioned conditions, we can finally define the typical field of applications for the cycloidal drive and the planetary gearboxes:

Table 1.2: Gearbox industrial applications

Cycloidal drive	Planetary gearbox	Both
Machine tools	Linear actuators	Printing
Robotics	Textile machines	Automotive
Tool changers	Material Handling	
Tilt System	Packaging machine	

Nowadays, the most relevant manufacturers of cycloidal gearboxes are Sumitomo ([15]) and Nabtesco ([17]). In order to figure this technology out, we are going to take a look of one example from the commercial catalogue of Sumitomo.

DRIVE 6000

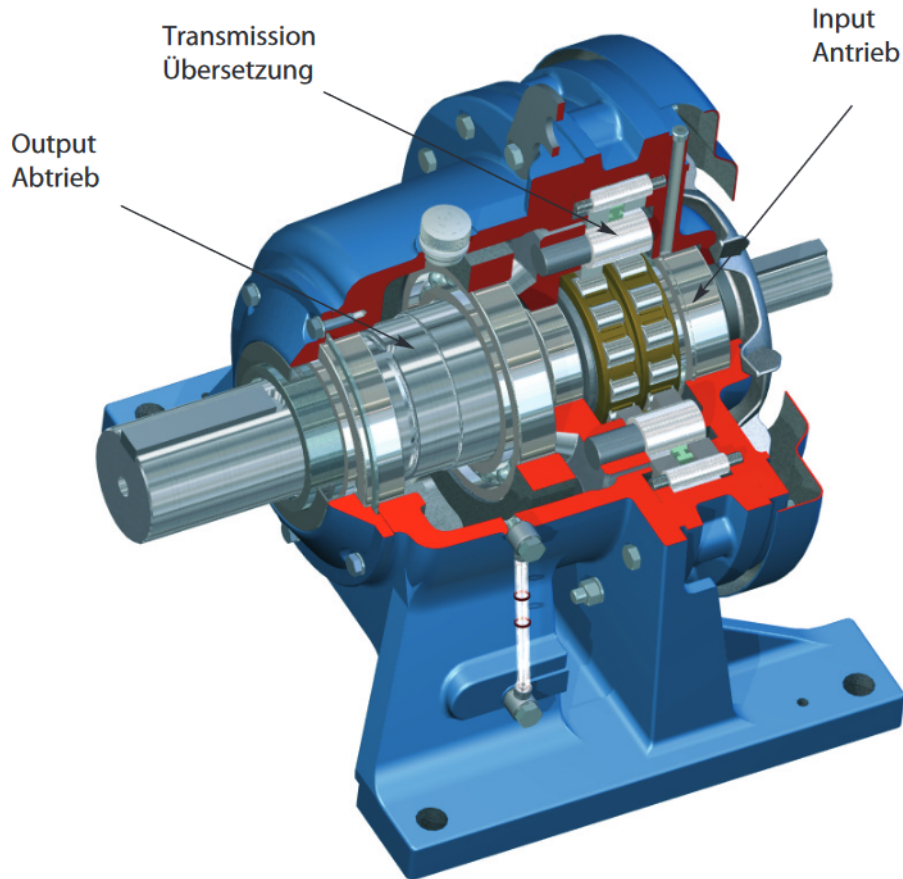


Figure 1.6: Sumitomo Drive 6000 ([15])

Referring to the model of the figure 1.6, since analysing the technical data we become aware of the extremely revolutionary properties of this reducer: for example for a reducer $0,37kW$, it is possible to have ratios variable between 25 and 731 with maximum size between 70 mm and 102 mm .

As Sumitomo ([15]) declares - to make the final summary- we can enumerate the pivotal benefits of this technology:

1. Extreme shock overload capacity:
Since the cycloidal gearbox's system distributes the load to numerous cycloid teeth, it can withstand extreme momentary intermittent shock overloads in emergency situations;

2. Compact size;
3. Overall economy:
Competitive initial cost, high reliability, long life and minimum of maintenance;
4. Capacity for frequent start- stop and severe reversing:
the inertia the cycloidal speed reducer is reduced to a minimum, so that it responds quickly in these applications;
5. Low noise:
when compared with the sliding tooth contact of conventional helical gears, the cycloidal system provides reduced noise level;
6. High efficiency at high ratios:
torque transmitting parts have a rolling action with minimal friction;
7. No thermal factor limitations:
Almost friction-less operation all but eliminates the conventional limitations due to heat;
8. High durability:
Tests on cycloidal reducers show negligible wear after 50,000 hours, and experience shows that future wear and tear is insignificant;

All in all, the most important disadvantage is the not extremely high efficiency especially at low load, the main goal of this work is to focus on the geometrical feature and the dynamic operating conditions that could let the efficiency raise up.

Chapter 2

Geometrical characterization and design of the cycloidal plate

Having assimilating all the peculiarities of the cycloidal reducers, a specific focus has to be given to the main geometrical features of the different elements forming a part in the cycloidal gearbox. Then, the fundamental goal of this chapter is to underline the specific features by raising the awareness of how the geometry impacts on the gearbox's performance. Undoubtedly, the geometry of the cycloidal plate will have a specific role due.

2.1 Analytical determination of the cycloidal geometry (theoretical and working profile)

The principal aim of this section is to summarize all the geometrical equations applied to cycloidal disc in order to get the mathematical equations of teeth profile. Firstly, it should be explained how the geometrical elements of the cycloidal wheel are obtained by generating equations for the teeth profile, equations for basic diameters and other geometrical features. Then, two fundamental definitions are introduced to design the cycloidal plate: the theoretical profile and the working one (referring to figure 2.1):

1. The theoretical profile is the curve achieved by rolling without slipping of a circle C_0 (rolling circle with radius r_{w0} and centre O_0) on the other circle C_1 (basic circle with radius r_1 and centre O_1): the trajectory of the point O_c (distant e_0 from O_0 and moving with the circle C_0) must be considered the theoretical profile of the cycloidal disc.
2. The working profile is an equidistant curve from the theoretical profile obtained

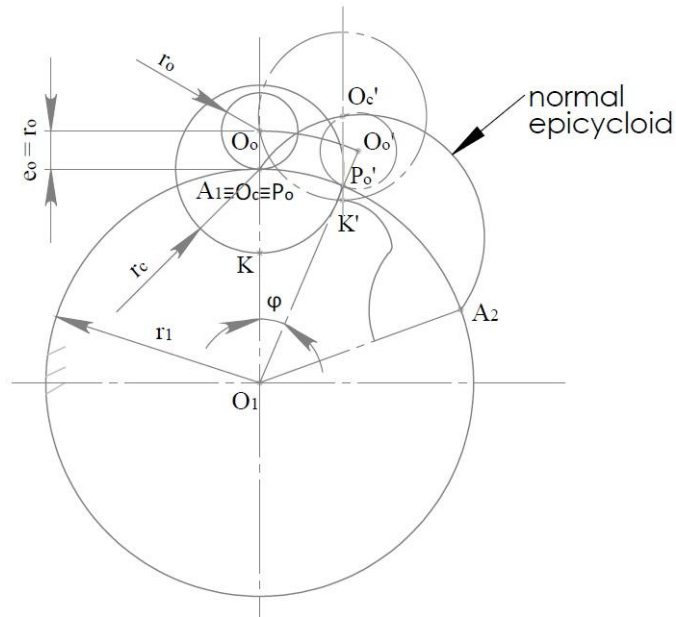


Figure 2.2: Curve generating for normal epicycloid([5])

Referring to figure 2.3, the geometry is produced in the same way as the normal epicycloid, except that O_c lies in the perimeter of rolling circle. In fact, we have $e_0 < r_c$.

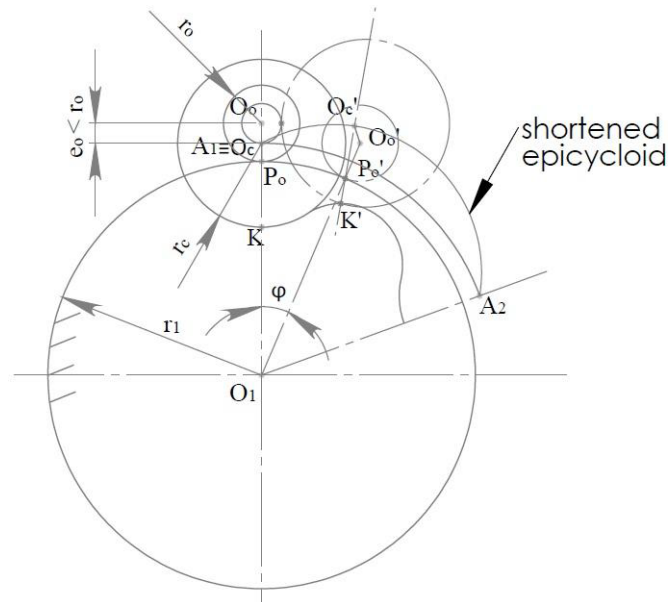


Figure 2.3: Curve generating for normal shortened([5])

The basic geometry could be defined by quantities in Table 2.1.

Table 2.1: Main geometrical quantities to define the external profile of the cycloidal plate

Symbol	Short definition
r_0	Radius of epicycloid
e_0	Epicycloids epicycle
r_c	Housing pins radius
r_1	Primitive radius
φ	Rotation angle of epicycle/of input shaft
ψ	Rotation angle of the wheel

In order to determine the teeth profile, two moving Cartesian coordinate systems are needed: $\xi O_0 \eta$ is linked to the generating circle C_0 and XO_1Y is connected with the basic circle (figure 2.1). Since r_c is the radius of the housing pins, the equation of the profile generating curve in the system $\xi O_0 \eta$ is:

$$\xi^2 + (\eta + e_0)^2 = r_c^2 \quad (2.1)$$

Where e_0 -the construction distance between O_c and O_0 -is called also eccentricity of the profile cutting instrument. At the same time, e_0 is related to the module circle and it is linked to the radius of C_0 , according to:

$$m = 2r_0 \quad (2.2)$$

$$e_0 = \frac{m}{2}(1 - x) \quad (2.3)$$

Where m is the module circle and it is used as a base linked to the parameters of the profile cutting instrument. Moreover, x is the coefficient of modification that could be demonstrated to be one of the most impacting geometrical feature of the reducer because of its effect on efficiency. We can add the following relationships:

$$r_{wo} = r_0 = \frac{m}{2} \quad (2.4)$$

$$a = r_1 + r_{wo} = \frac{mz_1}{2} + \frac{m}{2} = \frac{m}{2}(z_1 + 1) \quad (2.5)$$

To understand fully the forming process of the cycloidal disc, we should focus more on the process of profile cutting. At first, we define a as the distance between O_1 and O_0 and X as the profile cutting instrument that could be expressed as:

$$X = x \frac{m}{2} \quad (2.6)$$

Where x could be positive or negative, so we can have:

1. $x = 0$ no modification;
2. $0 < x < 1$ positive gears;
3. $x < 0$ negative gears;
4. $x = 1$ border gears

If we are referring to transmissions with a difference of teeth - between cycloidal plate's teeth and housing pins- equal to one, the practical choice is to have only positive coefficient of modification; this is to avoid that the teeth profile will be undercut. Referring to figure 2.4, we can define the following geometrical features:

1. Step of pith profile p :
 p indicates the distance between two homonymous points of the profile.

$$p = \pi m \quad (2.7)$$

2. Pitch diameter s :

$$s = 2\pi r_1 \quad (2.8)$$

3. Diameter of the theoretical dedendum circle d_{Tf_1} :

$$d_{Tf_1} = 2(r_1 + X) = m(z_1 + 1) \quad (2.9)$$

4. Diameter of the theoretical addendum circle d_{Ta_1} :

$$d_{Ta_1} = d_{Tf_1} + 2(2e_0) = m(z_1 + 2 - x) \quad (2.10)$$

5. Diameter of the working profile dedendum circle d_{f_1} :

$$d_{f_1} = d_{Tf_1} - 2r_c = m\left(z_1 + x - \frac{r_c}{m}\right) \quad (2.11)$$

6. Diameter of the working profile addendum circle d_{a_1} :

$$d_{a_1} = d_{Ta_1} - 2r_c = m\left(z_1 + 2 - x - \frac{r_c}{m}\right) \quad (2.12)$$

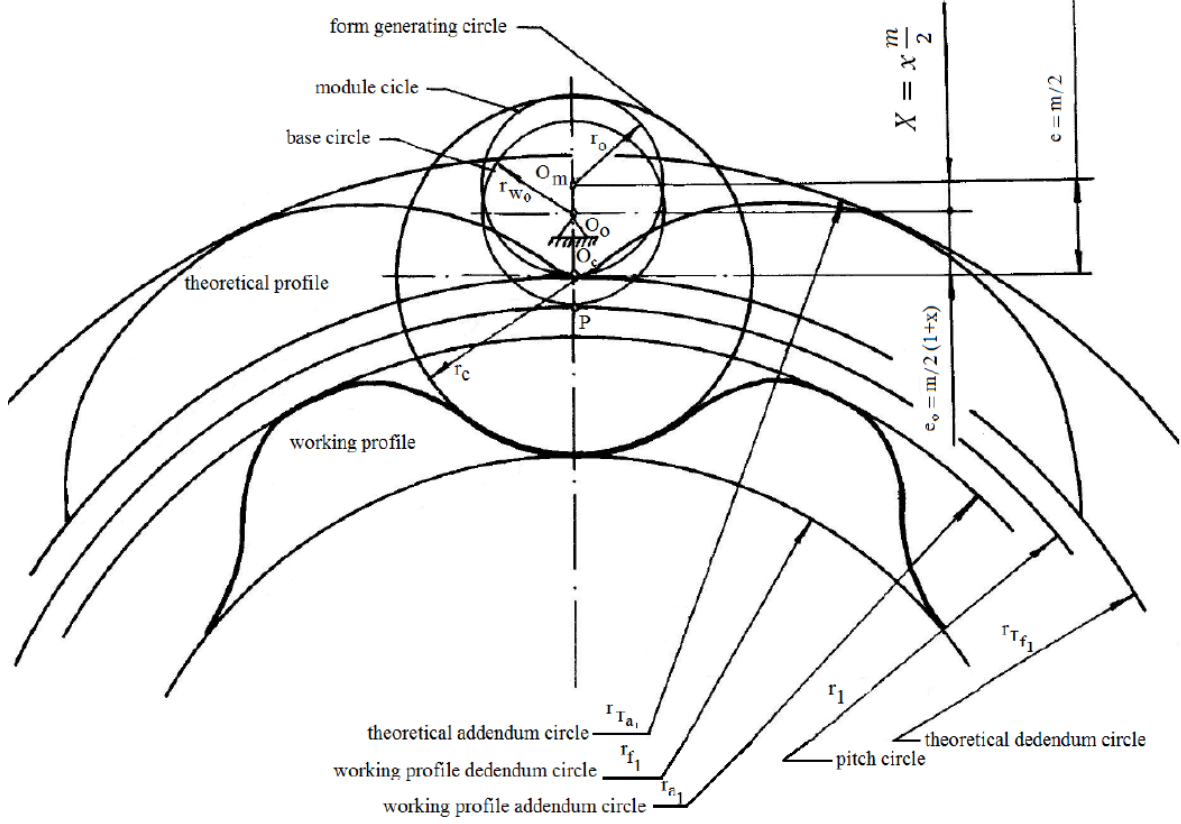


Figure 2.4: Gear dimensions([5])

The analyses of the formulas lead to the following conclusions:

1. The modification of the profile cutting instrument does not change the diameter of the pitch circle of the epicycloidal wheel;
2. By increasing x the tooth depth decreases;
3. The addendum and the dedendum circles coincide and the tooth depth is equal to zero when x is equal to 1.

Once all the geometrical features have been introduced, we are going to get the mathematical formulation of the theoretical and working profile. To make a summary - as it is clear in figure 2.1 -, there are the fixed reference system $X_1O_1Y_1$, the rotating ones XO_1Y and $\xi O_0\eta$. It is possible to link all these reference systems:

$$\begin{bmatrix} \xi \\ \eta \end{bmatrix} = \begin{pmatrix} \cos \psi & -\sin \psi \\ \sin \psi & \cos \psi \end{pmatrix} \begin{bmatrix} X_1 \\ Y_1 \end{bmatrix} \quad (2.13)$$

$$\begin{bmatrix} \vec{X}_1 \\ \vec{Y}_1 \end{bmatrix} = \begin{pmatrix} \cos \varphi & -\sin \varphi \\ \sin \varphi & \cos \varphi \end{pmatrix} \begin{bmatrix} \vec{X} \\ \vec{Y} \end{bmatrix} \quad (2.14)$$

$$\begin{bmatrix} \vec{\xi} \\ \vec{\eta} \end{bmatrix} = \begin{pmatrix} \cos \varphi \cos \psi - \sin \varphi \sin \psi & -\cos \psi \sin \varphi + \sin \psi \cos \varphi \\ \cos \psi \sin \varphi + \sin \psi \cos \varphi & \cos \varphi \cos \psi - \sin \psi \sin \varphi \end{pmatrix} \begin{bmatrix} \vec{X} \\ \vec{Y} \end{bmatrix} \quad (2.15)$$

$$\begin{bmatrix} \vec{\xi} \\ \vec{\eta} \end{bmatrix} = \begin{pmatrix} \cos(\psi + \varphi) & -\sin(\psi + \varphi) \\ \sin(\psi + \varphi) & \cos(\psi + \varphi) \end{pmatrix} \begin{bmatrix} \vec{X} \\ \vec{Y} \end{bmatrix} \quad (2.16)$$

The rotations of the circle C_1 and of the circle C_0 are not independent, but rather they are kinematically linked by the following relation, remembering that the number of teeth of the cycloidal disc is indicated with z_1 (ψ and φ shown in figure 2.1):

$$\frac{\psi}{\varphi} = \frac{r_1}{r_{aw}} = z_1 \quad (2.17)$$

The theoretical profile is the path of point O_c and it must be obtained by rolling without slipping of C_0 on C_1 , we can use the vector sum addition to get the theoretical profile:

$$\overrightarrow{O_1 O_c} = \overrightarrow{O_1 O_0} + \overrightarrow{O_0 O_c} = a\vec{Y}_1 - e_0\vec{\eta} \quad (2.18)$$

$$\overrightarrow{O_1 O_c} = a(\sin \varphi \vec{X} + \cos \psi \vec{Y}) - e_0[\sin(\psi + \varphi)\vec{X} + \cos(\psi + \varphi)\vec{Y}] \quad (2.19)$$

After some mathematical passages, we could gain the coordinates of the trajectory of the theoretical profile:

$$\begin{cases} X_T = a \sin \varphi - e_o \sin(\psi + \varphi) = a \sin \psi - e_o \sin[\psi(1 + z_1)] \\ Y_T = a \cos \varphi - e_o \cos(\psi + \varphi) = a \cos \psi - e_o \cos[\psi(1 + z_1)] \end{cases} \quad (2.20)$$

$$\begin{cases} X_T = \frac{m}{2} \left[(z_1 + 1) \sin \varphi - (1 - x) \sin(\varphi(z_1 + 1)) \right] \\ Y_T = \frac{m}{2} \left[(z_1 + 1) \cos \varphi - (1 - x) \cos(\varphi(z_1 + 1)) \right] \end{cases} \quad (2.21)$$

These equations make sense only if $0 < x < 1$. After that, we might get the equations for working profile: the working profile could be defined as the trajectory of the points equidistant from the theoretical profile. It is well-known that:

$$\overrightarrow{O_1 O_c} = \begin{bmatrix} X_T \\ Y_T \end{bmatrix} \quad (2.22)$$

Then, we can get the tangent vector to theoretical profile as follows (figure 2.5):

$$\vec{t} = \frac{1}{\|\overrightarrow{O_1 O_c}\|} \frac{d\overrightarrow{O_1 O_c}}{d\varphi} \quad (2.23)$$

$$\vec{t} = \frac{1}{\sqrt{\left(\frac{d}{d\varphi}X_T\right)^2 + \left(\frac{d}{d\varphi}Y_T\right)^2}} \frac{d\overrightarrow{O_1O_c}}{d\varphi} \quad (2.24)$$

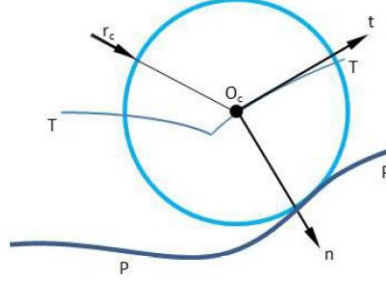


Figure 2.5: Geometric definition of the construction elements of working profile(P) by knowing the theoretical profile (T)

Because \vec{t} and \vec{n} are reference versors of orthogonal axes (figure 2.5), we could obtain the normal versor from the theoretical profile by knowing \vec{t} and, then, the trajectory of the point C :

$$\vec{n} \cdot \vec{t} = \vec{n} \cdot \begin{bmatrix} t_x \\ t_y \end{bmatrix} = 1 \implies \vec{n} = \begin{bmatrix} t_y \\ -t_x \end{bmatrix} \quad (2.25)$$

Then:

$$\overrightarrow{O_cC} = r_c \vec{n} \quad (2.26)$$

Finally, after some mathematical passages we are going to get the mathematical formulation of the working profile.

$$\begin{cases} X_W = X_T + r_c \frac{\frac{d}{d\varphi}Y_T}{\sqrt{\left(\frac{d}{d\varphi}X_T\right)^2 + \left(\frac{d}{d\varphi}Y_T\right)^2}} \\ Y_W = Y_T - r_c \frac{\frac{d}{d\varphi}X_T}{\sqrt{\left(\frac{d}{d\varphi}X_T\right)^2 + \left(\frac{d}{d\varphi}Y_T\right)^2}} \end{cases} \quad (2.27)$$

The main formulas of the theoretical profile and of the working one can be introduced in Matlab in order to lay the foundations of the following modelling work.

Design of theoretical and working profile of cycloidal plate

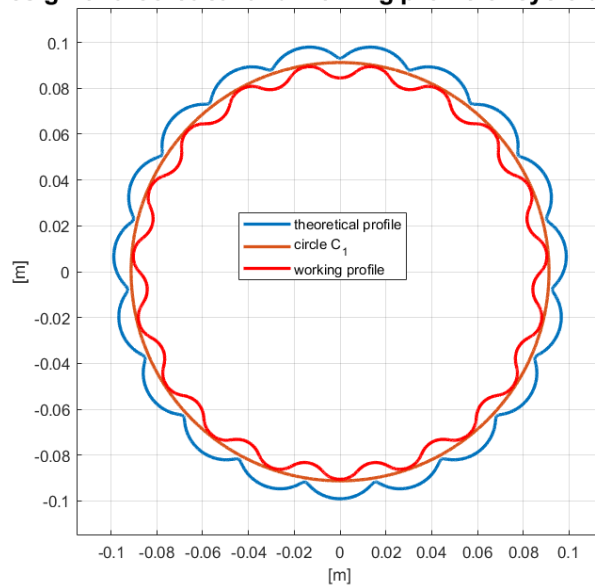


Figure 2.6: Matlab graphics to evaluate working and theoretical profile

Design of theoretical and working profile of cycloidal plate

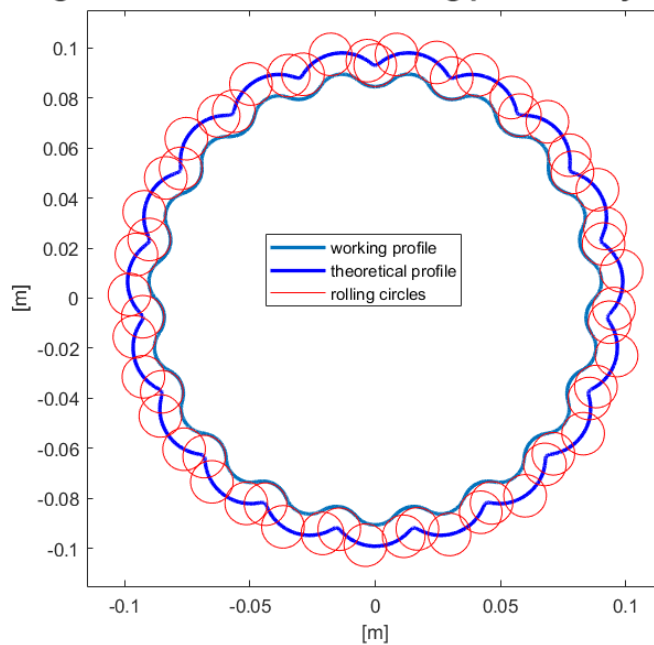


Figure 2.7: Matlab graphics to evaluate working and theoretical profile with rolling circles

2.2 Theoretical and working curvature radius of the cycloidal profile

To study the manufacturing practicability and the functionality of the cycloidal plate, it is important to analyse in detail the particular shape of the teeth in coupling with the pins. So, we are going to make a mathematical study on the external profile of the cycloid. At first, we are going to estimate the curvature radius of the theoretical profile ρ_T -using a well-known geometrical relationship to calculate the curvature radius since a curve given parametrically-:

$$\rho_T = \frac{(X_T'^2 + Y_T'^2)^{3/2}}{X_T' Y_T'' - Y_T' X_T''} \quad (2.28)$$

Where:

- $X_T' = \frac{dX_T}{d\varphi}$ and $Y_T' = \frac{d^2Y_T}{d\varphi}$;
- $X_T'' = \frac{d^2X_T}{d\varphi^2}$ and $Y_T'' = \frac{d^2Y_T}{d\varphi^2}$.

By using the equations of the theoretical profile (2.21), the equation of the theoretical curvature radius will be [5]:

$$\rho_T(\varphi) = \frac{m}{2}(z_1 + 1) \frac{[1 + (1 - x)^2 - 2(1 - x) \cos(z_1\varphi)]^{3/2}}{1 + (1 - x)^2(z_1 + 1) - (1 - x)(z_1 + 2) \cos(z_1\varphi)} \quad (2.29)$$

At this point, it is immediate to write the mathematical equation of the working curvature radius ρ_W and to get the graphic of figure 2.9:

$$\rho_W(\varphi) = \rho_T(\varphi) - r_c \quad (2.30)$$

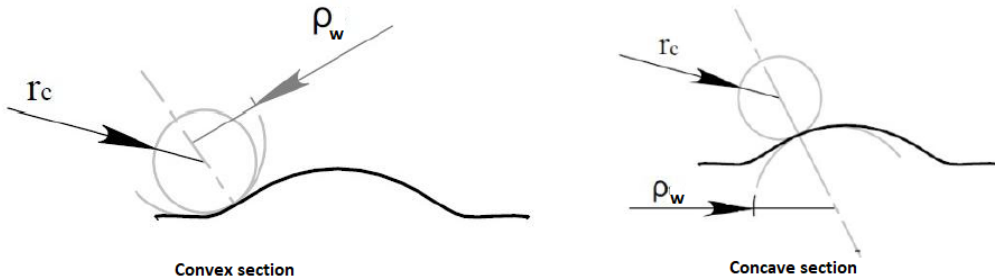


Figure 2.8: Convex and concave section

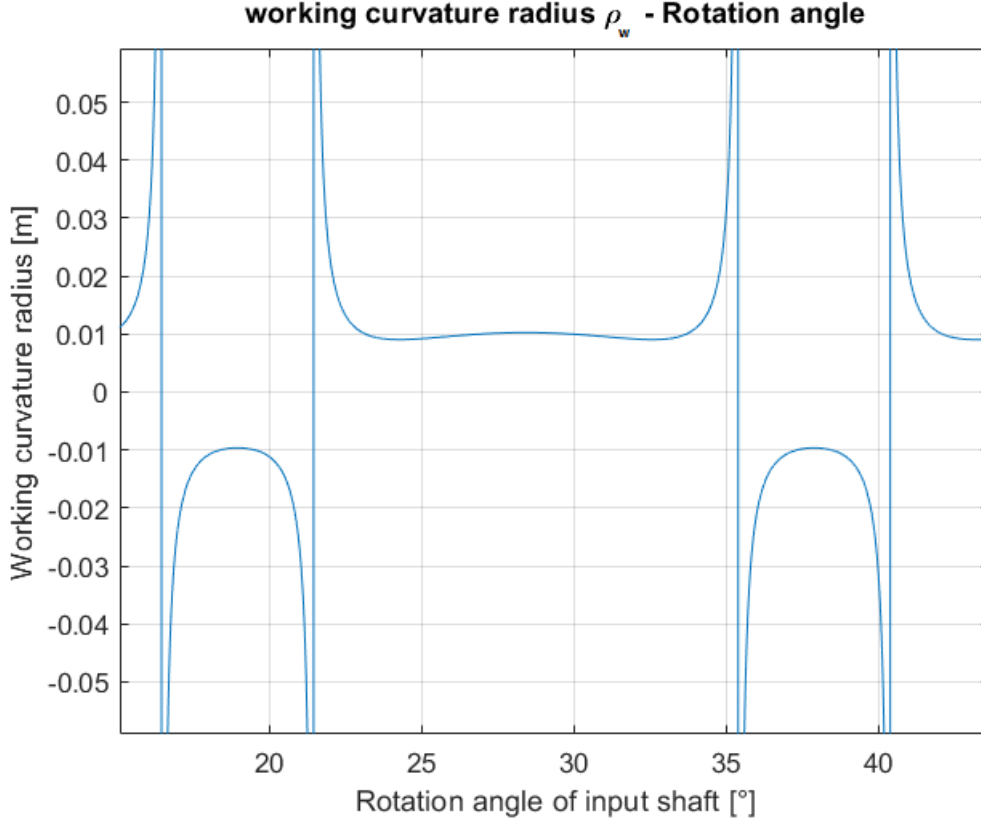


Figure 2.9: Working curvature radius ρ_W versus rotation angle φ

It is useful to analyze the trend of the curve ρ_W in order to evaluate any critical issues and design limits on the coupling of the teeth with the pins. By studying the trend of $\rho_W(\varphi)$ (figure 2.9), we may deduce:

1. Where the sign of ρ_W varies with a jump, then there is the transition of shape from convex ($\rho_W > 0$) to the concave ($\rho_W < 0$);
2. When the shape is concave, it should be avoided that $|\rho_W| > r_c$ as it would correspond to the physical condition of entry in the wheel in a concave section too small to guarantee the punctual contact foreseen with the housing pins, therefore, this contact would not be functional for the purpose of the transmission.

For the second points- in our case of analysis- we have $r_c = 8,5 \text{ mm}$ and- as it is deducible looking at the figure 2.9- the contact between wheel and pins is guaranteed.

2.3 Distinctive meshing angles

We are going to introduce the pressure angle α_W that is the angle between the tooth profile and a radial line to its pitch point. In involute teeth, it is defined as the angle formed by the radial line and the line tangent to the profile at the pitch point. The importance of the pressure angle consists in its giving the direction normal to the tooth profile, and because the pressure angle is strictly linked to the mechanical stresses introduced. According to [5], we have:

$$\alpha_W(\varphi) = \arcsin \frac{\cos(z_1\varphi) + x - 1}{\sqrt{1 + (1-x)^2 - 2(1-x)\cos(z_1\varphi)}} \quad (2.31)$$

In figure 2.10, the pressure angle α_W is plotted as a function of the rotation of the plate $\psi = z_1\varphi$ with different coefficients x . It is obvious that its maximum value is 90° and it can be positive or negative. Moreover, looking at figure 2.10, by increasing the value of x we obtain higher average values of the angle α_W during transmission.

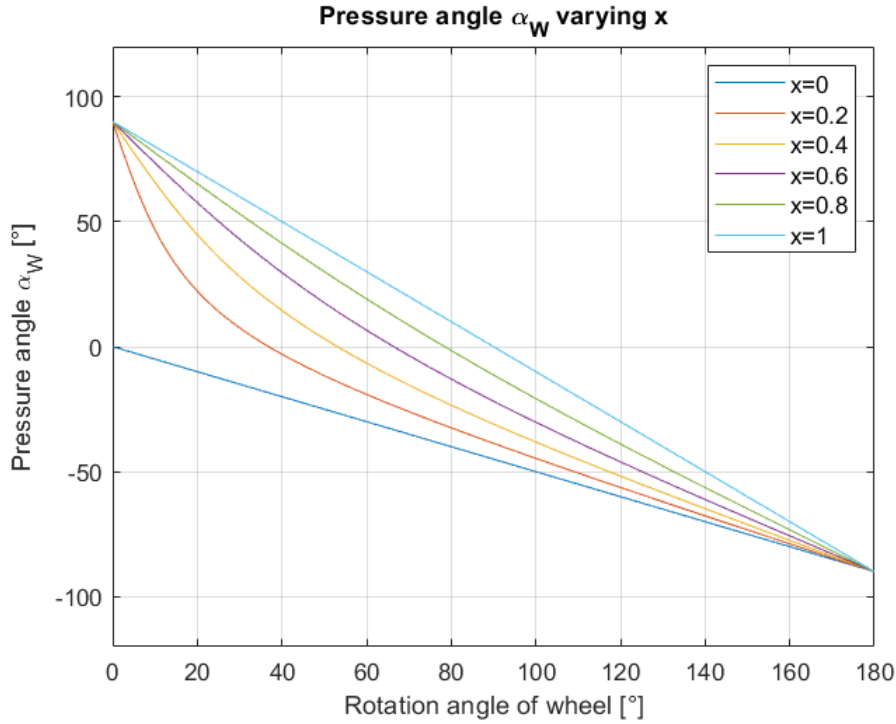


Figure 2.10: Pressure angle α_W

Another pivotal geometrical quantity in the analysis of the transmission is the transmitting angle θ , because of possible jamming. The transmitting angle is the angle between the direction of the net thrust exchanged between plate and housing

pin and the direction of the speed of the contact point seen belonging to plate. It must satisfy the following condition:

$$\theta_{max} \leq \theta_{allowable} \quad (2.32)$$

The introduction of $\theta_{allowable}$ is necessary to avoid that- in order to guarantee the motion's transmission- we have excessive excitement. Sometimes it is better to use γ - known as angle of motion transfer- instead of θ , where γ is the complementary of θ . Consequently, the relationship (2.32) will become:

$$\gamma_{min} \geq \gamma_{allowable} \quad (2.33)$$

In figure 2.11 it is possible to deduce the effects of correction coefficient x on the angle of motion transfer. The figure is obtained by the following formula for different x values:

$$\gamma(\varphi) = \arcsin \frac{(1-x) \sin(z_1 \varphi)}{\sqrt{1 + (1-x)^2 - 2(1-x) \cos(z_1 \varphi)}} \quad (2.34)$$

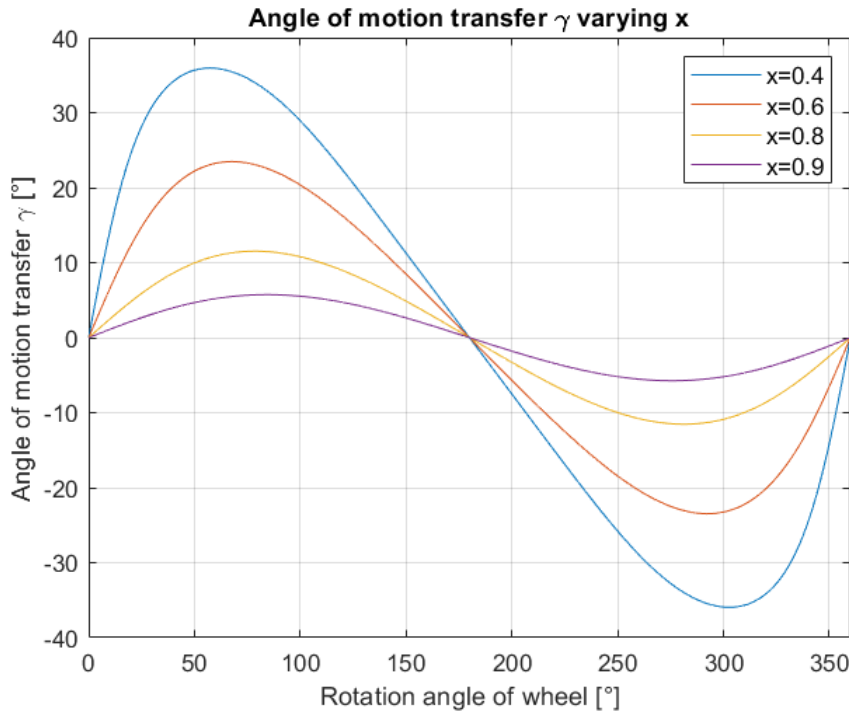


Figure 2.11: Angle of motion transfer γ

By raising up x we may have values of γ not appropriate for the motion, in fact, it is recommended $\gamma_{allowable} = 30^\circ$ during the decisive phases of motion. Finally, we should specify the values of the remaining parameter - except x - to uniquely define the external cycloidal profile:

Table 2.2: Main parameters to uniquely define the external geometry of the cycloidal disk

Symbol	Short name	Value
r_c	pin's radius	8,5 mm
z_1	teeth number	19
r_1	primitive radius	91,2 mm

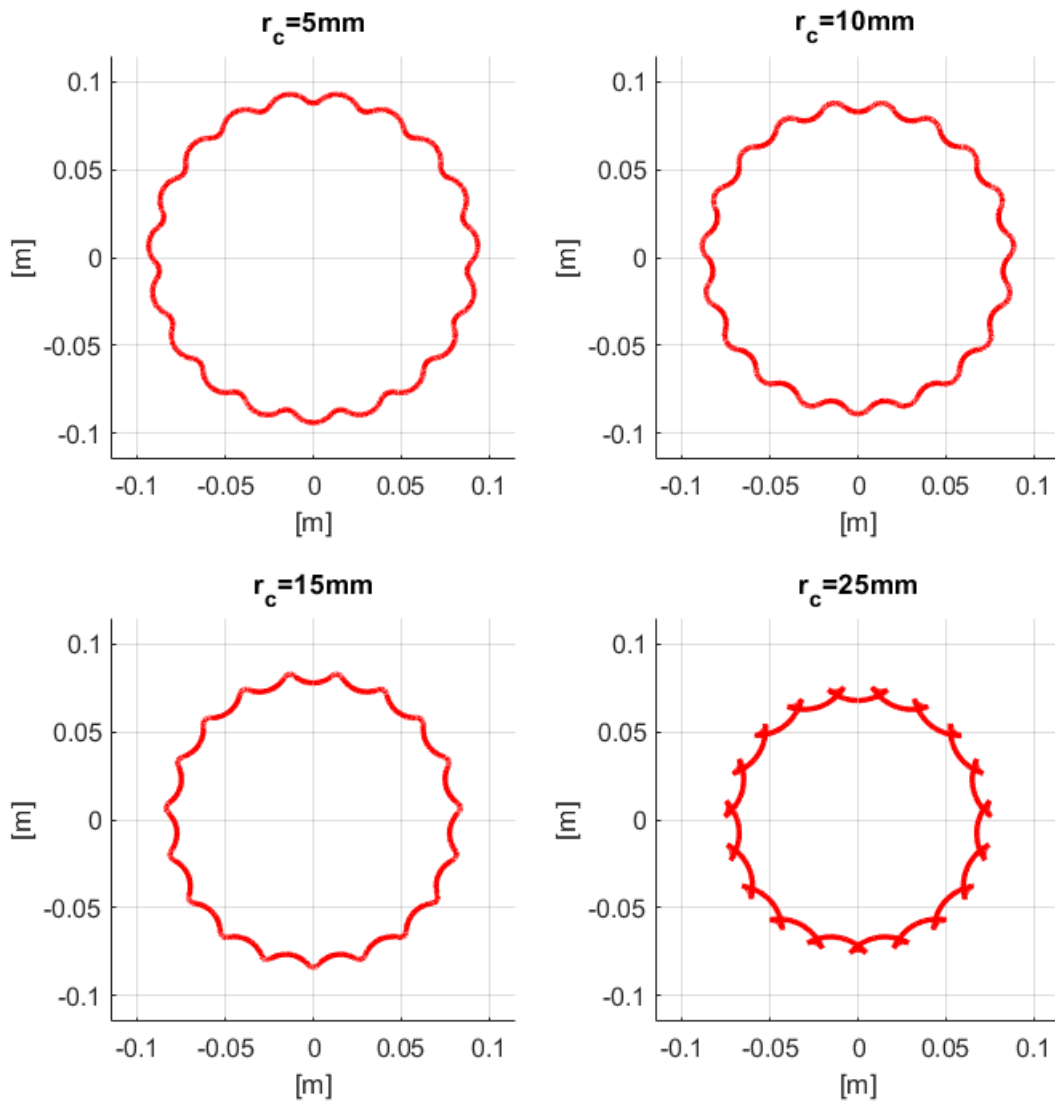
2.4 Parametric analysis on cycloidal plate

In this last section, the main goal is to make a parametric analysis in order to evaluate how the four basic parameters to define the plate's geometry impact on the general shape of the plate itself. Table 2.3 makes a summary of these four parameters and the starting value of each one: the simulations are based on varying only one parameter at a time, setting the others at the basic value.

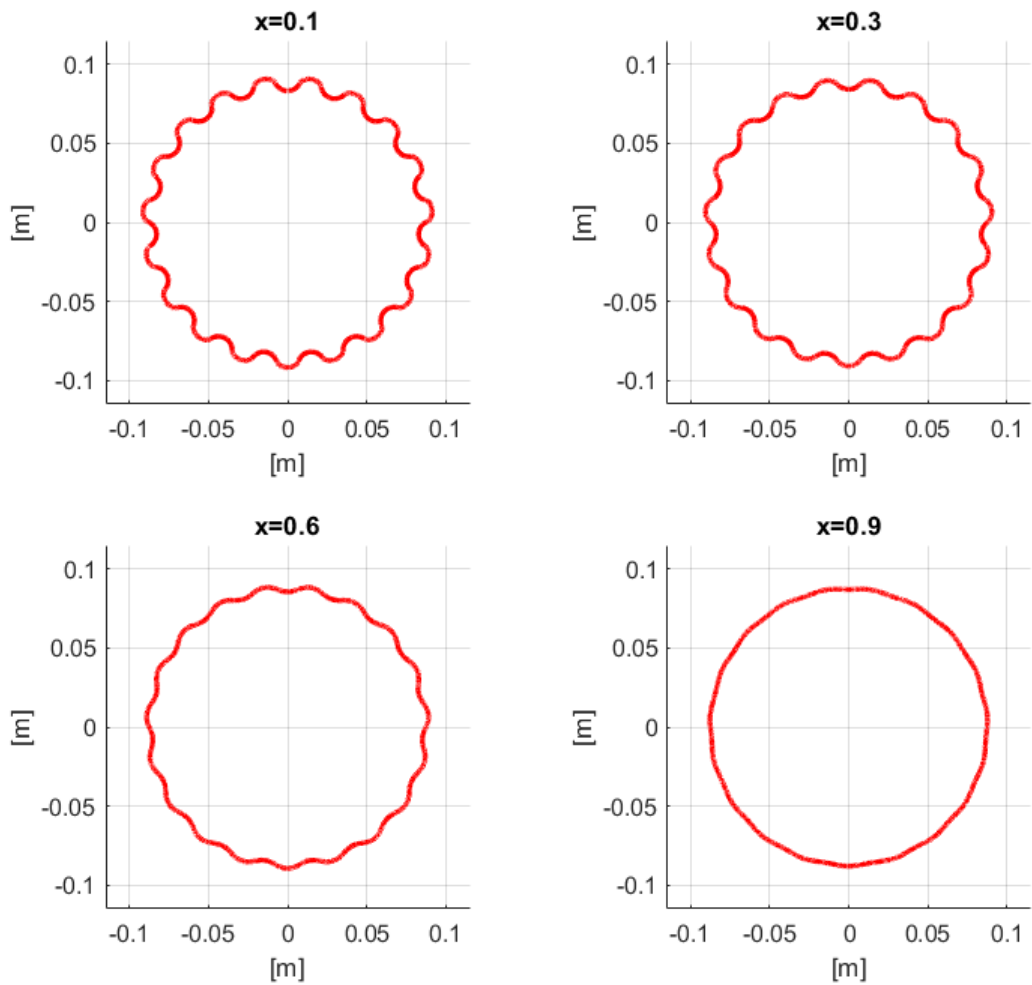
Table 2.3: Main parameters to uniquely define the external geometry of the cycloidal disk

Symbol	Short name	Value
r_c	pin's radius	8,5 mm
x	correction coefficient	0,37
z_1	teeth number	19
r_1	primitive radius	91,2 mm

The first simulation is obtained by varying r_c , the pins radius. The simulations were performed by varying only r_c but the same results would come out if we decided to varying $\frac{r_c}{r_1}$. As we can see in figure 2.13, if we increase r_c compared to r_1 , we will get external profile not technologically feasible (the last condition corresponds to $r_c = 25\text{ mm}$ or $\frac{r_c}{r_1} = 0,27$). Moreover, by raising $\frac{r_c}{r_1}$ we are going to get less sinuous forms that may not favor mechanical coupling between pins and cycloidal wheel: this is deducible analysing the figure 2.13.

Figure 2.12: Effect on plate geometry of varying r_c

In the second simulation (figure 2.13) we can take into consideration the influence of the correction coefficient x . This effect - as we have said before- consists mainly in the reduction of the depth of the teeth. This condition strongly hinders the coupling with the risk that the pins do not go to roll on the profile of the wheel but end up jumping on this.

Figure 2.13: Effect on plate geometry of varying x

In the last simulations- figure 2.14-, we have varied the number of teeth z_1 while the other parameters are maintained constant. This variation has, to a lesser extent, meaning in the design process because z_1 is determined by the desirable gear ratio. Anyways, in order to have a suitable shape for the cycloidal wheel, we should evaluate the right dimensions of the other parameters since setting z_1 .

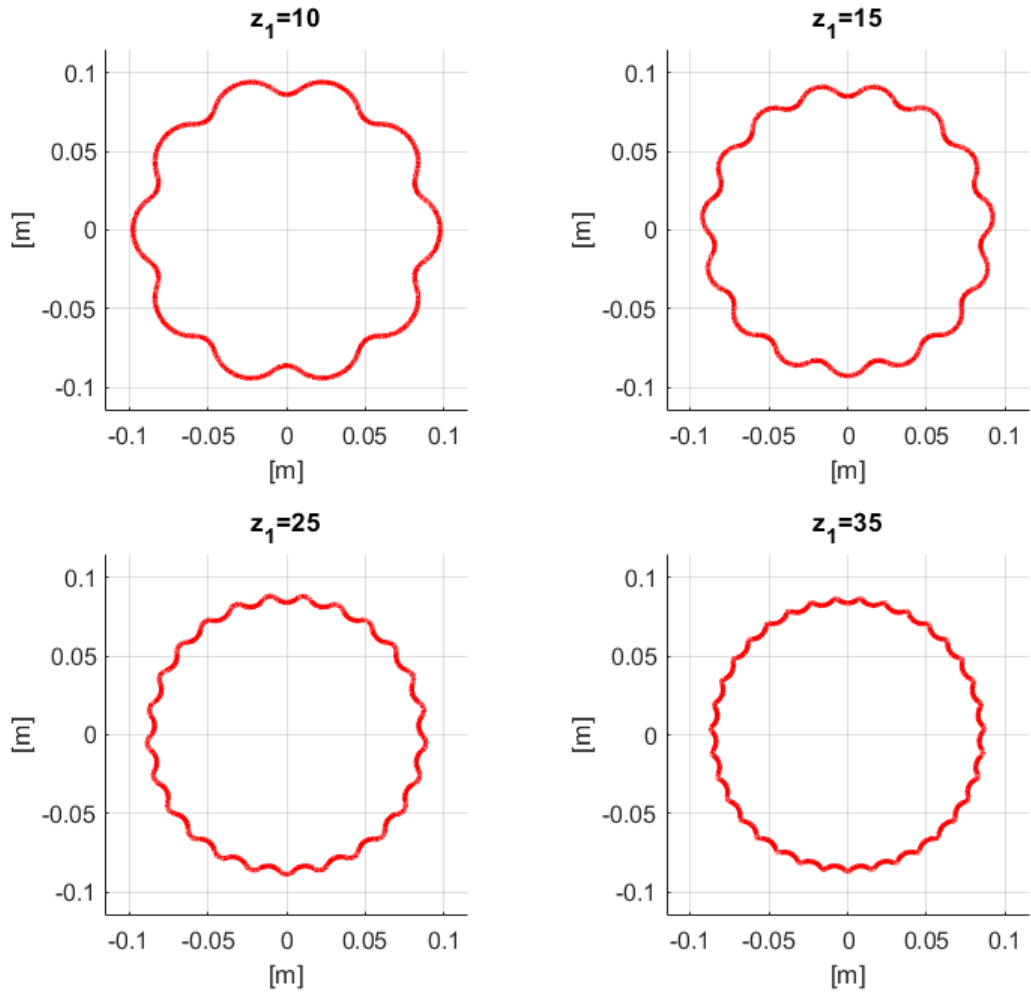


Figure 2.14: Effect on plate geometry of varying z_1

Chapter 3

Kinematic and dynamic analysis: rigid model bodies

The main aim of this chapter is to build the bases of a first model to explain the dynamic behaviour of the cycloidal reducer. The proposed model is the simplest obtained by imposing the perfect rigidity of the bodies; for this reason it is named rigid bodies model. Furthermore, the basic kinematics of this model will be maintained in the following models, while some modifications are introduced in the dynamic analysis. Then, the starting point consists in kinematic laws applied to the most relevant points of the coupling bodies, Afterwards, a particular focus will be made on the forces distribution and, finally, through two different approaches (analytical method and Newton's one) we are going to get the fundamentals laws to solve the dynamic problem. Using two different approaches lets to understand - by two different points of view, the first one more concise, the second one more intuitive - all the dynamics of the reducer.

3.1 Kinematic analysis

Before presenting all the main formulas of the kinematic analysis, the reference systems should be made clear: we have the fixed reference system X_0OY_0 whose center belongs to the input shaft axis, the second one $X_1O_1Y_1$ has the center coincident with the cycloidal plate's center and it is moving with the plate itself (figure 3.1).

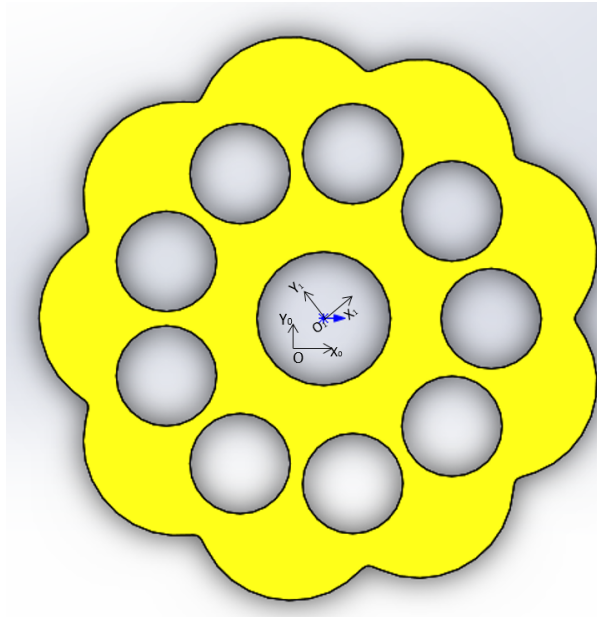


Figure 3.1: Reference systems used

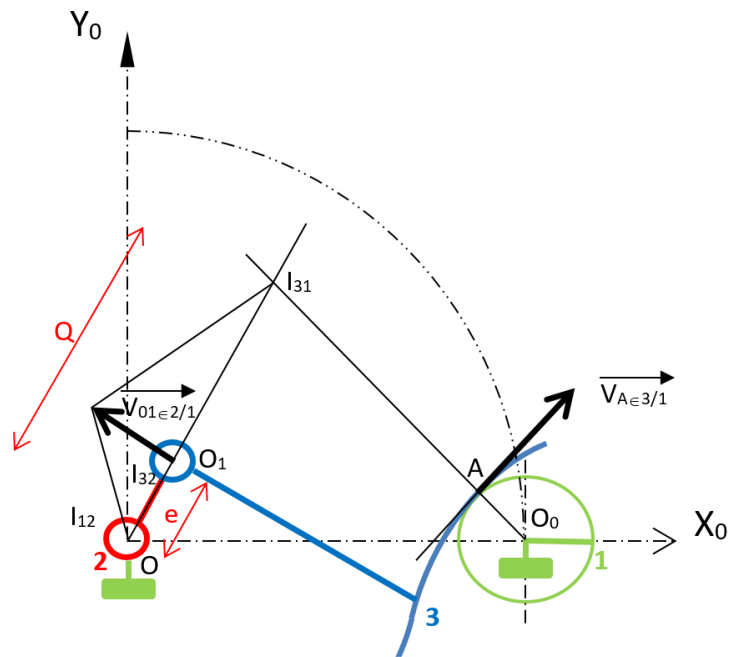


Figure 3.2: Setup of the cycloidal disk and of point of contact A (between cycloidal disk and a single housing pin), the main elements: 1 housing pin, 2 input shaft, 3 cycloidal plate

We are going to introduce the Kennedy theorem for the future developments: it states that the three instant centres shared by three rigid bodies in relative planar motion to another (whether or not connected), all lie on the same straight line -more details are in Appendix A-. Figure 3.2 shows the chosen setting: part 1 is the housing pin in contact, part 3 is the cycloidal plate, finally part 2 is the input shaft. It is well-known that O is the centre of input shaft rotation, while O_1 is the geometrical centre of the cycloidal disc. Part 2 has a rotating motion to the body 1 (fixed) on the centre O ; then the point O is the instantaneous centre of velocity (IVC) of the body 2, so $I_{12} = O$. Moreover, part 3 has a rotating motion to body 2 on the centre O_1 , then the point O_1 is the instantaneous centre of velocity of body 3 relatively to body 2, so $I_{23} = O_1$. Therefore, we will obtain- by applying the Kennedy theorem- the position of I_{31} . In fact, I_{31} is located at the intersection of the straight (OO_1) and the normal to the tangent at the point of contact A between cycloidal disk and housing pin. Since getting the position of the instantaneous centres of velocity I_{31} , we are going to write the Rivals theorem to get the velocity of the point O_1 :

$$\overrightarrow{V_{O_1 \in 2/1}} = \overrightarrow{OO_1} \times \overrightarrow{\omega_{2/1}} \quad (3.1)$$

$$\overrightarrow{V_{O_1 \in 3/1}} = \overrightarrow{I_{13}O_1} \times \overrightarrow{\omega_{3/1}} \quad (3.2)$$

While $\overrightarrow{V_{O_1 \in 2/1}}$ is the speed of the the point O_1 in-built with the body 2 relatively to the body 1, $\overrightarrow{V_{O_1 \in 3/1}}$ is the speed of the the point O_1 in-built with the body 3 relatively to the body one 1. Anyways, it must be valid that:

$$\overrightarrow{V_{O_1 \in 2/1}} = \overrightarrow{V_{O_1 \in 3/1}} \quad (3.3)$$

Getting to the main point:

$$\omega_{3/1} (Q - e) = -\omega_{2/1} e \quad (3.4)$$

$$\frac{\omega_{3/1}}{\omega_{2/1}} = -\frac{e}{Q - e} \quad (3.5)$$

Where e is the eccentricity between the axis of the input shaft and the other one of cycloidal wheel, while Q is the length of the segment $I_{31}O$. Then, while it appears clear that $\omega_{2/1}$ is the input speed of the mechanism, we should focus more on the contact between the internal lobes of the cycloidal disc and the rollers in-built with the output shaft. This contact could be demonstrated to be homo-kinetic, so the angular speed between the cycloidal plate and the output shaft is just the same. Then, $\omega_{3/1}$ is the output speed. All these remarks allow us to demonstrate by knowing $\omega_{3/1}/\omega_{2/1} = (z_2 - z_1)/z_1$:

$$Q = \frac{z_2 e}{z_2 - z_1} \quad (3.6)$$

The following achievements should guide to the derivation of the coordinate of point A - point of contact between the housing pin and the cycloidal disk- and its speed. Referring to figure 3.3, point A must belong to the line $I_{31}O_0$ with a distance from O_0 as equal to the radius of housing pins r_c , while r_2 is the distribution radius of the housing pins. We are able to deduce the position of the point A and the point I_{31} referring to the figure 3.5:

$$\begin{cases} X_A = r_2 - r_c \cos \chi \\ Y_A = r_c \sin \chi \end{cases} \quad (3.7)$$

$$\begin{cases} X_{I_{31}} = Q \cos \psi \\ Y_{I_{31}} = Q \sin \psi \end{cases} \quad (3.8)$$

Where we can get χ from basic of trigonometry applied to figure 3.3:

$$\chi = \arctan\left(\frac{Q \sin \psi}{r_2 - Q \cos \psi}\right) = \arctan\left(\frac{\sin \psi}{r_2/Q - \cos \psi}\right) \quad (3.9)$$

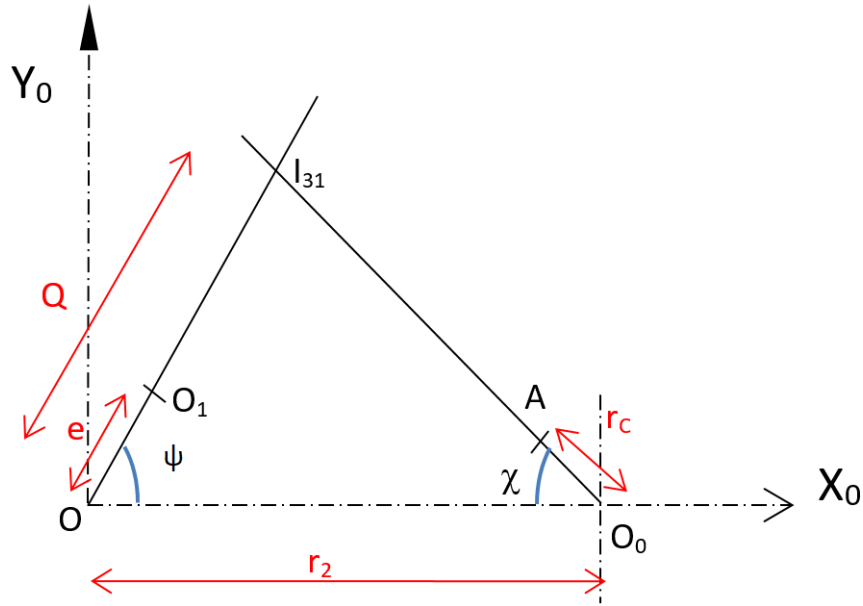


Figure 3.3: Setup of the cycloidal plate and of point of contact A (between cycloidal disk and a single housing pin)

For the following works on dynamics, it is relevant knowing the velocity of the point of contact A :

$$\overrightarrow{V_{A \in 3/1}} = \overrightarrow{I_{31}A} \times \overrightarrow{\omega_{3/1}} \quad (3.10)$$

Where:

$$\overrightarrow{I_{31}A} = \begin{bmatrix} r_2 - r_c \cos \chi - Q \cos \psi \\ r_c \sin \chi - Q \sin \psi \\ 0 \end{bmatrix} \quad (3.11)$$

By using some remarkable relations from goniometry:

$$\overrightarrow{I_{31}A} = \begin{bmatrix} r_2 - r_c \frac{\frac{r_2}{Q} - \cos \psi}{\sqrt{\frac{r_2}{Q} - 2 \cos \psi}} - Q \cos \psi \\ r_c \frac{\sin \psi}{\sqrt{\frac{r_2}{Q} - 2 \cos \psi}} - Q \sin \psi \\ 0 \end{bmatrix} \quad (3.12)$$

Then, we may move on to evaluate the velocity of the point A , referring this velocity to the rotating Cartesian system:

$$\overrightarrow{V_{A \in 3/1}} = \overrightarrow{I_{31}A} \times \overrightarrow{\omega_{3/1}} = \begin{bmatrix} r_2 - r_c \frac{\frac{r_2}{Q} - \cos \psi}{\sqrt{\frac{r_2}{Q} - 2 \cos \psi}} - Q \cos \psi \\ r_c \frac{\sin \psi}{\sqrt{\frac{r_2}{Q} - 2 \cos \psi}} - Q \sin \psi \\ 0 \end{bmatrix} \times \begin{bmatrix} 0 \\ 0 \\ \omega_{3/1} \end{bmatrix} \quad (3.13)$$

$$\overrightarrow{V_{A \in 3/1}} = \overrightarrow{I_{31}A} \times \overrightarrow{\omega_{3/1}} = \begin{bmatrix} \omega_{3/1} \left(r_c \frac{\sin \psi}{\sqrt{\frac{r_2}{Q} - 2 \cos \psi}} - Q \sin \psi \right) \\ -\omega_{3/1} \left(r_2 - r_c \frac{\frac{r_2}{Q} - \cos \psi}{\sqrt{\frac{r_2}{Q} - 2 \cos \psi}} - Q \cos \psi \right) \\ 0 \end{bmatrix} \quad (3.14)$$

In this way we have defined all the kinematics of the reducer by putting the pivotal achievements to fully resolve the dynamics.

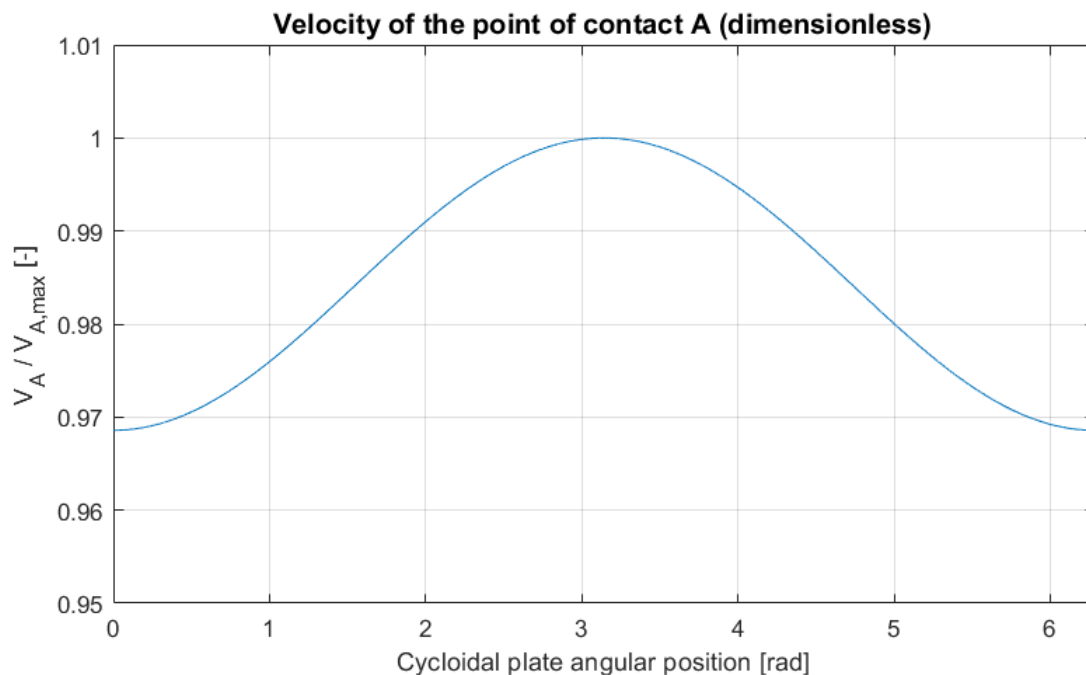


Figure 3.4: Velocity of point A (dimensionless)

3.2 Distribution of forces

The first step -that should be made before applying the fundamental dynamic laws- is to define the forces acting upon the cycloidal disc. The kind of interactions of the cycloidal disc between the other bodies are:

1. The force (normal E_x and tangential components $(1 - \mu_E)E_y$) exchanged between the cycloidal disc and the input shaft through the intermediate bearing;
2. The forces exchanged (normal $F_{N,i}$ and tangential components $\mu_p F_{N,i}$) between the cycloidal disc and the housing pins in contact;
3. The forces exchanged (normal $F_{k,j}$ and tangential components $\mu_s F_{k,j}$) between the cycloidal disc and the output rollers.

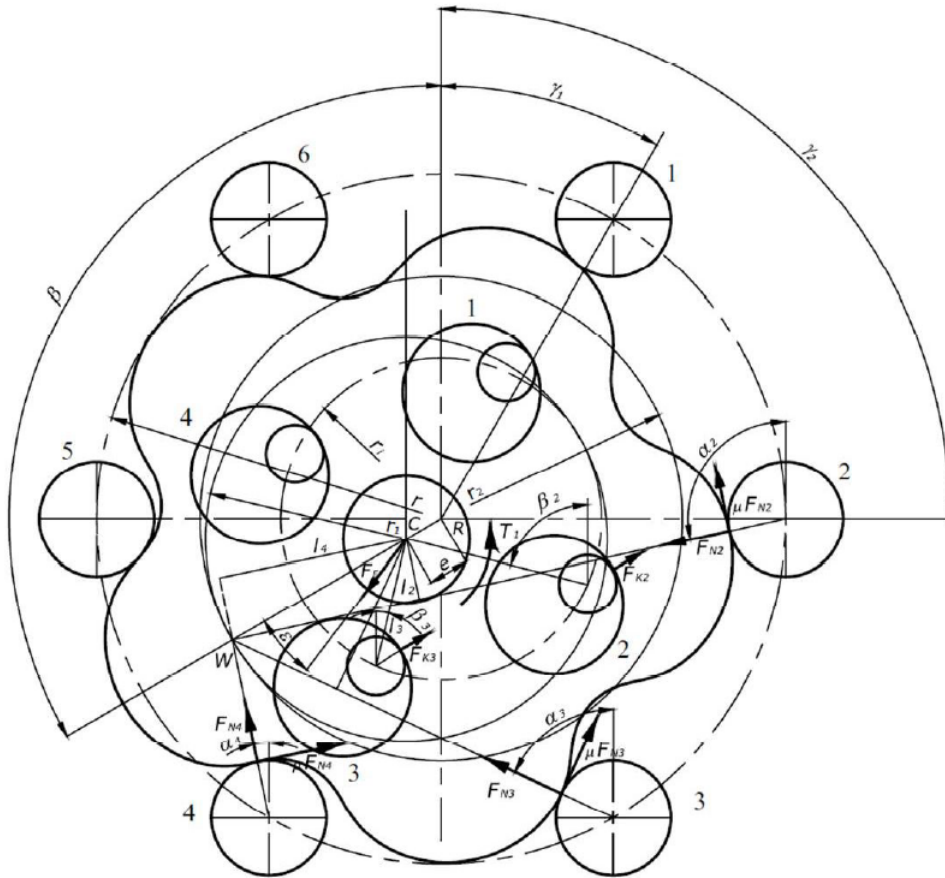


Figure 3.5: Distribution of forces exchanged between cycloidal plate and other bodies[1]

We are going to introduce the following hypotheses of the first model that we call rigid bodies model:

1. The output torque is constant;
2. All the bodies are strictly rigid, or better, no deformations are taken into account in this model;
3. Input speed is constant and output speed will be got through the gear ratio;
4. Input torque is unknown and it is going to be determined by solving the dynamic problem;
5. We are going to refer to a gearbox with only one disk- as the experimentation shows- the number of wheels does not impact on the trend of efficiency.

Without clearance between disk and pins, half of them are loaded and the others not at one time. Classically ([5],[6],[3]) the load distributions could be estimated by using the outcome of Kennedy theorem:

$$F_{N,i}(\psi_i) = \begin{cases} F_{max,N} \frac{r_2}{Q} \frac{\sin \psi_i}{\sqrt{1 + \left(\frac{r_2}{Q}\right)^2 - 2\frac{r_2}{Q} \cos \psi_i}} & \text{for } 0 \leq \psi_i \leq \pi \\ 0 & \text{for } \pi \leq \psi_i \leq 2\pi \end{cases} \quad (3.15)$$

It should be added the load distributions linked to the contact between rollers and cycloidal plate at one time:

$$F_{k,j}(\psi_j) = \begin{cases} F_{max,k} \sin \psi_j & \text{for } 0 \leq \psi_j \leq \pi \\ 0 & \text{for } \pi \leq \psi_j \leq 2\pi \end{cases} \quad (3.16)$$

We are going to demonstrate equation (3.15) as the outcome of Kennedy theorem. The main reference of all the following steps is figure 3.6.

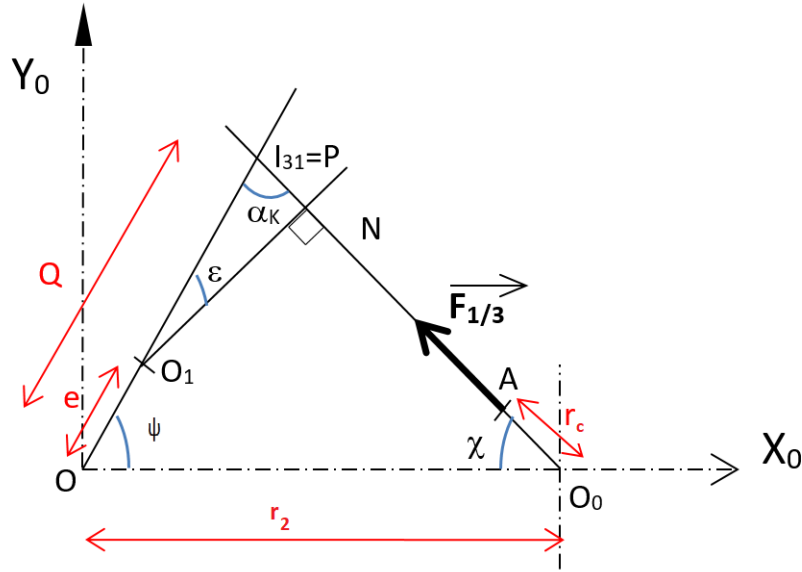


Figure 3.6: Setup of the geometry of the contact between cycloidal wheel and pin

From the literature ([5],[6],[3]), it is well-known:

$$F_{N,i}(\psi_i) = \begin{cases} F_{max,N} \sin \alpha_K & \text{for } 0 \leq \psi_i \leq \pi \\ 0 & \text{for } \pi \leq \psi_i \leq 2\pi \end{cases} \quad (3.17)$$

We can apply some geometrical remarks- looking at figure 3.15-:

$$\alpha_K = \pi - \psi - \chi = \pi - \psi - \arctan\left(\frac{\sin \psi}{r_2/Q - \cos \psi}\right) \quad (3.18)$$

After some mathematical passages, it is possible to demonstrate:

$$\sin \alpha_K = \frac{r_2}{Q} \frac{\sin \psi_i}{\sqrt{1 + \left(\frac{r_2}{Q}\right)^2 - 2\frac{r_2}{Q} \cos \psi_i}} \quad (3.19)$$

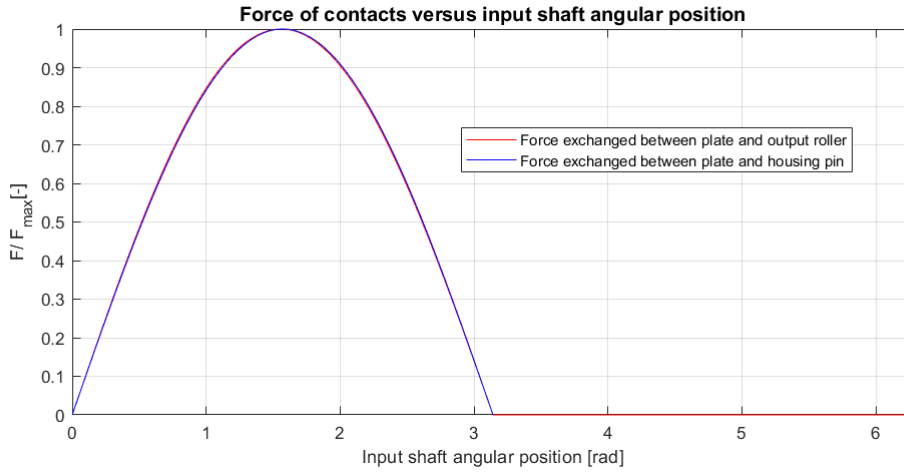


Figure 3.7: Forces of contacts versus input shaft rotation angle

3.3 Torques distribution

In order to obtain the relationship to estimate $F_{max,k}$, a balance of torques acting on the cycloidal disk should be introduced. Referring to figure 3.6, we should observe that:

1. The normal force of contact between the cycloidal disk and the output pins is acting along the direction of the segment AP applied at the point of contact A;
2. The normal force of contact between the cycloidal disk and the output rollers is directed along the direction of the segment O_1N .

The value of the real central disc's torque could be expressed by:

$$\vec{T}_2 = \sum_{i=1}^{z_2/2} \left(\vec{O_1A} \times F_{N,i} \frac{\vec{AP}}{\|\vec{AP}\|} \right) \cdot \vec{Z} \quad (3.20)$$

Where \vec{Z} is the versor normal to the plane which contains $X_1O_1Y_1$ and X_0OY_0 . Moreover:

$$\frac{\vec{AP}}{\|\vec{AP}\|} = -\frac{1}{\|\vec{AP}\|} \begin{bmatrix} r_2 - r_c \frac{\frac{r_2}{Q} - \cos \psi}{\sqrt{1 + \left(\frac{r_2}{Q}\right)^2 - 2\frac{r_2}{Q} \cos \psi}} - Q \cos \psi \\ r_c \frac{\sin \psi}{\sqrt{1 + \left(\frac{r_2}{Q}\right)^2 - 2\frac{r_2}{Q} \cos \psi}} - Q \sin \psi \\ 0 \end{bmatrix} \quad (3.21)$$

$$\vec{O_1A} = \vec{O_1P} + \vec{PA} = \begin{bmatrix} r_2 - r_c \frac{\frac{r_2}{Q} - \cos \psi}{\sqrt{1 + \left(\frac{r_2}{Q}\right)^2 - 2\frac{r_2}{Q} \cos \psi}} - e \cos \psi \\ r_c \frac{\sin \psi}{\sqrt{1 + \left(\frac{r_2}{Q}\right)^2 - 2\frac{r_2}{Q} \cos \psi}} - e \sin \psi \\ 0 \end{bmatrix} \quad (3.22)$$

Finally ([3]):

$$T_2 = r_2^2 F_{max,N} \sum_{i=1}^{z_2/2} \left(1 - \frac{e}{Q}\right) \int_{\psi_{2(i-1)}}^{\psi_{2i}} \frac{\sin^2 \psi_{2j}}{\|\vec{AP}\|} \left(\frac{r_c}{\sqrt{1 + \left(\frac{r_2}{Q}\right)^2 - 2\frac{r_2}{Q} \cos \psi} - 1} \right) d\psi \quad (3.23)$$

In the end, we have got a mathematical expression for the normal forces of contact between the cycloidal disk and the output rollers and between the housing pins and the cycloidal disc. Moreover, it has been proposed a theoretical direct way to find the maximum values of the exchanged forces without recalling the dynamic laws. Anyways, in simulations we are going to get these values from solving the dynamic problem. The approach above shows the most impacting geometrical features that have strict influence on the maximum values of exchanged forces.

3.4 Main dynamic equations derived from analytical mechanics

We are going to apply the dynamic principles in the form of analytical mechanics. Therefore, no elastic properties are introduced in dynamics, or better, we are going to admit that the values of the acting forces do not involve any deformations and these do not affect the efficiency and the overall dynamics of the reducer. We should remind that $X_1O_1Y_1$ is the mobile reference system, while X_0OY_0 is the fixed one. Then, the reference system $X_1O_1Y_1$ is clearly not inertial, while the reference system X_0OY_0 - because of being fixed- is undoubtedly inertial.

As the fundamentals of analytic mechanics suggest, the first step consists in writing the kinematic torsor of the cycloidal plate referring to X_0OY_0 :

$$\{C_{C_y/R_0}\} = \left\{ e\dot{\varphi}\vec{Y}_1 \mid -\frac{\dot{\varphi}}{z_1}\vec{Z} \right\}_{X_0OY_0} \quad (3.24)$$

The mathematical formulation explains how the cycloidal plate is moving on the plane where its motions is included.

So the cycloidal plate - moving with the reference system $X_1O_1Y_1$ - is revolving around the centre O_1 at a speed, that in steady state, is the output nominal speed of the reducer. Moreover, the point O_1 is revolving around the fixed point O at a speed that in steady state is the input speed. So, the kinematic torsor contains all these information about the motion of the cycloidal plate.

With the kinematic torsor, the dynamic torsor of the cycloidal plate could be written -through the mathematical derivative of the kinematic torsor adding the contribution of the inertia (mass and moment of inertia) of the cycloidal disc- :

$$\{D_{C_y/R_0}\} = \left\{ -m_{cy}e\dot{\varphi}^2\vec{X}_1 + m_{cy}e\ddot{\varphi}\vec{Y}_1 \mid -\frac{I_{zz}}{z_1}\ddot{\varphi}\vec{Z} \right\}_{X_1O_1Y_1} \quad (3.25)$$

Where m_{cy} is the mass of the cycloidal plate, while I_{zz} is its moment of inertia referred to the rotation axis \vec{Z} . Nevertheless, despite the mathematical derivation of the torsors above, in order to understand fully the dynamics, a physical analysis should be introduced:

1. $-m_{cy}e\dot{\varphi}^2\vec{X}_1$ may be interpreted as the dynamic force linked to the centripetal acceleration and its inertia to this kind of motion;
2. $m_{cy}e\ddot{\varphi}\vec{Y}_1$ may be interpreted as the dynamic force linked to the tangential acceleration and its inertia to this kind of motion;
3. $-\frac{I_{zz}}{z_1}\ddot{\varphi}\vec{Z}$ may be interpreted as the dynamic torque linked to angular acceleration of the disc and its inertia to this kind of motion.

Once the dynamic torsor of the cycloidal disk is defined, the main dynamic interactions between the cycloidal wheel and the other bodies could be analyzed. In the previous sections the dynamics of the exchanged forces has been kept into account. Then, in order to model the forces exchanged between the input shaft and the cycloidal plate, we should take into account the balance on the input shaft coupling - through the bearing - with the cycloidal plate. By applying the balance, it is consequential to admit that the exchanged force can be broken up into two components along \vec{X}_1 and \vec{Y}_1 . The point of application of these components is placed on the centre of the input shaft O , so- due to this shifting in action point of the \vec{Y}_1 component- we must have also a torque exchanged between the input shaft and cycloidal disc. This must be considered the input torque entering in the reducer. Then:

$$\{E_{C_y/R_0}\} = \left\{ E_x \vec{X}_1 + \text{sgn}(\omega_0)(1 - \mu_E) E_y \vec{Y}_1 \mid (1 - \mu_E) E_y e \vec{Z} \right\}_{X_0 O Y_0} \quad (3.26)$$

Where:

1. E_x is the X_1 -component of constraint force that is not involving any torque on the cycloidal disc;
2. $E_y(1 - \mu_E)$ is the Y_1 -component of constraint force, decreased by the value of the friction force. This component is involving torque on the cycloidal disc (input torque);
3. $(1 - \mu_E) E_y e$ is the input torque exchanged between cycloidal disc and input shaft.

Besides, the action of the housing pins on the cycloidal disc is analysed. Since the analysis of the previous sections, we know that there is a particular distribution of acting forces on cycloidal disc due to the contact with the housing pins. It is clear that half of the pins are loaded, the others are not exchanging forces. Moreover, it is demonstrated that this kind of interaction involves a factor of amplitude that - at this stage- is introduced in the equations as K_c . Then, for each instant we should sum all the coupling force exchanged with each pins, in such way we get \vec{C}_{O_i} that can be broken up in the two components along \vec{X}_1 and \vec{Y}_1 . So we can write the torsor in the moving reference system $X_1 O Y_1$ (where i stays for the i -th pin):

$$\{O_{C_y/R_0}\} = \left\{ \vec{C}_{O_i} = K_c \sum_i C_{X_i} \vec{X}_1 + K_c \sum_i C_{Y_i} \vec{Y}_1 \mid 0 \vec{Z} \right\}_{X_1 O_1 Y_1} \quad (3.27)$$

In order to apply the fundamental dynamic laws, the torsor must be referred to the inertial reference system $X_0 O Y_0$:

$$\{O_{C_y/R_0}\} = \left\{ \vec{C}_{O_i} = K_c \sum_i C_{X_i} \vec{X}_1 + K_c \sum_i C_{Y_i} \vec{Y}_1 \mid \sum_i (\vec{O A}_i \times \vec{C}_{O_i}) \right\}_{X_0 O Y_0} \quad (3.28)$$

In fact, we should add - as equation 3.28 shows- the torque around O introduced by the distribution of forces linked to the contact with housing pins. By solving the expression of torque, we will get:

$$\{O_{C_y/R_0}\} = \left\{ \overrightarrow{C_{O_i}} = K_c \sum_i C_{X_i} \overrightarrow{X_1} + K_c \sum_i C_{Y_i} \overrightarrow{Y_1} \mid \sum_i K_c M_{C_i} \overrightarrow{Z} \right\}_{X_0 O Y_0} \quad (3.29)$$

Lastly, the focus should be for the action of the output rollers on the cycloidal disk. Also in this case, the previous discussion about the distribution of coupling forces between cycloidal plate and output rollers, allows to introduce the factor of amplitude K_s . In the same way, the torsor of this action related to $X_1 O Y_1$ can be written as (where j stays for the j -th pin):

$$\{O_{S_y/R_0}\} = \left\{ \overrightarrow{S_{O_j}} = K_s \sum_j S_{X_j} \overrightarrow{X_1} + K_s \sum_j S_{Y_j} \overrightarrow{Y_1} \mid 0 \overrightarrow{Z} \right\}_{X_1 O_1 Y_1} \quad (3.30)$$

For the same reason, we refer the torsor to the reference system $X_0 O Y_0$:

$$\{O_{S_y/R_0}\} = \left\{ \overrightarrow{S_{O_j}} = K_s \sum_j S_{X_j} \overrightarrow{X_1} + K_s \sum_j S_{Y_j} \overrightarrow{Y_1} \mid \sum_j \left(K_s \overrightarrow{O S_j} \times \overrightarrow{S_{O_j}} \right) \right\}_{X_0 O Y_0} \quad (3.31)$$

$$\{O_{S_y/R_0}\} = \left\{ \overrightarrow{S_{O_j}} = K_c \sum_j S_{X_j} \overrightarrow{X_1} + K_c \mu_s \sum_j S_{x_j} \overrightarrow{Y_1} \mid K_s \sum_i M_{s_j} \overrightarrow{Z} \right\}_{X_0 O Y_0} \quad (3.32)$$

After introducing all the interactions through the torsor, it is possible to explain in detail the forces at work on the cycloidal disk. In the main equations there are two coefficients K_c and K_s that are strictly linked to the maximum value of the forces exchanged - coming from $F_{max,N}$ and $F_{max,k}$ of equations (3.15) and (3.16)-, while K_s can be obtained by the balance on the output shaft, K_c is unknown parameter determinable after solving the dynamic problem. The terms inside the sums are tied to the geometrical distribution of forces.

The idea of introducing the torsor's formulation comes from the issue to define in a strict and incisive way the interactions.

With the contact forces on the cycloidal disc, it is the time to apply the fundamental principles of dynamics: it is possible to have two different and alternative formulations, the Lagrange-Euler equation or the virtual work principle.

The starting step is to individuate the Lagrangian generalized coordinates able to make us describe the plate's motion. These must be linearly independent: the cycloidal plate is a rigid body moving on a plane. So x_1, y_1 (coordinates of the position of O_1 referring to $X_0 O Y_0$) and θ_Z (angular rotation around θ_{etaZ}) are the generalized coordinates of this dynamic problem applied on cycloidal plate. The main equations of Euler-Lagrange is well-known:

$$\frac{d}{dt} \frac{\partial \mathcal{L}}{\partial \dot{q}_k} - \frac{\partial \mathcal{L}}{\partial q_k} = Q_k \quad \text{with } k = 1, 2, 3 \quad (3.33)$$

Where $q_1 = x_1$, $q_2 = y_1$ and $q_3 = \theta_Z$, while \mathcal{L} is the Lagrangian of the system (cycloidal plate) and Q_k is due to the interactions of cycloidal plate with the other bodies (housing pins, input shaft, output rollers). As it is well-know, the Lagrangian \mathcal{L} could be obtained by summing the kinetic energy and the potential energy linked to the possible conservative forces acting. Afterwards, it is immediate to write the Lagrangian of the cycloidal disk because of its consisting only on kinetic energy of a rigid body translating and rotating on a plane:

$$\mathcal{L} = T - V = T = \frac{1}{2}m_{cy}\dot{x}_1^2 + \frac{1}{2}m_{cy}\dot{y}_1^2 + \frac{1}{2}I_{zz}\dot{\theta}_Z^2 \quad (3.34)$$

Then:

$$\frac{d}{dt} \frac{\partial \mathcal{L}}{\partial \dot{q}_1} = \frac{d}{dt} \frac{\partial \mathcal{L}}{\partial \dot{x}_1} = m_{cy}\ddot{x}_1 \quad (3.35)$$

$$\frac{d}{dt} \frac{\partial \mathcal{L}}{\partial \dot{q}_2} = \frac{d}{dt} \frac{\partial \mathcal{L}}{\partial \dot{y}_1} = m_{cy}\ddot{y}_1 \quad (3.36)$$

$$\frac{d}{dt} \frac{\partial \mathcal{L}}{\partial \dot{q}_3} = \frac{d}{dt} \frac{\partial \mathcal{L}}{\partial \dot{\theta}_Z} = I_{zz}\ddot{\theta}_Z \quad (3.37)$$

While:

$$\frac{\partial \mathcal{L}}{\partial q_1} = \frac{\partial \mathcal{L}}{\partial x_1} = 0 \quad (3.38)$$

$$\frac{\partial \mathcal{L}}{\partial q_2} = \frac{\partial \mathcal{L}}{\partial y_1} = 0 \quad (3.39)$$

$$\frac{\partial \mathcal{L}}{\partial q_3} = \frac{\partial \mathcal{L}}{\partial \theta_Z} = 0 \quad (3.40)$$

We are going to evaluate Q_1 , Q_2 and Q_3 :

$$\delta \vec{r}_k = \delta x_1 \vec{X}_1 + \delta y_1 \vec{Y}_1 + \delta \theta_Z \vec{Z} \quad (3.41)$$

$$Q_1 = \sum_{k=1}^N \vec{F}_{nc,k} \cdot \frac{\partial \vec{r}_k}{\partial q_1} = \sum_{k=1}^N \vec{F}_{nc,k} \cdot \vec{X}_1 \quad (3.42)$$

$$Q_1 = \sum_{k=1}^N \vec{F}_{nc,k} \cdot \vec{X}_1 = K_c \sum_i C_{X,i} + K_s \sum_j S_{X,j} + E_x \quad (3.43)$$

$$Q_2 = \sum_{k=1}^N \vec{F}_{nc,k} \cdot \frac{\partial \vec{r}_k}{\partial q_2} = \sum_{k=1}^N \vec{F}_{nc,k} \cdot \vec{Y}_1 \quad (3.44)$$

$$Q_2 = \sum_{k=1}^N \vec{F}_{nc,k} \cdot \vec{Y}_1 = K_c \sum_i C_{Y,i} + K_s \mu_s \sum_j S_{X,j} + (1-E)E_y \quad (3.45)$$

$$Q_3 = \sum_{k=1}^N \overrightarrow{F_{nc,k}} \cdot \frac{\partial \overrightarrow{r}_k}{\partial q_3} = \sum_{k=1}^N \overrightarrow{F_{nc,k}} \cdot \overrightarrow{Z} \quad (3.46)$$

$$Q_3 = \sum_{k=1}^N \overrightarrow{F_{nc,k}} \cdot \overrightarrow{Z} = K_c \sum_i M_{C,i} + K_s \sum_j M_{S,j} + e(1-E)E_y \quad (3.47)$$

The following kinematic relationship hold:

$$\begin{cases} \ddot{x}_1 = -e\dot{\varphi}^2 \\ \ddot{y}_1 = e\ddot{\varphi} \\ \theta_Z = \frac{\varphi}{z_1} \end{cases} \quad (3.48)$$

The first two equations of (3.48) describe the particular motion of the point O_1 around O (not uniform circular motion generally). The last one is the equation of the gear ratio between the input angular position and the output angular position. Then, the following equations are the final result:

$$\begin{cases} K_c \sum_i C_{X_i} + K_s \sum_j S_{X_j} + E_x + m_{cy}e\dot{\varphi}^2 = 0 \\ K_c \sum_i C_{y_i} + K_s \mu_s \sum_j S_{X_j} + E_y(1 - \mu_E) - m_{cy}e\ddot{\varphi} = 0 \\ K_c \sum_i M_{C_i} + K_s \mu_s \sum_j M_{S_j} + E_y e(1 - \mu_E) + \frac{I_{zz}}{z_1} \ddot{\varphi} = 0 \end{cases} \quad (3.49)$$

The same equations could be obtained starting off by the torsor's formulation in order to apply the virtual work principle for each linearly independent directions. It is renowned that the Lagrangian-Euler equation is equivalent to the virtual work principle.

Along the \overrightarrow{X}_1 direction:

$$\sum \left(\overrightarrow{F} \cdot \delta \overrightarrow{X}_1 \right) = 0 \quad (3.50)$$

$$K_c \sum_i C_{X_i} + K_s \sum_j S_{X_j} + E_x + m_{cy}e\dot{\varphi}^2 = 0 \quad (3.51)$$

Along the \overrightarrow{Y}_1 we are going to have:

$$\sum \left(\overrightarrow{F} \cdot \delta \overrightarrow{Y}_1 \right) = 0 \quad (3.52)$$

$$K_c \sum_i C_{y_i} + K_s \mu_s \sum_j S_{X_j} + E_y(1 - \mu_E) - m_{cy}e\ddot{\varphi} = 0 \quad (3.53)$$

Regarding the balance to the rotation around the axis \overrightarrow{Z}

$$\sum \left(\overrightarrow{M}_Z \cdot \delta \theta_Z \right) = 0 \quad (3.54)$$

$$K_c \sum_i M_{C_i} + K_s \mu_s \sum_j M_{S_j} + E_y e(1 - \mu_E) + \frac{I_{zz}}{z_1} \ddot{\varphi} = 0 \quad (3.55)$$

Finally, we have a system of equations:

$$\begin{cases} K_c \sum_i C_{X_i} + K_s \sum_j S_{X_j} + E_x + m_{cy} e \dot{\varphi}^2 = 0 \\ K_c \sum_i C_{y_i} + K_s \mu_s \sum_j S_{X_j} + E_y(1 - \mu_E) - m_{cy} e \ddot{\varphi} = 0 \\ K_c \sum_i M_{C_i} + K_s \mu_s \sum_j M_{S_j} + E_y e(1 - \mu_E) + \frac{I_{zz}}{z_1} \ddot{\varphi} = 0 \end{cases} \quad (3.56)$$

This dynamic problem can not be resolved because the number of unknown parameters (E_x , E_y , K_c , K_s , φ and their first and second derivatives) is bigger than the number of equations. Anyway, we may apply the virtual work principle to the input shaft:

$$\sum \left(\vec{M}_Z \cdot \delta \vec{\theta}_Z \right) = 0 \quad (3.57)$$

$$K_s \sum_i M_{s_j} \vec{Z} - \frac{I_{zzOS}}{z_1} \ddot{\varphi} \vec{Z} + C_s \vec{Z} = 0 \quad (3.58)$$

Where I_{zzOS} is the moment of inertia of the output shaft, while C_s is the constant output load imposed on the output shaft. Then:

$$\begin{cases} K_c \sum_i C_{X_i} + K_s \sum_j S_{X_j} + E_x + m_{cy} e \dot{\varphi}^2 = 0 \\ K_c \sum_i C_{y_i} + K_s \mu_s \sum_j S_{X_j} + E_y(1 - \mu_E) - m_{cy} e \ddot{\varphi} = 0 \\ K_c \sum_i M_{C_i} + K_s \mu_s \sum_j M_{S_j} + E_y e(1 - \mu_E) + \frac{I_{zz}}{z_1} \ddot{\varphi} = 0 \\ K_s \sum_j M_{s_j} - \frac{I_{zzOS}}{z_1} \ddot{\varphi} - C_s = 0 \end{cases} \quad (3.59)$$

By now, the dynamic problem is still not solvable because the larger number of unknown variables (five) in comparison with the equations (four). The main aim of this dynamic analysis is to simulate the real working condition of the cycloidal reducer at the test bench. Then, the measurements are taken in a steady state to estimate the efficiency.

At that point the hypothesis of steady state for the input are proposed, this allows to write the following relationships:

$$\ddot{\varphi}(t) = 0; \quad \dot{\varphi}(t) = \omega_0 \quad (3.60)$$

Consequently:

$$\begin{cases} K_c \sum_i C_{X_i} + K_s \sum_j S_{X_j} + E_x + m_{cy} e \omega_0^2 = 0 \\ K_c \sum_i C_{y_i} + K_s \mu_s \sum_j S_{X_j} + E_y(1 - \mu_E) = 0 \\ K_c \sum_i M_{C_i} + K_s \mu_s \sum_j M_{S_j} + E_y e(1 - \mu_E) = 0 \\ K_s \sum_j M_{s_j} - C_s = 0 \end{cases} \quad (3.61)$$

The first three equations of the system (3.61):

$$K_c \sum_i C_{X_i} + K_s \sum_j S_{X_j} + E_x + m_{cy} e \omega_0^2 = 0 \quad (3.62)$$

$$K_c \sum_i C_{y_i} + K_s \mu_s \sum_j S_{X_j} + E_y (1 - \mu_E) = 0 \quad (3.63)$$

$$K_c \sum_i M_{C_i} + K_s \mu_s \sum_j M_{S_j} + E_y e (1 - \mu_E) = 0 \quad (3.64)$$

It can be reduced to an algebraical system in the form:

$$\begin{pmatrix} \sum_i C_{X_i} & 1 & 0 \\ \sum_i C_{Y_i} & 0 & 1 - \mu_E \\ \sum_i M_{C_i} & 0 & (1 - \mu_E)e \end{pmatrix} \begin{bmatrix} K_c \\ E_x \\ E_y \end{bmatrix} = \begin{bmatrix} -m_{cy} e \omega_0^2 - K_s \sum_j S_{X_j} \\ -K_s \mu_s \sum_j S_{X_j} \\ K_s \sum_j M_{S_j} \end{bmatrix} \quad (3.65)$$

We can evaluate E_y analytically by using Cramer's rule, then:

$$E_y = \frac{\det \begin{pmatrix} \sum_i C_{Y_i} & -K_s \mu_s \sum_j S_{X_j} \\ \sum_i M_{C_i} & K_s \sum_j M_{S_j} \end{pmatrix}}{\det \begin{pmatrix} \sum_i C_{Y_i} & 1 - \mu_E \\ \sum_i M_{C_i} & (1 - \mu_E)e \end{pmatrix}} \quad (3.66)$$

$$E_y = \frac{K_s \left(\sum_i C_{Y_i} \sum_j M_{S_j} + \mu_s \sum_j S_{X_j} \sum_i M_{C_i} \right)}{\left(\sum_i C_{Y_i} e - \sum_i M_{C_i} \right) (1 - \mu_E)} \quad (3.67)$$

We can also add the main equation of torque balance acting on output shaft, where C_S is the output torque (T_{out}), and we can add the analytic solution of the system to get the input torque (T_{in}):

$$T_{out} = C_S = K_s \sum_j M_{S_j} \quad (3.68)$$

$$\vec{T}_{in} = \left(E_y (1 - \mu_E) \vec{Y}_1 \right) \times \left(e \vec{X}_1 \right) \quad (3.69)$$

$$\vec{T}_{in} = E_y (1 - \mu_E) e \vec{Z} \quad (3.70)$$

$$T_{in} = E_y (1 - \mu_E) e \quad (3.71)$$

$$T_{in} = K_s e \frac{\sum_i C_{Y_i} \sum_j M_{S_j} + \mu_s \sum_j S_{X_j} \sum_i M_{C_i}}{\sum_i C_{Y_i} e - \sum_i M_{C_i}} \quad (3.72)$$

So with these elements we can evaluate the instantaneous efficiency of gearbox transmission:

$$\eta = \frac{T_{out} \omega_{out}}{T_{in} \omega_{in}} \quad (3.73)$$

$$\frac{\omega_{out}}{\omega_{in}} = \frac{1}{z_1} \quad (3.74)$$

$$\eta = \frac{T_{out}}{T_{in}} \frac{1}{z_1} \quad (3.75)$$

$$\eta = \frac{K_s \sum_j M_{S_j}}{e E_y (1 - \mu_E)} \frac{1}{z_1} \quad (3.76)$$

$$\eta = \frac{\sum_j M_{S_j} \left(\sum_i C_{Y_i} e - \sum_i M_{c_i} \right)}{e z_1 \left(\sum_i C_{Y_i} \sum_j M_{s_j} + \mu_s \sum_j S_{X_j} \sum_i M_{c_i} \right)} \quad (3.77)$$

Then, we are going to simulate a working condition in which the input speed and the output load are imposed, the output speed is determined by the gear ratio and, finally, the input torque is obtained by solving the dynamic problem. This operating condition is comparable with the working state reproduced through the test's bench. Moreover - as the equation 3.77 shows - with the hypothesis of rigid bodies the efficiency does not depend on the constant output load (whose factor of amplitude is K_s). For this main reason we should focus on other mathematical models.

3.5 Main dynamic equations derived from Newton method

Even if the analytic method is extremely concise, proposing also briefly the Newton method could allow to achieve a better comprehension of the dynamic behaviour of the reducer, seeing the acting forces in free body diagram. We are going to propose the Newton's method applied to the cycloidal disk with the main hypotheses of the rigid bodies model. Then, this approach is alternative to the analytic mechanics.

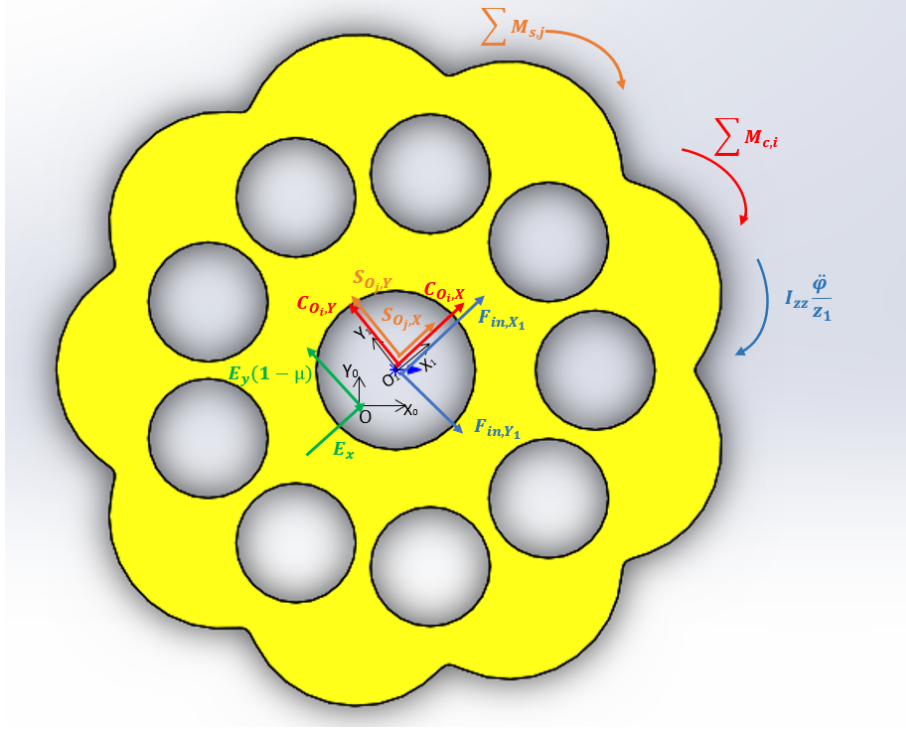


Figure 3.8: Free-body diagram of cycloidal disk with the applied forces and torques (rigid bodies model)

According to figure 3.8, writing the relative acceleration formula is immediate:

$$\vec{a}_{O_1} = \vec{a}_O + \vec{a}_{O_1/O,n} + \vec{a}_{O_1/O,t} \quad (3.78)$$

Where:

1. \vec{a}_{O_1} is the absolute acceleration of the point O_1 - centre of the moving reference system $X_1O_1Y_1$;
2. \vec{a}_O is the absolute acceleration of the point O - centre of the fixed reference system X_0OY_0 . It is clear that $\vec{a}_O = \vec{0}$;
3. $\vec{a}_{O_1/O,n}$ is the normal acceleration of the point O_1 related to X_0OY_0 ;
4. $\vec{a}_{O_1/O,t}$ is the tangential acceleration of the point O_1 related to X_0OY_0 .

Moreover, It is well-known that the point O_1 is moving along a circumference of radius e and centre in O . Since knowing that and referring to the bases of $X_1O_1Y_1$, we get:

$$\vec{a}_{O_1} = -e\dot{\varphi}^2 \vec{X}_1 + e\ddot{\varphi} \vec{Y}_1 \quad (3.79)$$

With the acceleration of point O_1 , we can get the inertial force applied to the disc relating all the dynamic equations to the movable (and not inertial) reference system $X_1O_1Y_1$. Then:

$$\vec{F}_{in} = -m_{cy}\vec{a}_{O_1} = m_{cy}e\dot{\varphi}^2 \vec{X}_1 - m_{cy}e\ddot{\varphi} \vec{Y}_1 = -F_{in,X_1} \vec{X}_1 + F_{in,Y_1} \vec{Y}_1 \quad (3.80)$$

After getting the inertial forces acting on the cycloidal disk with the purpose to refer the dynamic equations to $X_1O_1Y_1$, the focus should be for the coupling forces exchanged with cycloidal disk with others bodies. Referring to the figure 3.8, we have:

1. $C_{O_i,X}$ and $C_{O_i,Y}$, that are the axis components of the resultant of the forces exchanged between the housing pins and the cycloidal disc -at one time-;
2. $S_{O_j,X}$ and $S_{O_j,Y}$, that are the axis components of the resultant of the forces exchanged between the output rollers and the cycloidal disc -at one time-;
3. E_X and $E_y(1 - \mu_E)$, that are the axis components of the resultant force exchanged between the input shaft and the cycloidal disc -at one time-;
4. $K_c \sum_i M_{c,i}$, that is the torque - related to O_1 - imposed by the distribution of forces exchanged between the housing pins and the cycloidal disc -at one time-;
5. $K_c \sum_j M_{s,j}$, that is the torque - related to O_1 - imposed by the distribution of forces exchanged between the output rollers and the cycloidal disc -at one time-;
6. $I_{zz} \frac{\ddot{\varphi}}{z_1}$, that is the torque linked to the plate's moment of inertia.

By applying the balance of forces in the two independent directions- \vec{X}_1 and \vec{Y}_1 - and the balance of the overall torques acting on a point O_1 about the axis \vec{Z} , we get the same equations as before.

Chapter 4

Experimentation on dynamic behaviour and on performances

In this chapter we focus on the methodology of the experimental part of this work. We should point out that the following measurements are coming from the Lodz's test bench, the main part of the experimentation were made in partnership between SUPMECA and University of Lodz. Anyway, we have got acquainted with a similar experimental bench provided by PSA. Moreover, the experimental analysis has a cardinal role in the following modelling and computational works, for this reason, we concentrate on the main outcomes of the measurements. The last part of this chapter is dedicated to the results of simulations of the previous rigid bodies model in order to check if there is overlapping between previsions and experimentation and which parts of the mathematical model must be developed to adapt the modelling to the experimentation.

4.1 Test Bench

A two discs drive was used in this research work (figures 4.1,4.2,4.3,4.4). Each disc has 19 teeth (z_1) and cooperates with housing equipped in 20 teeth(z_2). In this case the total ratio of the gear is:

$$i = \frac{\omega_{in}}{\omega_{out}} = \frac{z_1}{z_2 - z_1} = 19 \quad (4.1)$$

The main parameters of the cycloidal reducer are presented in the following table:

Table 4.1: Basic data of the tested cyclo gearbox

Rotational speed of input shaft	1500	rpm
Power	7,5	kW
Gear box ratio	19	-

In order to increase the gearbox efficiency brass washer were introduced. It lowers the friction between the parts.



Figure 4.1: Tested cycloidal drive: cyclo gearbox



Figure 4.2: Tested cycloidal drive: cycloidal plate

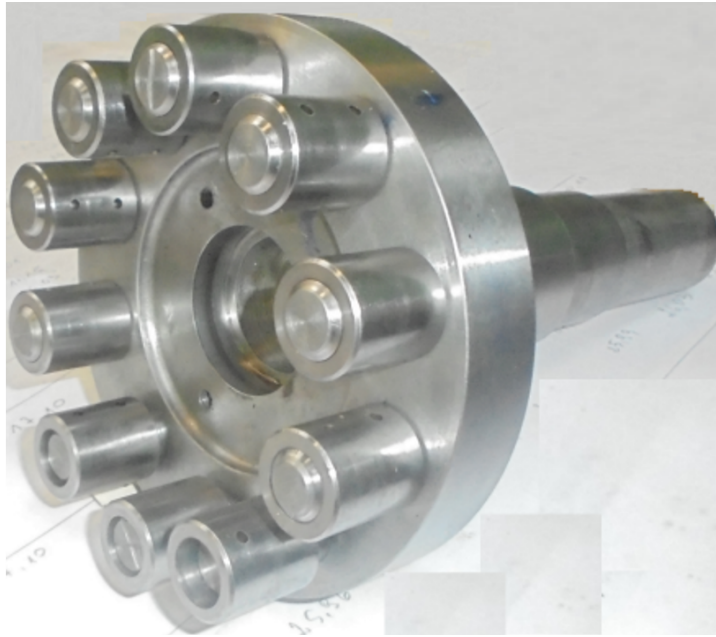


Figure 4.3: Tested cycloidal drive: output shaft and output rollers



Figure 4.4: Tested cycloidal drive: housing with pins

The cycloid drive was tested on the bench assembled at AML (figure 4.5).

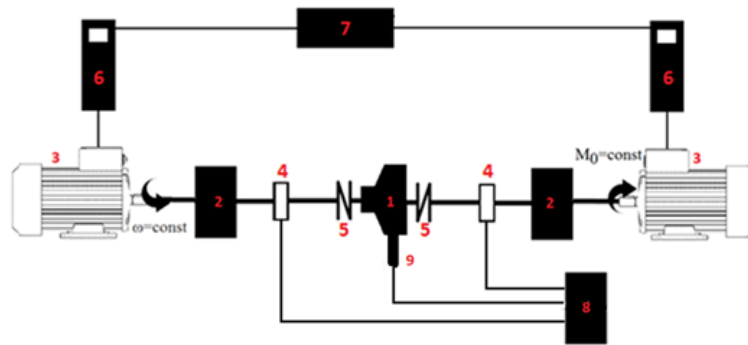


Figure 4.5: 1-cycloidal gearbox, 2-planetary gear set, 3-electric motor, 4-torque and speed meters, 5-clutch (Radex N50), 6-inverters, 7-inverter control system, 8-data acquisition system, 9-oil temperature sensor

The test rig consists of:

1. Two electrical motors “3” (200 kW each), which can operate as motor or generator. The common DC voltage cable allows the transmission of electrical energy from the generator to the engine. In this way, the external power supply is charged only to cover energy losses much smaller than appear in the working drive system.
2. Two ABB frequency converters “5”, which in the power supply has the rectifier bridge and input filter to reduce harmonic distortion from an external power supply.
3. The CPU “7” (Fig. 3.), which allows to plan and execute an experiment. Changing the parameters of electrical machines can be realized by step, trapezoidal or sinusoidal function. A limitation of electrical parameters are: frequency converters and motors “3”.

4. The CPU “8”, to capture, archive and process data from the test bench. This unit operates separately from the CPU “7” to prevent mutual interference and increase safety.
5. An oil cooling system were used to keep the desired temperature inside the cycloid housing.
6. The oil temperature sensor were mounted at the bottom of the cycloid gear housing. It allows for observation of oil average temperature during bench operation.

In order to reduce the vibration of test rig components, a set of laser sensors “Shaf-tAlign” made by Prüftechnik was used to coaxial setting of all shafts and clutches in the drive line. After reaching the required accuracy in setting the cooperating connections, the test can be started. The control system “7” allows to set up the speed on the input shaft and the torque on the output shaft. So when the torque increased at the braking side, the speed was kept at the constant level. Conversely, if the speed increased, the torque on the braking unit could be constant. Of course during transient conditions, the torque and speed can vary due to the moment of inertia.

The measurement system consists of:

1. Two torque and speed sensors HBM T40b, which were mounted on the input and output shaft of the cycloidal gearbox.
2. Temperature sensor which measure the oil temperature in the gearbox.

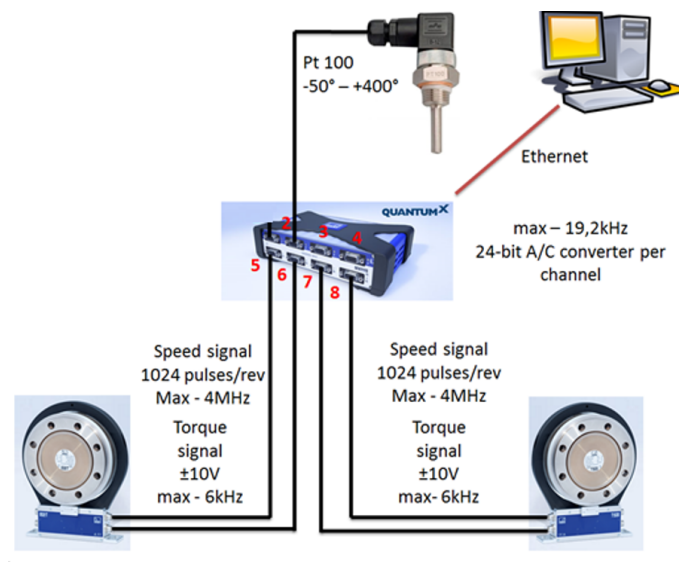


Figure 4.6: Data acquisition system

A schematic view of the data acquisition hardware is shown in figure 4.6.

4.2 Methodology and results

Tests were carried out at constant torque on the output shaft of the tested gear. The speed increased from 0 *rpm* to the maximum value was kept constant for 20 *s* and then decreased to 0 *rpm* again. A sample of acquired data is shown on the figure 4.7.

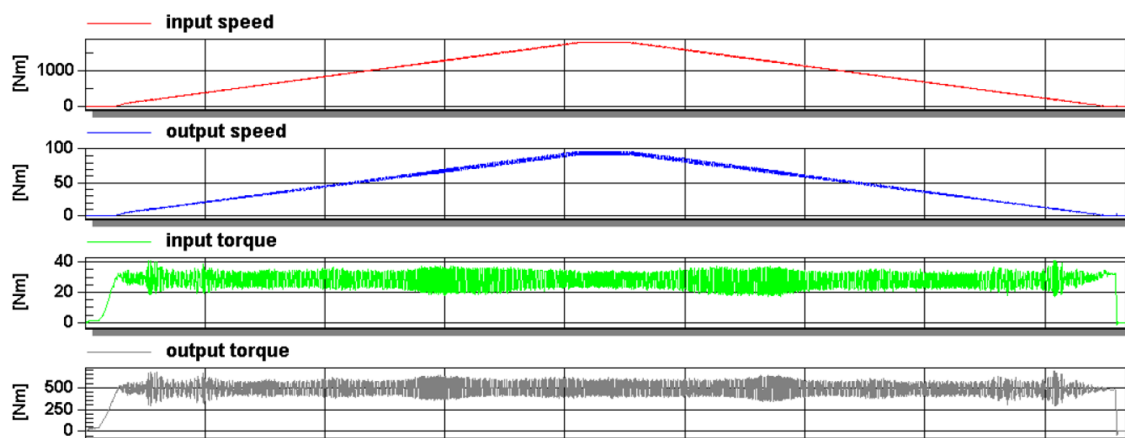


Figure 4.7: A sample of measured signals

The torques and speed values acquired during these 20 *s* were averaged. The archived values were used to calculate the instant efficiency according to the formula:

$$\eta = \frac{T_{out} \omega_{out}}{T_{in} \omega_{in}} \quad (4.2)$$

The viscosity of the oil was checked on a separate test bench before and after the test.

We report the detailed experimental data obtained at the input speed of 1200 *rpm* to give an example of the most relevant measures (directly measured and indirectly obtained) that we have focused on:

Table 4.2: Measurements at 1200 rpm

viscosity	oil temp.	n_{in}	n_{out}	speed ratio	T_{in}	T_{out}	η
mm^2/s	$^{\circ}C$	<i>rpm</i>	<i>rpm</i>	-	<i>Nm</i>	<i>Nm</i>	-
41,1	34,4	1202,0	63,2	19,01	2,99	29,8	0,52
39,8	35,2	1202,0	63,2	19,01	5,99	82,7	0,73
43,9	32,8	1199,0	63,1	19,00	8,71	126,9	0,77
42,1	33,8	1202,0	63,2	19,01	11,41	173,7	0,80
42,3	33,7	1202,0	63,2	19,01	13,86	222,2	0,84
41,5	34,1	1202,0	63,2	19,01	16,35	268,0	0,86
41,0	34,4	1202,0	63,2	19,01	18,82	313,9	0,88
39,3	35,5	1202,0	63,2	19,01	21,31	355,8	0,88
40,1	35,0	1202,0	63,2	19,01	23,54	400,7	0,90
39,4	35,4	1202,0	63,2	19,01	26,28	449,2	0,90

The data for input speed as equal to 1000 rpm:

Table 4.3: Measurements at 1000 rpm

viscosity	oil temp.	n_{in}	n_{out}	speed ratio	T_{in}	T_{out}	η
mm^2/s	$^{\circ}C$	<i>rpm</i>	<i>rpm</i>	-	<i>Nm</i>	<i>Nm</i>	-
42,1	33,	1001	52,7	19,00	3,01	30,7	0,54
41,1	34,4	1001	52,7	19,00	6,11	83,2	0,72
44,4	32,5	1001	52,7	19,00	9,02	131,9	0,77
45,0	32,1	1001	52,7	19,00	11,45	178,9	0,82
44,1	32,6	1001	52,7	19,00	13,70	219,8	0,84
44,2	32,6	1001	52,7	19,00	16,66	271,1	0,86
43,0	33,3	1001	52,7	19,00	19,07	316,9	0,87
42,2	33,7	1001	52,7	19,00	21,58	361,9	0,88
42,0	33,9	1001	52,7	19,00	24,14	408,2	0,89
41,9	33,9	1001	52,7	19,00	26,67	450,5	0,89

4.3 Processing of experimental data

We are going to analyze the experimental data coming from the measurements taken at the test bench: it should be noted that the data taken are more than the quantities (speed and torque) used to evaluate the efficiency: we are focusing only on the data absolutely necessary to evaluate the efficiency.

The measurements got through the test bench, have been taken at different input speeds set by the inverters of the control system. This is motivated by the interest in discovering whether the dynamic behaviour is changing with varying the input speed. All information are summarized in the graphic of the figure 4.8.

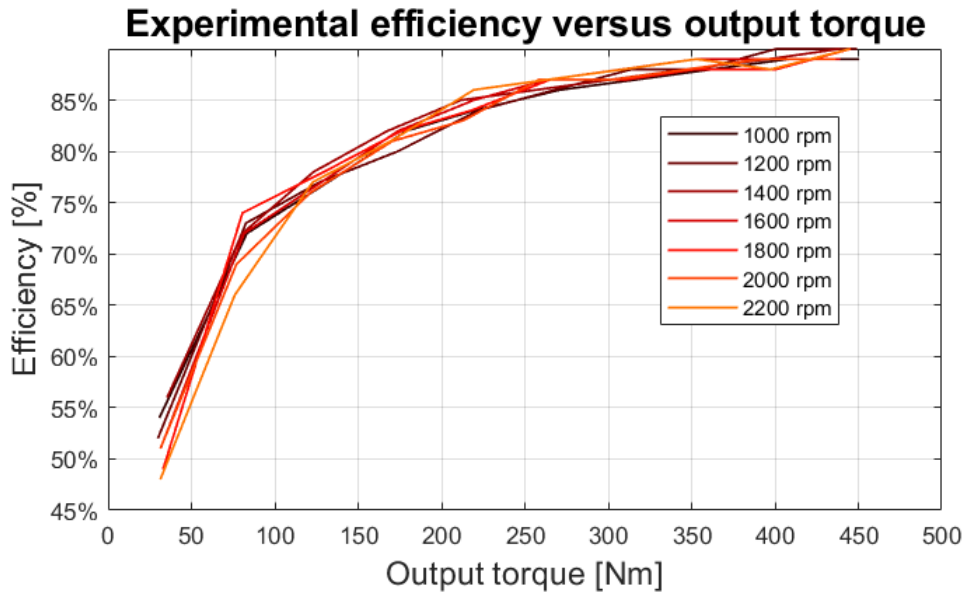


Figure 4.8: Efficiency as a function of output load (experimental data)

It is immediate that the efficiency does not significantly depend on the input speed, but the dependence from the output load is very considerable: increasing the output load leads to a higher efficiency. So the mathematical model- that we are going to develop- should keep into account all these effects. Another way to display the same effect of the figure 4.8, is to plot the input torque measured as a function of the output load for different input speeds (figure 4.9): the conclusions are very similar to those coming from figure 4.8.

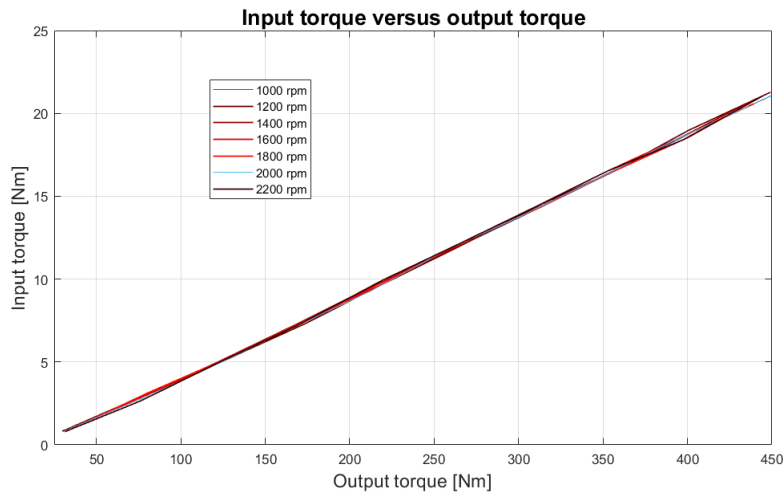


Figure 4.9: Input torque as a function of output load (experimental data)

To better display the effect of variable input speed at a fixed output load, we can analyze figure 4.10 where no important dependence from input speed is displayed.

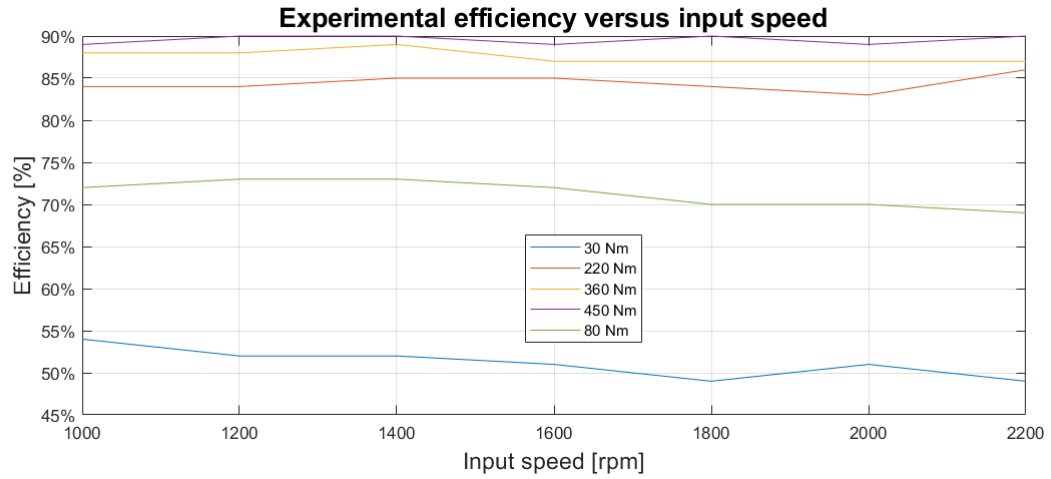


Figure 4.10: Efficiency as a function of input speed (experimental data)

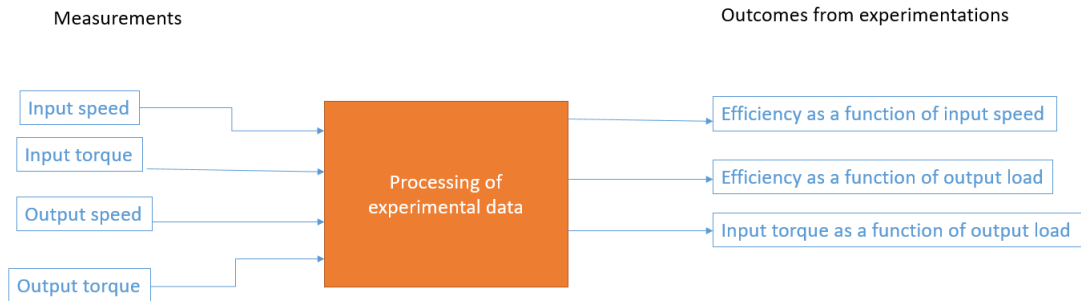


Figure 4.11: Summary schedule of the data processing

All the main idea concerning the data processing are summarized in figure 4.11.

4.4 Simulations coming from rigid bodies model

As we have already observed, the rigid bodies model is not able to explain the dependence of efficiency on load as figure 4.12 shows.

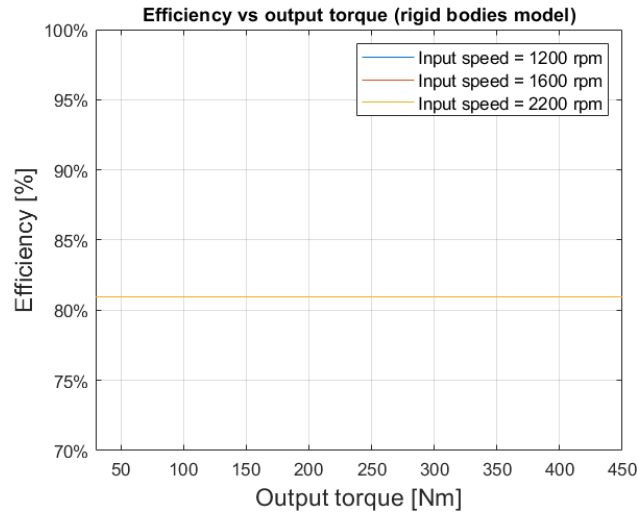


Figure 4.12: Efficiency as a function of load (theoretical previsions from rigid bodies model)

In order to evaluate the coherence of the used model, the coefficient of Coulombian friction is allowed to change. The default value in the simulations ($\mu = 0,05$) is suggested by the literature in the case of contact between steel ad steel with a lubricating film and bodies in mutual rolling. In figure 4.13 we can observe the simulation's results.

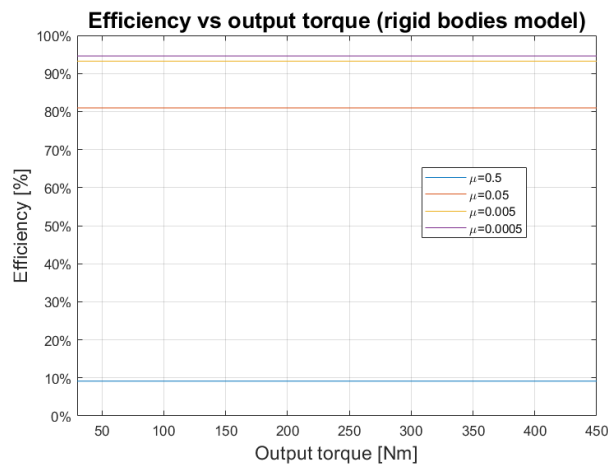


Figure 4.13: Efficiency as a function of load varying μ (theoretical previsions from rigid bodies model)

Although this model is incapable of explaining the experimental results, it allows to visualize in detail the dynamics of the exchanged forces. Table 4.4 gives a summary of all the parameters introduced as an input of the simulations on Matlab.

Table 4.4: Parameters of simulation

Main geometrical reducer's features and dynamic parameters			
Cycloidal disc		Housing	
Symbol and description	Value	Symbol and description	Value
z_1 number of teeth	19	z_2 number of housing pins	20
r_1 primitive radius	91,2 mm	r_c housing pins' radius	8,5 mm
x correction coefficient	0,38	r_2 pins' distribution radius	96,0 mm
e_0 eccentricity	3,0 mm		
Output rollers		Dynamic parameters	
Symbol and description	Value	Symbol and description	Value
R_s roller distribution radius	62,0 mm	m_{cy} cycloidal disc mass	1,27 kg
N_c number of output rollers	10	μ_p housing pins' friction coef.	0,05
r_c output rollers's radius	13,0 mm	μ_s output rollers' friction coef.	0,05
		μ_E bearing friction coef.	0,05

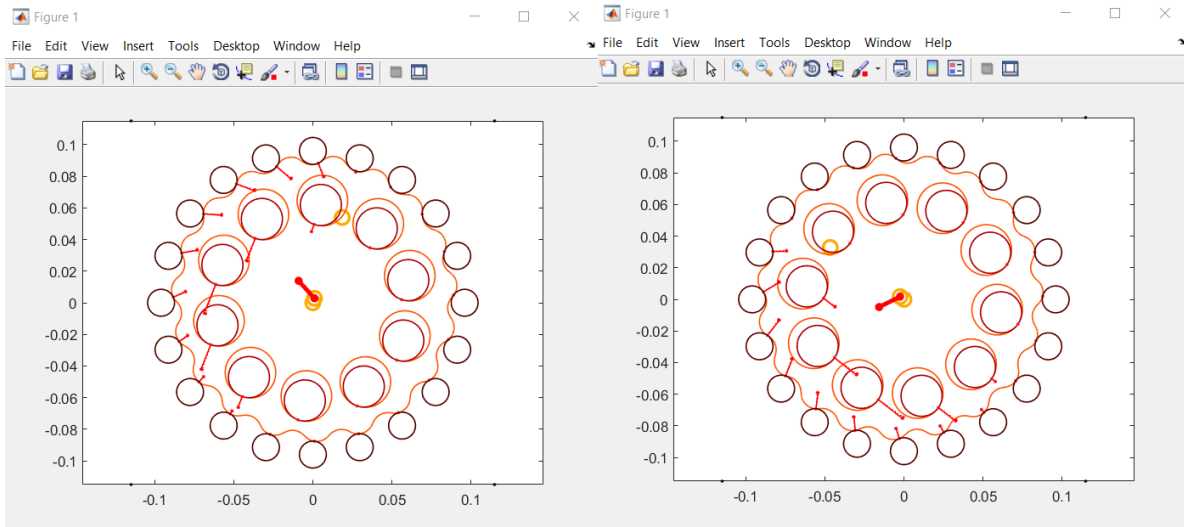


Figure 4.14: Two frames from the animation of the dynamics of normal forces obtained through Matlab

The rigid body model allows us to obtain simulations that recreate the dynamics of forces in a really explanatory way as figure 4.14.

4.5 Conclusions

The last note we would like to add in this chapter concerns the question of the modeling of friction force. There are several models for the mathematical modeling of friction, the most relevant are summarized in Appendix B. However, having observed that there is a lack of dependency on speed, it allows us to realize that the Coulombian friction model would be able to describe effectively the exchange of the friction forces. In fact, in this model, friction has only dependence on normal forces since the introduction of a constant coefficient that is function of contacting materials and other operating conditions independent of operating speeds. In the following developed models we will still discuss the validity of the Coulombian model in the overall mathematical model of the reducer.

As previously mentioned, in the simulations carried out it was preferred to use the value of friction coefficient taken from the manuals. However,- using the rigid bodies model- by varying the friction coefficient it is found that the saturated value of experimental efficiency (about 0.9) is obtained with a coefficient of friction of approximately 0.011 (figure 4.15). This could be explained by the fact that the lubricated rolling of the various mechanical components could use less friction than that foreseen by the manuals. Anyway, the rigid body model remains unable to describe the change in efficiency with output load, and this is the reason why other mathematical models will be developed.

In general, by observing the efficiency data, we discover the existence of two regions:

1. A first region for small output load values, where the variation in efficiency is considerable;
2. A second region for high output load values, where increasing the external load does not involve important variations on the efficiency that saturates to a constant value; in this field the rigid bodies model could describe the physical reality.

By averaging the data we obtain an effective reference experimental curve in first approximation for all the input speeds. For this reason, the rigid body model is considered effective in the optimization process as it has a low cost in terms of processing times.

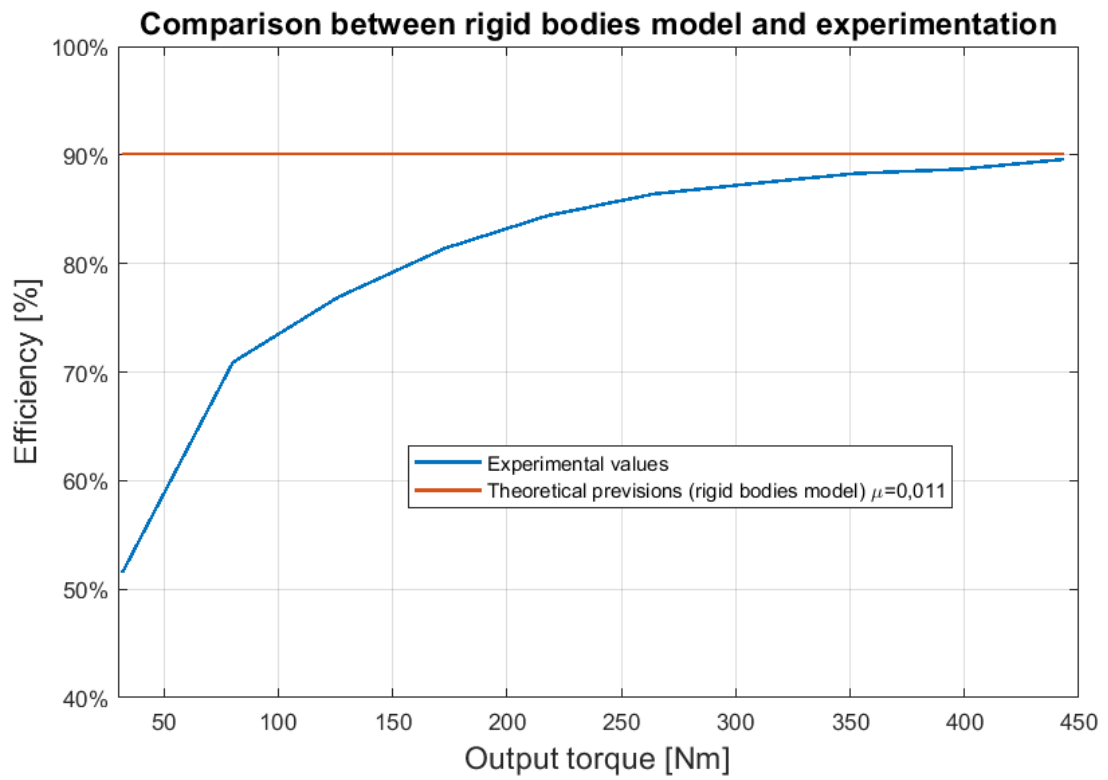


Figure 4.15: Efficiency coming from rigid bodies model and experimentation

Chapter 5

Optimization of the machine's main parameters with rigid bodies model

In this chapter, it is pointed out one of the most relevant outcome from rigid bodies model, that is the possibility of setting up a first attempt of optimization of the machine performance. As we know, the most obvious performance consists in the transmission efficiency: when we have to choose a reducer in a particular application, the transmission efficiency is the critical parameter that makes possible to select a specific model. However, another important aspect- that we should consider in applications- is the problem of vibrations in working conditions. This is why in the first section we are going to briefly analyze this topic and the optimization process will keep into account both the efficiency and the parameters that describe the vibrations (torque acyclism and the harmonic ratio).

5.1 Main vibration problems of cycloidal reducers

Although this thesis work is expressly focused on performance in terms of efficiency, also the issue of mechanical vibrations is here mentioned. In fact, as we know, this is a particularly important theme in mechanical design in view of applications. The cycloidal gearbox- if well designed- can boast a minimum vibration level. However, the eccentricity between the axes of rotation of the disk and the input shaft can cause considerable amount of torsional vibrations. This effect is usually reduced by introducing more than one disk, two or three, mounted in counter-phase in order to reduce the peaks of net vibration: each disk introduces torsional vibrations associated with the eccentricity of the axes and due to the rotation of the input shaft, by placing the cut-off discs, these vibrations add up and tend to shrink mutually. The experimentation carried out in Lodz has shown that the number of wheels has

no impact on efficiency, but it allows to reduce torsional vibrations and stresses for each wheel. In the main model that we are developing, we may keep into account of the vibrations effect by analyzing the input torque as a function of the simulation time, as figure 5.1 shows.

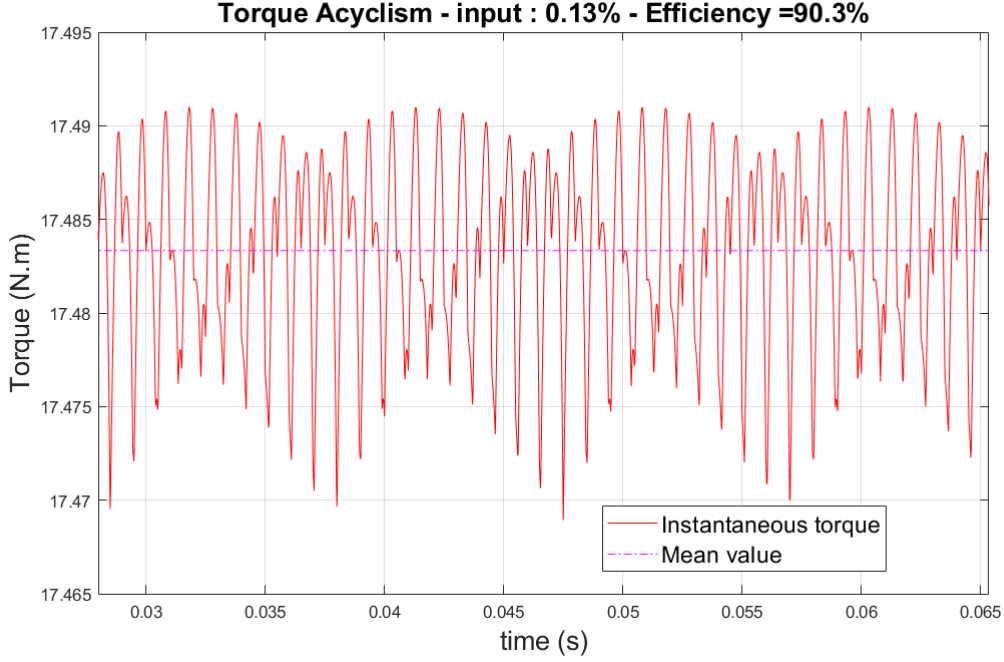


Figure 5.1: Instantaneous input torque (output torque as equal to 300 Nm)

Having the input torque as a function of time, it is possible to evaluate a quantity strictly linked to the vibration level that is the torque acyclism, defined as follows:

$$TA = \max \left(\frac{T_{in}(t) - T_{in,m}}{T_{in,m}} \right) \quad (5.1)$$

Where $T_{in}(t)$ is the instantaneous value of input torque coming from simulation, $T_{in,m}$ is its mean value. Moreover, it is common, in vibration analysis, introducing the Fourier transformation and we can define another quantity that describes the vibration level linked to the spectral diagram and this is the harmonic ratio, defined as follows:

$$HR = \max \left[\mathcal{F} \left(\frac{T_{in}(t) - T_{in,m}}{T_{in,m}} \right) \right] \quad (5.2)$$

Where \mathcal{F} indicates the Fourier transformation.

5.2 Influence of the profile modification coefficient

By varying the profile modification coefficient x , an efficiency optimum is obtained for a value around 0,09. This is coherent with the observation that a low correction coefficient gives a larger angle of motion transfer. The transmission could become more efficient with a low correction coefficient.

Moreover, by increasing the correction coefficient the torsional vibrations decrease and this is why the external shape tends to become more similar to a circumference than to a gear.

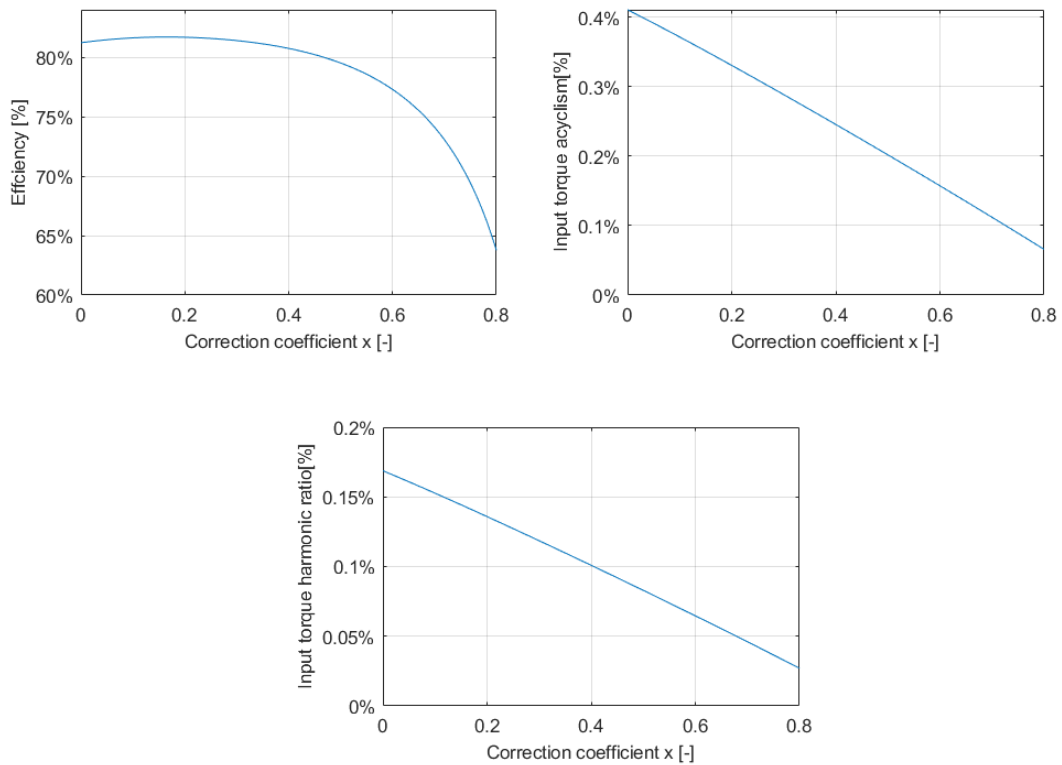


Figure 5.2: Influence of the profile modification coefficient

5.3 Influence of the pins radius

We also discover that the larger is the pins radius - in a limit imposed by the geometry- the better is the efficiency. The increment of this quantity causes no significant variations of the torque acyclism and of the harmonic ratio (figure 5.3).

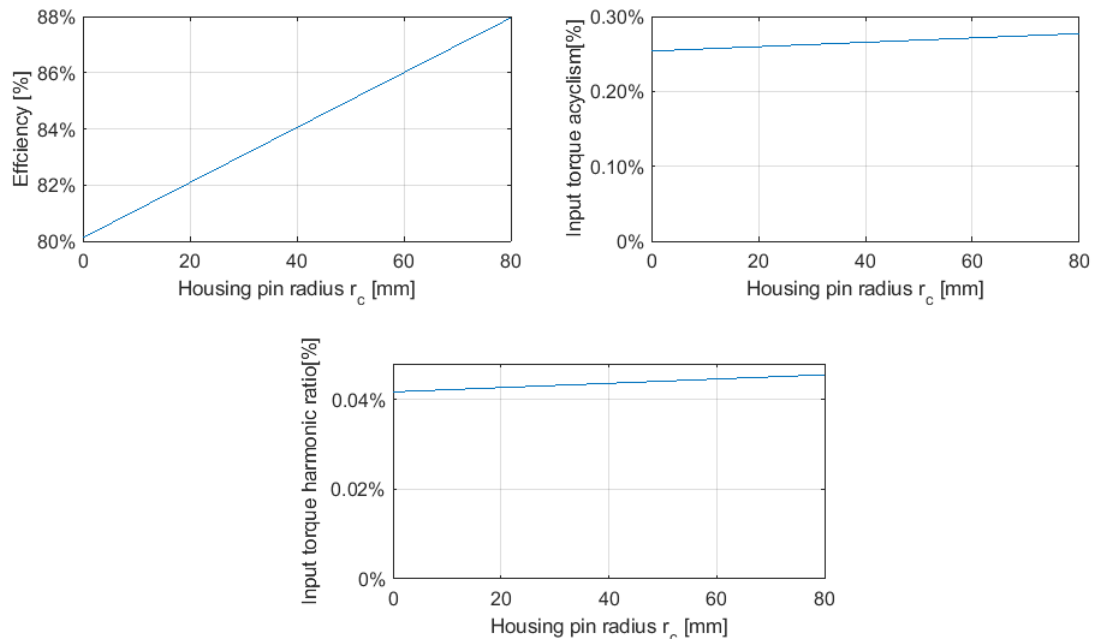


Figure 5.3: Influence of the pins radius

5.4 Influence of the teeth number

This parameter also affects the number of housing pins. The larger the number of teeth is great, the larger is the efficiency. This analysis seems to be not so realistic. The harmonic ratio remains constant and the torque acyclism overall declines with a modulation of a even or odd number of teeth (figure 5.4). The variation in the number of teeth involves the variation of the reduction ratio of the gearbox itself: this parameter is set by the particular application to which the gearbox is applied. We need to act on the cycloidal reducer's geometric features and on the number of teeth of the disk. However, due to the geometrical considerations made in chapter 2, increasing the number of teeth must involve changes in the characteristic dimensions of the disk.

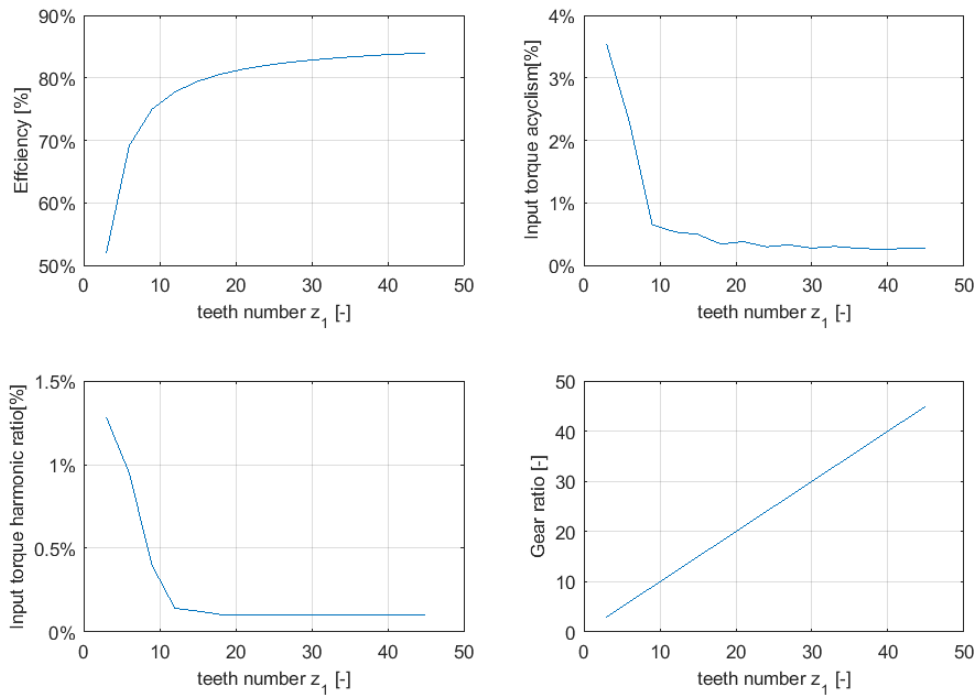


Figure 5.4: Influence of the teeth number

5.5 Influence of the output rollers number

The efficiency no longer varies from a number of output rollers greater than five. The torque acyclism and the harmonic ratio, after the low limit is exceeded, remain constant with a small modulation of an even or odd number of rollers.

The effect of having a greater number of rollers is to more effectively distribute the forces that allow the balance of the torque at the output. As well as being deducible from the basic model equations, the number of rollers does not change the dynamic behavior of the machine. Without any doubt, having a very small number of rollers can lead to an increase in operating vibrations and a lower efficiency, precisely because the balancing forces to the output torque are badly distributed (figure 5.5).

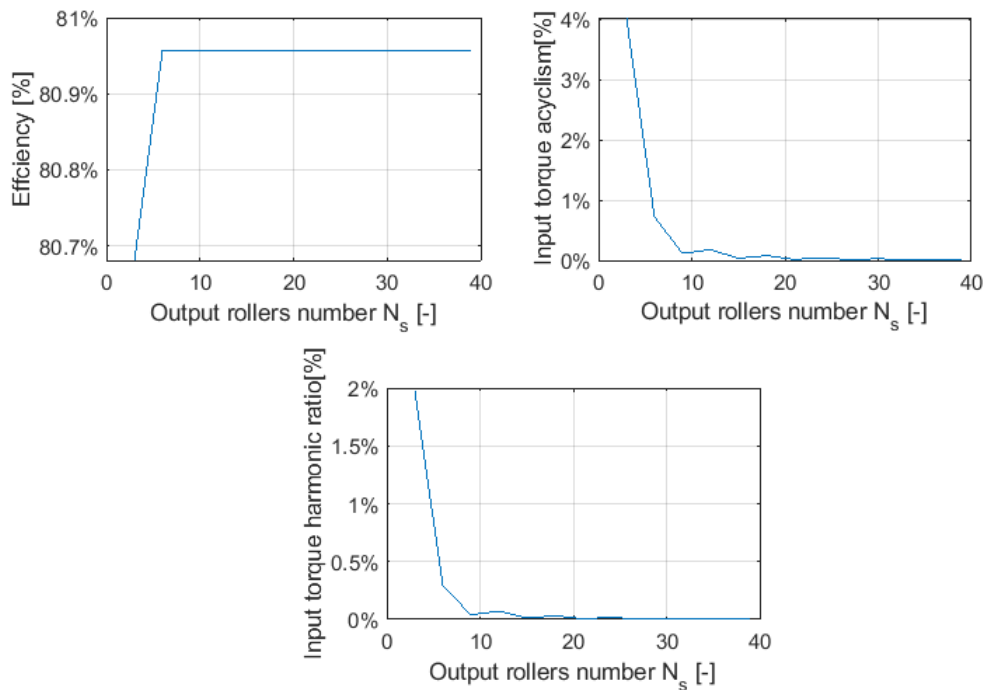


Figure 5.5: Influence of the output rollers number

5.6 Influence of friction coefficient

Lastly, the effect of the friction coefficient on the performance of the machine will be analyzed: this is not a parameter that can be changed during the design process, but it is markedly dependent on the working conditions. As known, this depends on the roughness of the surfaces in contact, on the extent of surface wear, on the presence of a lubricant film and- to a first approximation- does not depend on the sliding speed of the bodies in contact.

Obviously, it is expected that increasing the amount of friction is going to decrease efficiency, while the effect on the magnitude of the level of torsional vibrations in operation is interesting. Increasing the amount of friction forces leads to increasing vibrations because the forces balance varies. However, there is a maximum value of the coefficient of friction above which the amount of friction can be increased to reduce the vibration level. Anyway, in this field of friction coefficient, the values of efficiency would be inadmissible.

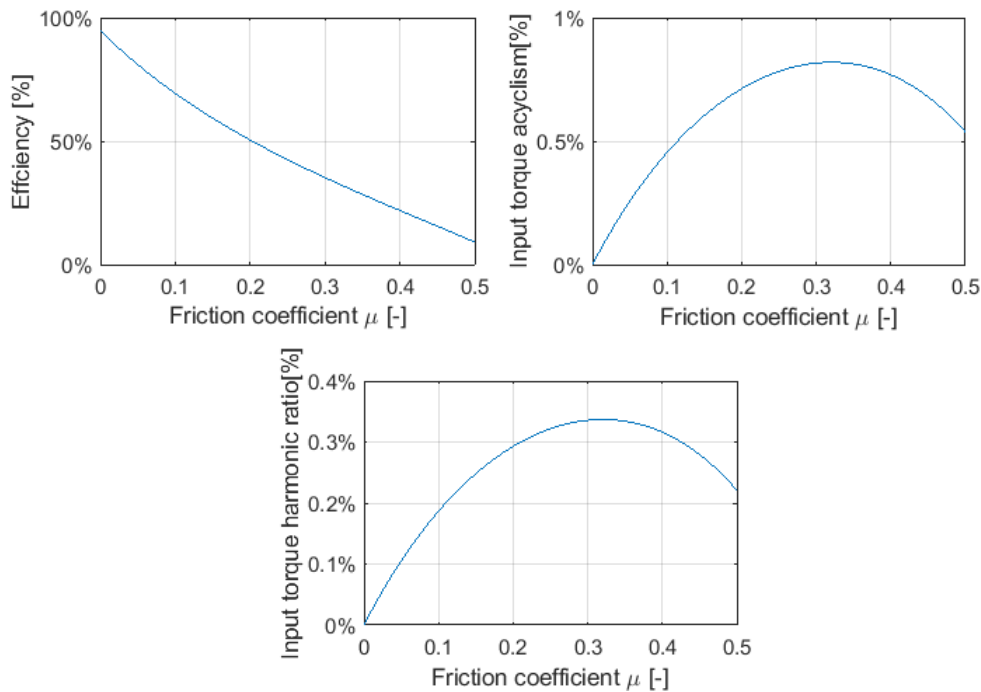


Figure 5.6: Influence of friction coefficient

It could be observed that for extremely low values of friction coefficient we have not got efficiency as equal to one. Since the main equations of the proposed model, we can not introduce $\mu = 0$, so the lower μ used for simulations is equal to 0,001. For the value of μ , the efficiency is around 0,98.

5.7 Optimizing the gearbox's performance

In this chapter we have analyzed some effect of variations of some parameters on the efficiency: the most impacting quantities are undoubtedly the correction coefficient x , the friction coefficient μ and the teeth number z_1 . Anyways, the correction coefficient is not allowed to be too small because if x is lowered, the external shape of cycloidal disk tends to be a circumference, causing difficulties of meshing with the housing pins. Moreover, the friction coefficient μ depends on the operating working conditions and this dependence underlines how important is for the cycloidal reducer to have the best condition in cleaning, surface finishing and maintenance. Finally, the number of teeth z_1 involves setting the gear ratio that is linked mainly to the particular application.

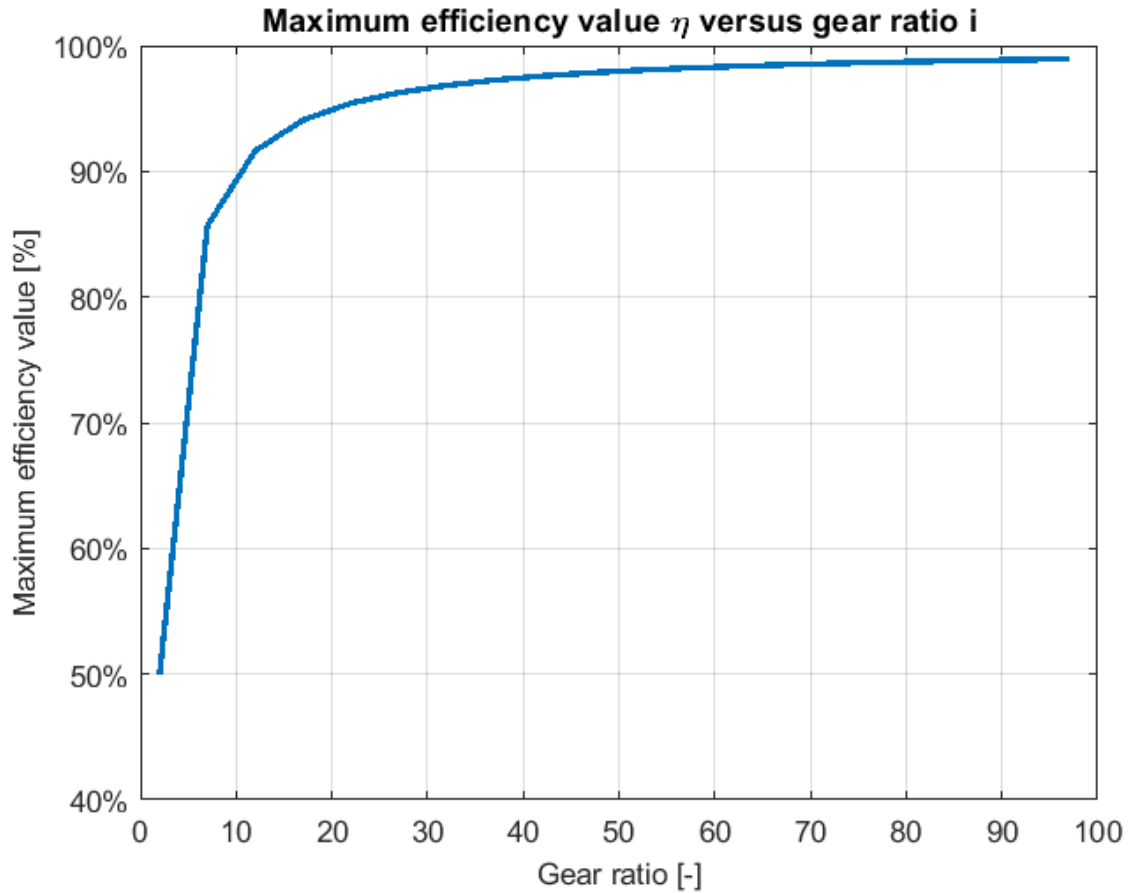


Figure 5.7: Maximum efficiency value as a function of gear ratio

To summarize, if we set the values of all the geometric parameters and the friction coefficient in a such way to raise up the efficiency, we would get a graph that draws attention to the fact that as great is the gear ratio, as significant is the transmission efficiency (figure 5.7). In fact, to get figure 5.7, we have set $\mu = 0,005$ ad $x = 0,1$: if z_1 - or equally i - was made to vary up to very high values, the gear ratio would raise up and at the limit it would tend to become unitary.

By now, it is possible to make a comparison between theoretical efficiency values of cyclo gearbox and typical efficiency values of traditional planetary reducers (figure 5.8).

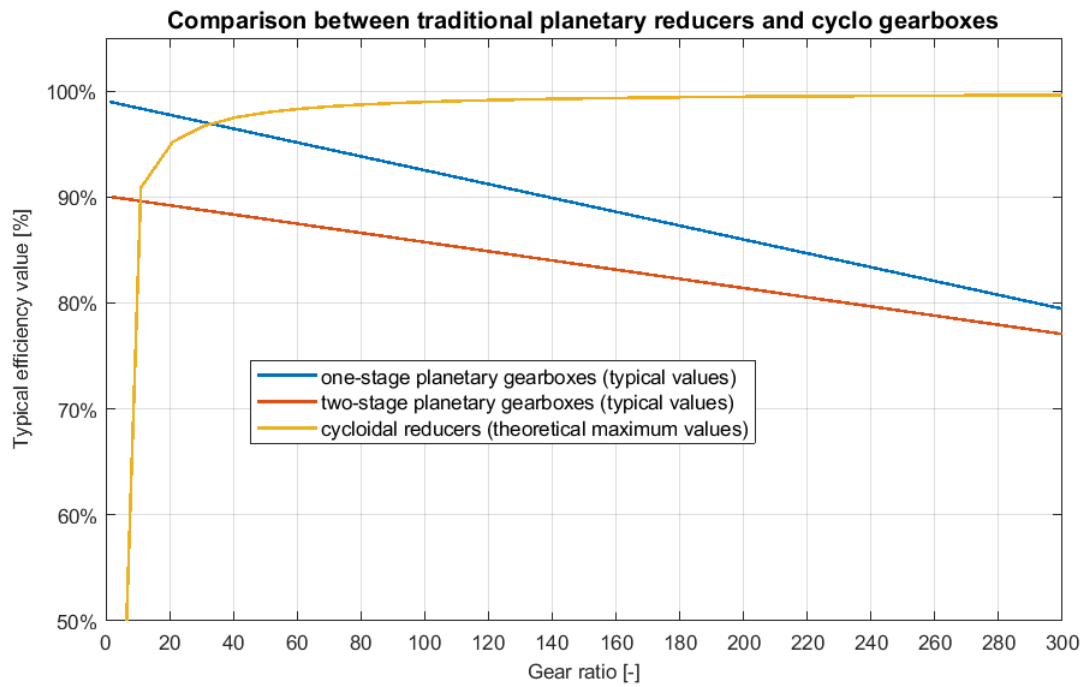


Figure 5.8: Comparison between theoretical efficiency values of cyclo gearbox and typical efficiency values of traditional planetary reducers

Chapter 6

Linear and non-linear stiffness model of the cycloidal disk

This is the key chapter where the behaviour of the cycloidal reducer is going to be explained in order to have a significant overlap with the experimentation. So far we have developed the basic equations and formed the rigid bodies model: we have observed that- within the limits of the aforesaid model- the transmission efficiency should be constant as the load varies. This behavior can be more or less satisfactory at high loads, while it does not explain the behavior of the gearbox at low loads. Therefore, dynamic elastic effects are introduced, mainly due to the cycloidal disk. The proposed model deals- in a simple way- with possible elastic effects. This the reason is why:

1. On the one hand, we will lay the foundations of a first model that takes into account the deformability of the disk and, then, we will develop it further;
2. We want to obtain a model that starts as a slight modification of the starting model without major modifications, precisely because the rigid bodies model allows to describe the behavior of the gearbox with saturated efficiency;
3. Finally, the addition of elastic effects complicates the model in the main form, this affects the cost of processing that increases exponentially as well as introducing complex mathematical operations (resolutions of differential equations).

On this basis, we are going to impute all the elastic effects on the single disk in the coupling with the input shaft, moreover, we will try not to complicate the model immediately, however, we will come to a non-linear deformability model in order to justify the experimentation.

6.1 Motivations in adding an elastic mobility

We are going to introduce a stiffness mobility along the direction of force transmission between the input shaft and the cycloidal disk. The main reasons why we have introduced this stiffness mobility are summarized in the following points:

1. We would include, in such way, the overall elastic dynamic effects of the bodies of the reducer on its dynamic behaviour;
2. Between the input shaft and the cycloidal disk there is the eccentric bearing whose presence, in a first approximations, is included as being in-built in the input shaft. Since referring to Hertz theory of contact, it is well-known that the relationship between force and deformation in mechanical contact could be strictly non-linear;
3. Because of the small axial length of the disk, the contact between the input shaft is not attributable to the case of two cylinders of infinite length in contact, neither to the case of two spheres in contact;
4. The idea of introducing elastic mobility only between input shaft and cycloidal disk, could be considered the direct consequences of others works whose focus is the analysis of strength and stress distribution. It could be proved that the most stressed sections of cycloidal plate are those closer to the coupling with the input shaft- in direction of the force \vec{E} - so the most relevant elastic effects must have involved by this mechanical joint;
5. The constants -that are going to be introduced- are not strictly experimental but, coming from the simulation's work with the main aim to demonstrate if the proposed model, are able to explain the experimentation. They are a sort of shape constants.

6.2 Dynamic equations with elastic properties

We should add a further hypothesis to the rigid bodies model in order to get the stiffness model: we are using the same kinematic relationships of the previous model, anyways this could be coherent with the resulting achievements if the displacements along y_1 are negligible.

We can refer to figure 6.1 to understand where and how we have imagined to introduce an ideal spring that will involve all the aforesaid elastic effects. This ideal spring acts along the \vec{Y}_1 that, as it was explained in chapter 3 - is moving with the cycloidal wheel.

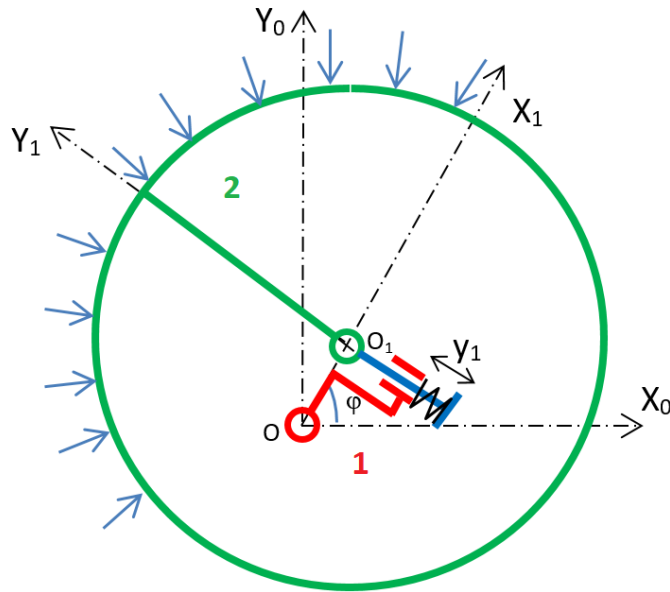
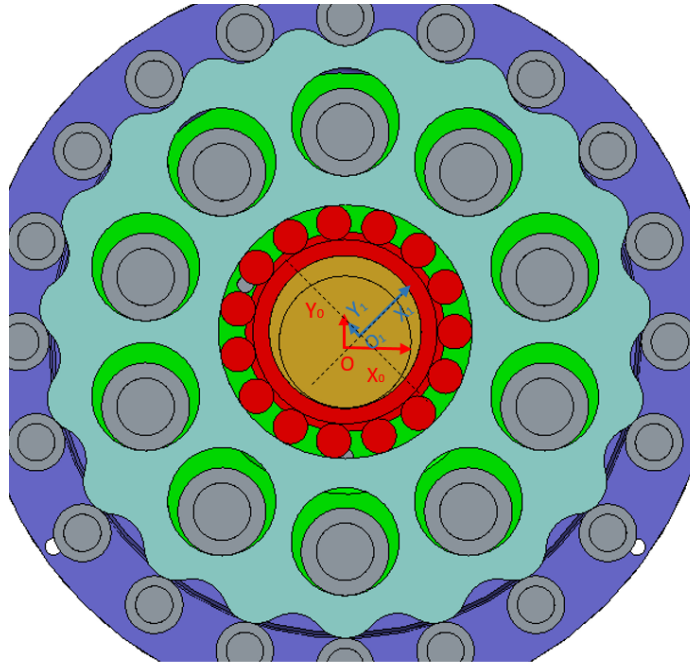


Figure 6.1: Model for y_1 mobility introducing a contact stiffness: the element 1 stays for the input shaft, the element 2 stays for the cycloidal disk's internal coupling surface (O_1 is the cycloidal disc's centre, O input shaft's centre)

In this way we have introduced an adding mobility along the direction of exchanged force, linked to the transmission of the torque on the input shaft.

In the first instance, the elastic retraction force has the following mathematical definition:

$$\overrightarrow{F_{el}(y_1)} = -k_{cy}|y_1|^p \operatorname{sgn}(y_1) \overrightarrow{Y_1} \quad (6.1)$$

While the input torque could be expressed as follows:

$$\overrightarrow{T_{in}(y_1)} = (e\overrightarrow{X_1}) \times \overrightarrow{F_{el}(y_1)} = -e k_{cy}|y_1|^p \overrightarrow{Z} \quad (6.2)$$

Where:

1. k_{cy} is the stiffness constant;
2. p is the exponent of non-linearity in general cases; if p is posed as equal to 1, we will get the Hooke law; otherwise the relationship between force and deformation is non-linear -as Hertz theory suggests in contact mechanics-.

With the expression of elastic force, we are interested in obtaining the expression of associated potential energy mainly because we will have all the elements to apply the Lagrange-Euler equation at a later stage. We should remind that θ_Z stays for the angular rotation of the disk around its axis and y_1 is position of O_1 (center of the disk) and coincides with the liner deformation of the spring, the potential associated to the spring is:

$$V(y_1, \theta_Z) = - \int \overrightarrow{F_{el}(y_1)} \cdot d\overrightarrow{Y_1} - \int [\overrightarrow{F_{el}(y_1)} \times (e\overrightarrow{X_1})] \cdot d(\theta_Z \overrightarrow{Z}) \quad (6.3)$$

$$V(y_1, \theta_Z) = - \int \overrightarrow{F_{el}(y_1)} \cdot d\overrightarrow{Y_1} - \int (F_{el}(y_1) e\overrightarrow{Z}) \cdot d(\theta_Z \overrightarrow{Z}) \quad (6.4)$$

Where:

1. $-\int \overrightarrow{F_{el}(y_1)} \cdot d\overrightarrow{Y_1}$ is linked to the linear deformation along the axis of the spring (the direction of the versor $\overrightarrow{Y_1}$);
2. $-\int (F_{el}(y_1) e\overrightarrow{Z}) \cdot d(\theta_Z \overrightarrow{Z})$ is the potential energy that is born because the action of the elastic force involves a torque (the input torque) around the axis of the cycloidal wheel.

Then:

$$V(y_1, \theta_Z) = \int k_{cy} y_1^p dy_1 + e k_{cy} y_1^p \int d\theta_Z \quad (6.5)$$

$$V(y_1, \theta_Z) = \frac{1}{p+1} y_1^{p+1} + e k_{cy} y_1^p \theta_Z + C \quad (6.6)$$

Assuming that $V(y_1 = 0, \theta_Z = 0) = 0$, we will obtain:

$$V(y_1, \theta_Z) = \frac{1}{p+1} y_1^{p+1} + e k_{cy} y_1^p \theta_Z \quad (6.7)$$

However, the expression (6.1) has a numerical problem because, if $p \neq 1$, it could involve complex number without physical meaning. Moreover, we will lose the deformation's sign that makes valid the equation (6.1). For these reason we should rewrite the equations (6.1) (6.9) and the equation (6.7) as follows:

$$\overrightarrow{F_{el}(y_1)} = -k_{cy} y_1 |y_1|^{p-1} \overrightarrow{Y_1} \quad (6.8)$$

$$\overrightarrow{T_{in}(y_1)} = (e \overrightarrow{X_1}) \times \overrightarrow{F_{el}(y_1)} = -e k_{cy} y_1 |y_1|^{p-1} \overrightarrow{Z} \quad (6.9)$$

$$V(y_1, \theta_Z) = \frac{1}{p+1} k_{cy} |y_1|^{p+1} + e k_{cy} |y_1|^p \theta_Z \quad (6.10)$$

As in rigid bodies model we can write the kinematic torsor with the velocity of point O_1 :

$$\{C_{C_y/R_0}\} = \left\{ e\dot{\varphi} \overrightarrow{Y_1} + (\dot{y}_1 \overrightarrow{Y_1} - y_1 \dot{\varphi} \overrightarrow{X_1}) \mid \frac{\dot{\varphi}}{z_1} \overrightarrow{Z} \right\} \quad (6.11)$$

Where:

1. $e\dot{\varphi} \overrightarrow{Y_1}$ is the absolute speed of the pint O_1 referring to X_0OY_0 ;
2. $\dot{y}_1 \overrightarrow{Y_1} - y_1 \dot{\varphi} \overrightarrow{X_1}$ is the relative speed of the center of the cycloidal plate (the cycloidal center is not in-built with O_1 due to the introduction of the spring referring to the $X_1O_1Y_1$);
3. $\frac{\dot{\varphi}}{z_1} \overrightarrow{Z}$ is the rotation angular speed of the cycloidal plate rotating around its axis.

With the kinematic torsor, the dynamic torsor of the cycloidal plate could be written as (referring the torsors to X_0OY_0):

$$\{D_{C_y/R_0}\} = \left\{ m_{cy}(-e\dot{\varphi}^2 - 2\dot{y}_1\dot{\varphi} - \dot{y}_1\ddot{\varphi})\overrightarrow{X_1} + m_{cy}(e\ddot{\varphi} + \ddot{y}_1 - y_1\dot{\varphi}^2)\overrightarrow{Y_1} \mid -\frac{I_{zz}}{z_1}\ddot{\varphi}\overrightarrow{Z} \right\}_{X_0OY_0} \quad (6.12)$$

We must remind of the derivative of rotating versors $\overrightarrow{X_1}$ and $\overrightarrow{Y_1}$:

$$\dot{\overrightarrow{X_1}} = \frac{d\overrightarrow{X_1}}{dt} = \dot{\varphi}\overrightarrow{Y_1} \quad (6.13)$$

$$\dot{\overrightarrow{Y_1}} = \frac{d\overrightarrow{Y_1}}{dt} = -\dot{\varphi}\overrightarrow{X_1} \quad (6.14)$$

The torsor standing for the interactions between the input shaft and the cycloidal disc- since submitting the previous hypotheses (elastic deformation and negligible displacements)- is:

$$\{E_{C_y/R_0}\} = \left\{ E_x \vec{X}_1 - k_{cy} y_1 |y_1|^{p-1} \vec{Y}_1 \mid -k_{cy} y_1 |y_1|^{p-1} e \vec{Z} \right\}_{X_0 O Y_0} \quad (6.15)$$

All the other torsors - the one that describes the interaction between plate and pins and the other one that stays for the interaction between plate and rollers- are in the same form of the rigid bodies model:

$$\{O_{C_y/R_0}\} = \left\{ \vec{C}_{O_i} = K_c \sum_i C_{X_i} \vec{X}_1 + K_c \sum_i C_{Y_i} \vec{Y}_1 \mid \sum_i K_c M_{C_i} \vec{Z} \right\}_{X_0 O Y_0} \quad (6.16)$$

$$\{O_{S_y/R_0}\} = \left\{ \vec{S}_{O_j} = K_s \sum_j S_{X_j} \vec{X}_1 + K_s \sum_j S_{Y_j} \vec{Y}_1 \mid \sum_j K_s M_{S_j} \vec{Z} \right\}_{X_0 O Y_0} \quad (6.17)$$

We can write the general form of the virtual displacement:

$$\delta \vec{r}_k = \delta x_1 \vec{X}_1 + \delta y_1 \vec{Y}_1 + \delta \theta_Z \vec{Z} \quad (6.18)$$

By using the torsors and the virtual work principle we obtain the main equations of the dynamic problem.

Along the \vec{X}_1 direction:

$$\sum \left(\vec{F} \cdot \delta \vec{X}_1 \right) = 0 \quad (6.19)$$

$$K_c \sum_i C_{X_i} + K_s \sum_j S_{X_j} + E_x + m_{cy} (e \dot{\varphi}^2 + 2 \dot{y}_1 \dot{\varphi} + \ddot{y}_1) = 0 \quad (6.20)$$

Along the \vec{Y}_1 we are going to have:

$$\sum \left(\vec{F} \cdot \delta \vec{Y}_1 \right) = 0 \quad (6.21)$$

$$K_c \sum_i C_{y_i} + K_s \mu_s \sum_j S_{X_j} - k_{cy} y_1 |y_1|^{p-1} + m_{cy} (-e \ddot{\varphi} + \ddot{y}_1 - y_1 \dot{\varphi}^2) = 0 \quad (6.22)$$

Regarding the balance to the rotation around the axis \vec{Z}

$$\sum \left(\vec{M}_Z \cdot \delta \theta_Z \right) = 0 \quad (6.23)$$

$$K_c \sum_i M_{C_i} + K_s \mu_s \sum_j M_{S_j} - e k_{cy} y_1 |y_1|^{p-1} + \frac{I_{zz}}{z_1} \ddot{\varphi} = 0 \quad (6.24)$$

Then, by using equations (6.56) and (6.57) -adding the hypothesis of steady state- we could get a system of equations whose unknown variables are K_c and y_1 . The

unknown-variable y_1 is present in the first and second derivative: anyway, by posing the right initial conditions and taking the stationary solution lets to have a displacement y_1 in a steady state.

$$\begin{cases} K_c \sum_i M_{C_i} + K_s \mu_s \sum_j M_{S_j} - k_{cy} y_1 |y_1|^{p-1} e = 0 \\ K_c \sum_i C_{y_i} + K_s \mu_s \sum_j S_{X_j} - k_{cy} y_1 |y_1|^{p-1} + m_{cy} (\ddot{y}_1 - y_1 \dot{\varphi}^2) = 0 \end{cases} \quad (6.25)$$

By making explicit the variable K_c as a function of y_1 and its derivative, the following differential equations are obtained:

$$K_c = \frac{1}{\sum_i M_{C_i}} \left(-K_s \mu_s \sum_j M_{S_j} + k_{cy} y_1 |y_1|^{p-1} e \right) \quad (6.26)$$

$$m_{cy} \ddot{y}_1 + k_{cy} y_1 |y_1|^{p-1} \left(1 - e \frac{\sum_i C_{Y_i}}{\sum_i M_{C_i}} \right) - m_{cy} \omega_0^2 y_1 = K_s \mu_s \sum_j S_{X_j} - K_s \sum_j M_{S_j} \frac{\sum_i C_{Y_i}}{\sum_i M_{C_i}} \quad (6.27)$$

The equation above is a non-linear differential equations with time-variant coefficient whose solution could be determined numerically by using Matlab/Simulink. So with these elements we can evaluate the efficiency of the gearbox transmission:

$$T_{out} = C_s \quad (6.28)$$

$$T_{in} = |\vec{T}_{in}| = e k_{cy} |y_1|^p \quad (6.29)$$

$$\frac{\omega_{out}}{\omega_{in}} = \frac{1}{i} = \frac{1}{z_1} \quad (6.30)$$

$$\eta = \frac{T_{out} \omega_{out}}{T_{in} \omega_{in}} = \frac{C_s}{z_1 e k_{cy} |y_1|^p} \quad (6.31)$$

After getting the main equations with the use of torsor linked with the virtual work principle, we are going to obtain the same equations through solving the Euler-Lagrange equation.

The main equation of Euler-Lagrange is well-known:

$$\frac{d}{dt} \frac{\partial \mathcal{L}}{\partial \dot{q}_k} - \frac{\partial \mathcal{L}}{\partial q_k} = Q_k \quad (6.32)$$

Where $q_1 = x_1$, $q_2 = y_1$ and $q_3 = \theta_Z$ -with the same meaning of the rigid bodies model- while \mathcal{L} is the Lagrangian of the system (cycloidal plate) and Q_k is due to the interactions of cycloidal plate with the other bodies.

$$\mathcal{L} = T - V \quad (6.33)$$

$$T = \frac{1}{2} m_{cy} \vec{V}_{O_1} \cdot \vec{V}_{O_1} + \frac{1}{2} I_{zz} \dot{\theta}_Z^2 \quad (6.34)$$

$$V = \frac{1}{p+1} k_{cy} |y_1|^{p+1} + e k_{cy} |y_1|^p \theta_Z \quad (6.35)$$

Where $\overrightarrow{V_{O_1}}$ can be determined using Rivals theorem:

$$\overrightarrow{V_{O_1}} = \overrightarrow{V_O} + \overrightarrow{V_{O_1/O,dr}} + \overrightarrow{V_{O_1/O,rel}} \quad (6.36)$$

$$\overrightarrow{V_{O_1}} = \overrightarrow{V_{O_1/O,dr}} + \overrightarrow{V_{O_1/O,rel}} \quad (6.37)$$

$$\overrightarrow{V_{O_1}} = e\dot{\varphi} \overrightarrow{Y_1} + (\dot{y}_1 \overrightarrow{Y_1} - y_1 \dot{\varphi} \overrightarrow{X_1}) \quad (6.38)$$

Finally:

$$\frac{d}{dt} \frac{\partial \mathcal{L}}{\partial \dot{q}_1} = \frac{d}{dt} \frac{\partial T}{\partial \dot{x}_1} \quad (6.39)$$

$$\frac{d}{dt} \frac{\partial T}{\partial \dot{x}_1} = m_{cy} (e\dot{\varphi}^2 + 2\dot{y}_1 \dot{\varphi} + y_1 \ddot{\varphi}) \quad (6.40)$$

$$\frac{d}{dt} \frac{\partial \mathcal{L}}{\partial \dot{q}_2} = \frac{d}{dt} \frac{\partial T}{\partial \dot{y}_1} \quad (6.41)$$

$$\frac{d}{dt} \frac{\partial T}{\partial \dot{y}_1} = m_{cy} (-e\ddot{\varphi} + \ddot{y}_1 + y_1 \dot{\varphi}^2) \quad (6.42)$$

$$\frac{d}{dt} \frac{\partial \mathcal{L}}{\partial \dot{q}_3} = \frac{d}{dt} \frac{\partial T}{\partial \dot{\theta}_Z} \quad (6.43)$$

$$\frac{d}{dt} \frac{\partial T}{\partial \dot{\theta}_Z} = I_{zz} \ddot{\theta}_Z = I_{zz} \frac{\ddot{\varphi}}{z_1} \quad (6.44)$$

While:

$$\frac{\partial \mathcal{L}}{\partial q_1} = \frac{\partial V}{\partial x_1} = 0 \quad (6.45)$$

$$\frac{\partial \mathcal{L}}{\partial q_2} = \frac{\partial V}{\partial y_1} = k_{cy} y_1 |y_1|^{p-1} \quad (6.46)$$

$$\frac{\partial \mathcal{L}}{\partial q_3} = \frac{\partial V}{\partial \theta_Z} = e k_{cy} y_1 |y_1|^{p-1} \quad (6.47)$$

We are going to evaluate Q_1 , Q_2 and Q_3 :

$$\delta \overrightarrow{r}_k = \delta x_1 \overrightarrow{X_1} + \delta y_1 \overrightarrow{Y_1} + \delta \theta_Z \overrightarrow{Z} \quad (6.48)$$

$$Q_1 = \sum_{k=1}^N \overrightarrow{F_{nc,k}} \cdot \frac{\partial \overrightarrow{r}_k}{\partial q_1} = \sum_{k=1}^N \overrightarrow{F_{nc,k}} \cdot \overrightarrow{X_1} \quad (6.49)$$

$$Q_1 = \sum_{k=1}^N \overrightarrow{F_{nc,k}} \cdot \overrightarrow{X_1} = K_c \sum_i C_{X,i} + K_s \sum_j S_{X,j} + E_x \quad (6.50)$$

$$Q_2 = \sum_{k=1}^N \overrightarrow{F_{nc,k}} \cdot \frac{\partial \overrightarrow{r_k}}{\partial q_2} = \sum_{k=1}^N \overrightarrow{F_{nc,k}} \cdot \overrightarrow{Y_1} \quad (6.51)$$

$$Q_2 = \sum_{k=1}^N \overrightarrow{F_{nc,k}} \cdot \overrightarrow{Y_1} = K_c \sum_i C_{Y,i} + K_s \mu_s \sum_j S_{X,j} \quad (6.52)$$

$$Q_3 = \sum_{k=1}^N \overrightarrow{F_{nc,k}} \cdot \frac{\partial \overrightarrow{r_k}}{\partial q_3} = \sum_{k=1}^N \overrightarrow{F_{nc,k}} \cdot \overrightarrow{Z} \quad (6.53)$$

$$Q_3 = \sum_{k=1}^N \overrightarrow{F_{nc,k}} \cdot \overrightarrow{Z} = K_c \sum_i M_{C,i} + K_s \sum_j M_{S,j} \quad (6.54)$$

Finally, summarizing all the steps and continuing with the substitutions of the terms, we will obtain the three main dynamic equations:

$$K_c \sum_i C_{X_i} + K_s \sum_j S_{X_j} + E_x + m_{cy}(e\dot{\varphi}^2 + 2\dot{y}_1\dot{\varphi} + \ddot{y}_1) = 0 \quad (6.55)$$

$$K_c \sum_i C_{y_i} + K_s \mu_s \sum_j S_{X_j} - k_{cy}y_1|y_1|^{p-1} + m_{cy}(-e\ddot{\varphi} + \ddot{y}_1 - y_1\dot{\varphi}^2) = 0 \quad (6.56)$$

$$K_c \sum_i M_{C_i} + K_s \mu_s \sum_j M_{S_j} - ek_{cy}y_1|y_1|^{p-1} + \frac{I_{zz}}{z_1}\ddot{\varphi} = 0 \quad (6.57)$$

6.3 Dynamic equations with elastic properties (Newton's method)

We can obtain the free-body diagram for the stiffness model by varying the following forces:

1. The force $E_y(1 - \mu_E)\overrightarrow{Y_1}$ should be replaced by the elastic forces $\overrightarrow{F_{el}(y_1)} = -k_{cy}y_1|y_1|^{p-1}\overrightarrow{Y_1}$;
2. The two components of inertial force should be changed because we must take into account the effects of y_1 displacements deformations on kinematic laws.

In order to get the effective inertial force in the case of having y_1 displacements, we are going to adapt the kinematic equations, starting off by writing the relative velocity formula:

$$\overrightarrow{V_{O_1}} = \overrightarrow{V_O} + \overrightarrow{V_{O_1/O,dr}} + \overrightarrow{V_{O_1/O,rel}} \quad (6.58)$$

Where $\overrightarrow{V_{O_1/O,dr}}$ is the dragging velocity linked to the motion of the reference system $X_1O_1Y_1$, while $\overrightarrow{V_{O_1/O_0,dr}}$ is the relative speed related to $X_1O_1Y_1$ and associated to the displacements y_1 .

$$\overrightarrow{V_{O_1}} = e\dot{\varphi} \overrightarrow{Y_1} + (\dot{y}_1 \overrightarrow{Y_1} - y_1\dot{\varphi} \overrightarrow{X_1}) \quad (6.59)$$

Then:

$$\overrightarrow{a_{O_1}} = \frac{d\overrightarrow{V_{O_1}}}{dt} = (-e\ddot{\varphi}^2 - 2\dot{y}_1\dot{\varphi} - y_1\ddot{\varphi})\overrightarrow{X_1} + (e\ddot{\varphi} + \ddot{y}_1 - y_1\dot{\varphi}^2)\overrightarrow{Y_1} \quad (6.60)$$

Therefore, the two axis components of inertia force should be:

$$\begin{cases} F_{in,X_1} = m_{cy}(e\dot{\varphi}^2 + 2\dot{y}_1\dot{\varphi} + y_1\ddot{\varphi}) \\ F_{in,Y_1} = m_{cy}(-e\ddot{\varphi} + \ddot{y}_1 + y_1\dot{\varphi}^2) \end{cases} \quad (6.61)$$

By applying the fundamental laws of dynamic it is immediate getting the same equations coming from the analytic method with torsors.

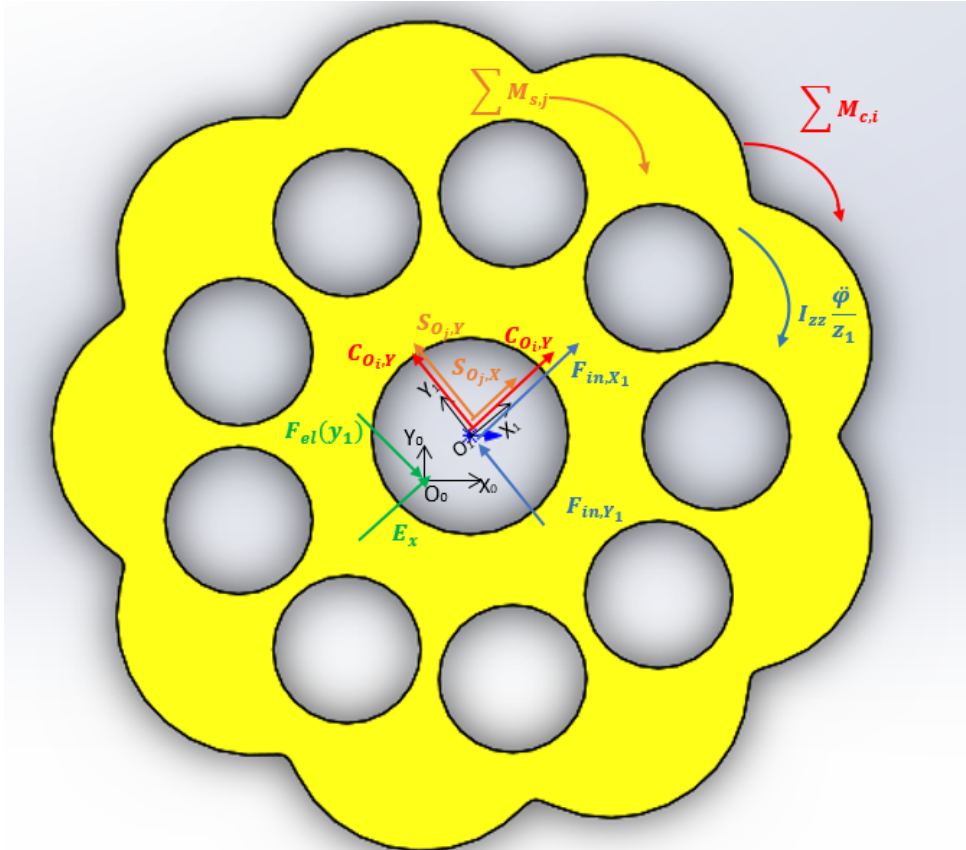


Figure 6.2: Free body diagram in the case of stiffness model

6.4 Mathematical formulation of dynamic problem

In this section the main focus is on the mathematical aspects of the following equation:

$$m_{cy}\ddot{y}_1 + k_{cy}y_1|y_1|^{p-1} \left(1 - e^{\frac{\sum_i C_{Y_i}}{\sum_i M_{C_i}}}\right) - m_{cy}\omega_0^2 y_1 = K_s \mu_s \sum_j S_{X_j} - K_s \sum_j M_{S_j} \frac{\sum_i C_{Y_i}}{\sum_i M_{C_i}} \quad (6.62)$$

The equation (6.62) is a second order non-linear differential equation. The non-linearity of the equation is due to $y_1|y_1|^{p-1}$ when $p \neq 1$. Moreover, the coefficient of $y_1|y_1|^{p-1}$ is time-dependent, while the coefficients of the second derivative (\ddot{y}_1) and of y_1 are constant. The right term is time-dependent in a periodic way because all the basic addenda are periodic: they are linked to the forces distribution on the cycloidal plate and they are varying as cycloidal wheel rotates. Basic methods for initial value problems, beginning with the simple Euler scheme, and working up to the extremely popular Runge–Kutta fourth order method (ode45), may be implemented by the Matlab/Simulink to solve the dynamic problem.

However, as it is known from the relevant literature, the resolution of equations of this type can easily lead to numerical divergence. It was observed in the first attempts to solve this equation. To override the problem of the divergence in a simple but not optimal way from the mathematical point of view, we have reduced the interval of discretization in time used by Simulink for the resolution of the equation. This can be done immediately via the Simulink numerical resolution settings. In such way, it determined a significant increase in processing times, whose effect is amplified by the fact that the general algorithm -to get the efficiency as a function of the load- requires a very long times to solve the differential equations whose generic form is basically (6.62). Nevertheless, the reduction of the discretization interval appears a fast and effective way to avoid incurring numerical problems that would be more effectively addressed by a mathematician than by an engineer.

If it was be desirable to get an analytic solution of the equation, the Harmonic Balance method could be introduced. This is used to calculate the steady-state response of nonlinear differential equations when the forcing term is a period function as in our case. However, analytic resolution falls outside the interests of this thesis work, whose focus is on the practical aspects rather than the strictly mathematical and numerical ones.

Furthermore, we should add that the equation (6.62) is based on the hypothesis of steady state. We should write the Cauchy problem by setting the initial values

problem, that for us are in the main form:

$$\begin{cases} m_{cy}\ddot{y}_1 + k_{cy}y_1|y_1|^{p-1} \left(1 - e^{-\frac{\sum_i C_{Y_i}}{\sum_i M_{C_i}}}\right) - m_{cy}\omega_0^2 y_1 = F(t) \\ y_1(t=0) = 0 \\ \dot{y}_1(t=0) = 0 \end{cases} \quad (6.63)$$

These are not the actual initial conditions of the physical problem, but in the beginning these are unknown. To solve the problem, the simulation was performed and only at the stationary response the solution was eventually taken into account. Finally, we have added in Appendix E a little explanation of the main blocks used in Simulink to solve the main equation (6.62) and in Appendix D the basic phenomenology of non-linear mass-spring system.

6.5 Linear stiffness model: research of the experimental stiffness coefficient

So far we have developed a method to explain the dynamics considering the consequences of having elastic properties concentrated on the contact between the high-speed shaft and the cycloidal plate. The first attempt is to force the elastic property to linear behaviour. By posing $p = 1$ from the general stiffness model, we are going to obtain the so-called linear stiffness model. That model foresees the linearity of relationship between retraction force and deformation. As the appendix C underlines, for two cylinders in external contact, the relationship would be really linear. However, the equation is:

$$m_{cy}\ddot{y}_1 + k_{cy}y_1 \left(1 - e^{-\frac{\sum_i C_{Y_i}}{\sum_i M_{C_i}}}\right) - m_{cy}\omega_0^2 y_1 = K_s \mu_s \sum_j S_{X_j} - K_s \sum_j M_{S_j} \frac{\sum_i C_{Y_i}}{\sum_i M_{C_i}} \quad (6.64)$$

By now, we must give a physical meaning to the stiffness constant k_{cy} that in the linear stiffness model we will call as linear stiffness coefficient, whose units are N/m . The value suggested by literature is far from the real one because the real case is particularly different from the ideal reference case of two cylinders in external contact. In fact, we have at most two cylindrical bodies in contact, the first one in contact with its internal surface, the second one with its external surface. However, there are the eccentric bearing rollers in between. So we are going to estimate whether it would be possible to carry out a value of k_{cy} that could make possible the overlap between experimentation and mathematical prevision.

In order to reach that purpose, we can solve the following system:

$$\begin{cases} m_{cy}\ddot{y}_1 + k_{cy}y_1 \left(1 - e^{-\frac{\sum_i C_{Y_i}}{\sum_i M_{C_i}}}\right) - m_{cy}\omega_0^2 y_1 = F(t) \\ F(t) = K_s \mu_s \sum_j S_{X_j} - K_s \sum_j M_{S_j} \frac{\sum_i C_{Y_i}}{\sum_i M_{C_i}} \\ \bar{\eta} = \frac{C_s}{z_1 k_{cy} |y_1|} = \eta_{sp}(C_s, \omega_0) \end{cases} \quad (6.65)$$

Where $\eta_{sp}(C_s, \omega_0)$ consists in the experimental curves obtained thorough the experimental test bench and we are aware that the main dependence is for the output load C_s , rather than for the input speed ω_0 , while $|y_1|$ is the average value of the deformation during the simulation time. The mathematical problem is not easily solved by the Matlab/Simulink tools. Moreover, we can make explicit the linear stiffness coefficient k_{cy} as a function of the experimental efficiency:

$$k_{cy} = \frac{C_s}{z_1 \eta_{sp}(C_s, \omega_0) |y_1|} \quad (6.66)$$

By substituting in the main dynamic differential equation:

$$m_{cy}\ddot{y}_1 + \frac{C_s}{z_1 \eta_{sp}(C_s, \omega_0) |y_1|} y_1 \left(1 - e^{-\frac{\sum_i C_{Y_i}}{\sum_i M_{C_i}}}\right) - m_{cy}\omega_0^2 y_1 = F(t) \quad (6.67)$$

It would become particularly artificial to introduce an equation of this kind on Simulink, since Simulink is a solver of time equations and whose resolution algorithm goes on passing through successive sequences. The mean value ($|y_1|$) of the unknown function ($|y_1(t)|$) in the simulation time intervals is present in the basic equation (6.67) and with the basic blocks of Simulink is not easily possible to solve the overall equation because of this presence. In such way we will find the specific values of linear stiffness coefficient that makes possible to have, for each particular value of the output load, the values of the experimental efficiency.

We discovered that- using the linear stiffness model to approximate the experimental data- the linear stiffness coefficient has an almost square relationship with the load (figure 6.3). We will be forced to introduce empirical relationship suggesting that the chosen model is not able to effectively explain physical reality and experimental data. As a physical interpretation we have that the increase of the load involves a variation in the linear stiffness of the disk so that the experimental efficiency can be simulated.

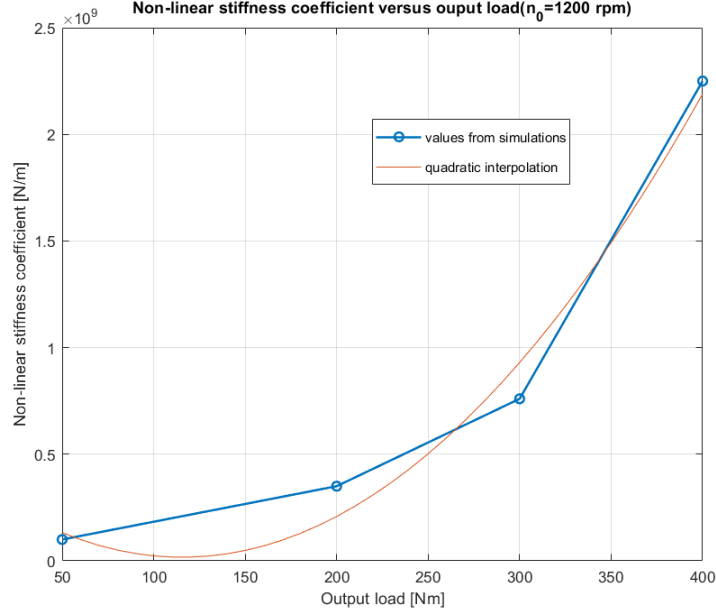


Figure 6.3: Relationship between k_{cy} and output load C_s in order to approximate the experimental efficiency

6.6 Linear stiffness model: comparison between experimentation and simulations

As a criterion to determine the validity of the model and its capability of approximating the experimentation, it was to choose the model whose shape parameters were constant and did not depend neither on the input speed, nor on the load. The linear model can not describe the experimentation without admitting a variability of the linear stiffness coefficient as a function of the output load. In the following simulations we can observe the effect of increasing the stiffness in determining a general increase in transmission efficiency, this is because a more rigid system responds- at the same stress given by the forcing $F(t)$ - with lesser deformations and forces that are globally produced lower. This translates into smaller input torque and higher efficiency. The behavior of the efficiency as a function of stiffness saturates at high value of stiffness and then reverses for high stiffness values, precisely because in the determination of the input torque, both the stiffness and the deformation participates. From the comparison with the experimental data, it is observed that the increase in experimental efficiency is much greater than the theoretical forecasts with the linear stiffness model. However, the model has two advantages: the first is the lack of dependence of efficiency on the input speed (as the experimentation

shows), the second is the dependence, even though small, of the efficiency on the output torque.

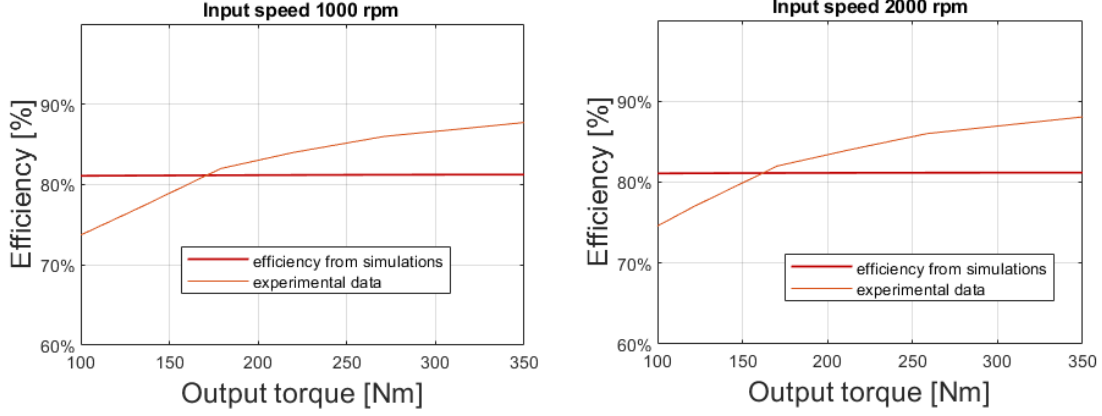


Figure 6.4: Simulations' results to evaluate the efficiency with the linear model ($p = 1$) at two different speeds with $k_{cy} = 10^9 \frac{N}{m}$

6.7 Non-linear stiffness model: motivations

From the linear stiffness model we have concluded that a mobility along the direction of force transmission between high-speed shaft and cycloidal plate could explain why the efficiency depends on the output load. Although, the linearity in deformations does not imply the same increase of efficiency as the experimentation shows. For this reason we are going to introduce a relationship of non-linearity between force and deformation with the main purpose to find shape constants -as we will see later p and k_{cy} - that let to reach an overlap between previsions and experimental data. Physically, the following observations could clarify this new way forward:

1. The theories of contact explain that the relationship between deformation and normal contact force may be strictly non-linear. In fact, as table 6.1 shows, in the elementary case of contact we have that k_{cy} depends on the geometry of contacting bodies, on the material properties and on some sizes of the bodies. Instead, p depends only on the geometry of contacting bodies. In the particular case of analysis, we can not find a similar elementary case to apply the basic equations. Anyways, we can expect that the experimental p is not too far from the typical coefficient of the table 6.1. The same applies to k_{cy} ;
2. Another reason why we can not have the theoretical value for p consists in the fact that we are going to consider the dynamic effects only on the contact

between input shaft and cycloidal wheel. Actually, we have a lot of points of contact at that time: the contacts between pins and teeth and between rollers and plate's lobes. Nevertheless, if all these contacts were added in dynamics, the model would become really complicated and the processing time of the Matlab/Simulink code would increase exponentially. Moreover, we have that significant stressed zones of the wheel is near to the coupling with the high-speed shaft;

3. if the model becomes reliable, we will prove that most of the dynamic effects must be involved between input shaft and cycloidal disk and that the increase of the efficiency could be a direct consequence of the importance of the contact dynamics;
4. As we have already specified, the constants introduced p and k_{cy} will be evaluated to get an overlap between theoretical and experimental efficiency. These are shape constants indeed, so for future developments we may evaluate these experimentally and later we could check if the experimental values are near to the values coming from the computational and modelling work. This last check could be proved the validity of the model chosen itself.

By now, we are able to compare the effect in variation of the coefficient p by keeping constant k_{cy} (while p is varying). If we choose a value of k_{cy} that does not allow to have intersection with the line representing for the linear behaviour, we tend to have a hardening behaviour of the spring (figure 6.5 left).

At the same time we can estimate the effect of raising up k_{cy} , while p is imposed equal to 2,5: for the same value of the deformation, there is a greater retraction force. In that way, we increase the hardening behaviour of the spring (figure 6.5 right).

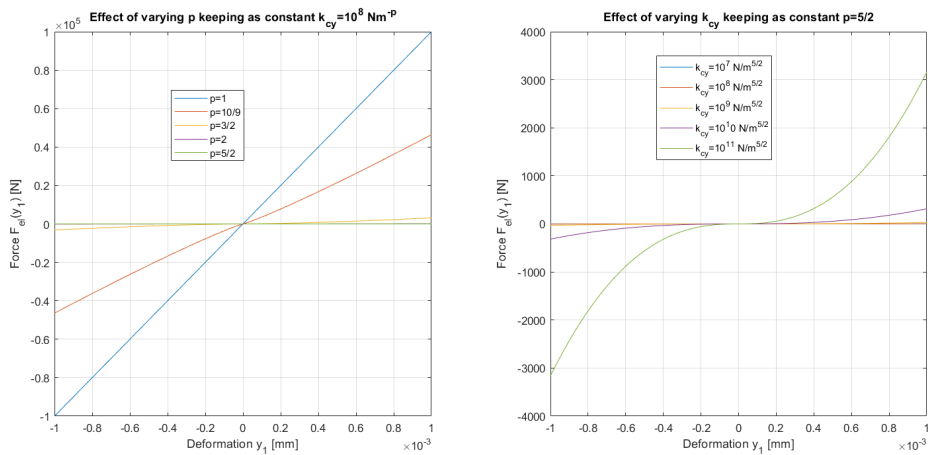


Figure 6.5: Effects of varying p and k_{cy}

More details about Hertz theory and Palmgren formula- summarized in the table 6.1- are in the Appendix C.

Table 6.1: Stiffness coefficient and exponent of non-linearity in the general theoretical cases proposed

General case	Stiffness coefficient k_{cy}	Exponent of non-linearity p
Sphere and a half-space and two spheres	$\left(\frac{16E^*R}{9}\right)^{3/2}$	3/2
Two cylinders with parallel endless axes	$\left(\frac{\pi}{4}E^*L\right)$	1
Cylinders not infinitely long with parallel axes (Palmgren formula)	$8,075 \cdot 10^4 \frac{N}{m^2} L^{8/9} d^{10/9}$	10/9

6.8 Non-linear stiffness model: research of the shape factors

The procedure for calculating the coefficients k_{cy} and p in the non-linear stiffness model is similar to the linear case. Everything is complicated by having two constants to be determined in order to obtain the overlap between theoretical and experiential values. A variation of the non-linearity exponent p is expected around 10/9 and beyond, but not so far from this last value. Precisely because, although it is true that we are not in the elementary cases of Appendix C, we are not so distant from these physical conditions. The values taken from the previous model (linear stiffness model) are the starting points of the new model and gradually we are going to move away in small steps in order to get a significant approximation between theoretical previsions - from the new model (non-linear stiffness model)- and experimentation.

Afterwards, we can write the main differential equation in the general case with $p \neq 1$:

$$m_{cy}\ddot{y}_1 + k_{cy}y_1|y_1|^{p-1} \left(1 - e^{-\frac{\sum_i C_{Y_i}}{\sum_i M_{C_i}}}\right) - m_{cy}\omega_0^2 y_1 = K_s \mu_s \sum_j S_{X_j} - K_s \sum_j M_{S_j} \frac{\sum_i C_{Y_i}}{\sum_i M_{C_i}} \quad (6.68)$$

By adding the experimental data of efficiency and the mathematical equation of efficiency coming from the basic theory, we are going to have the following system

of equation where the unknown variable are p and k_{cy} :

$$\begin{cases} m_{cy}\ddot{y}_1 + k_{cy}y_1|y_1|^{p-1} \left(1 - e^{-\frac{\sum_i C_{Y_i}}{\sum_i M_{C_i}}}\right) - m_{cy}\omega_0^2 y_1 = F(t) \\ F(t) = K_s \mu_s \sum_j S_{X_j} - K_s \sum_j M_{S_j} \frac{\sum_i C_{Y_i}}{\sum_i M_{C_i}} \\ \bar{\eta} = \frac{C_S}{z_1 k_{cy} |y_1|^p} = \eta_{sp}(C_S) \end{cases} \quad (6.69)$$

Finally, we could rewrite the differential equation by making explicit the value of the non-linear stiffness constant k_{cy} :

$$k_{cy} = \frac{C_S}{z_1 \eta_{sp}(C_S) |y_1|^p} \quad (6.70)$$

$$m_{cy}\ddot{y}_1 + \frac{C_S}{z_1 \eta_{sp}(C_S) |y_1|^p} y_1 |y_1|^{p-1} \left(1 - e^{-\frac{\sum_i C_{Y_i}}{\sum_i M_{C_i}}}\right) - m_{cy}\omega_0^2 y_1 = F(t) \quad (6.71)$$

At the end, by changing gradually the value of k_{cy} and of p and checking the overlap between experimental efficiency and theoretical one, we get the shape values of these constants.

6.9 Non-linear stiffness model: comparison between experimentation and simulations

In this section we are going to analyze the results coming from the non-linear stiffness model. We have carried out that the shape constant able to get the overlap:

Table 6.2: Values of constants coming from computational work

Stiffness coefficient k_{cy}	Exponent of non-linearity p
$1,5 \cdot 10^{10} \text{ N/m}^{2,35}$	2,35

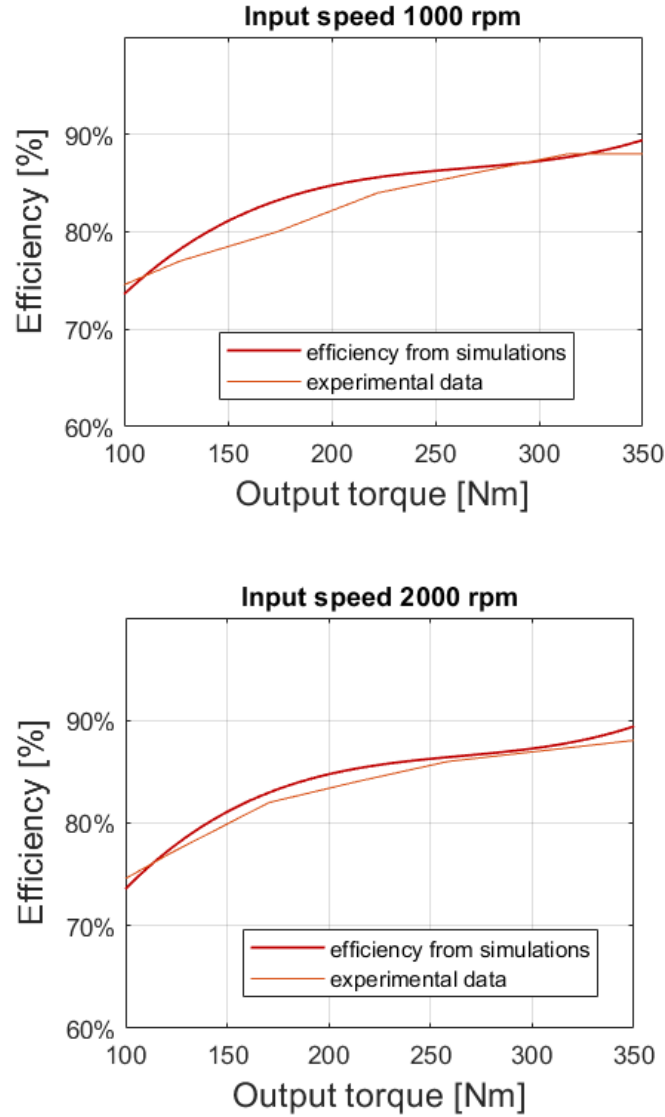


Figure 6.6: Simulations' results to evaluate the efficiency with the non-linear model ($p = 2,35$) at two different speed with $k_{cy} = 1,5 \cdot 10^{10} \frac{N}{m^{2,35}}$

We find a significant closeness between theoretical and experimental values of efficiency with the choice summarized in table 6.2. This confirms the validity of the hypotheses posed, admitting however that further investigations should be made to promote the main ideas of the non-linear stiffness model (figure 6.6). Since looking at the response in terms of deformation $y_1(t)$ (figure 6.7) as simulation time changes, we may see the typical response of the spring-mass system, whose spring is non-linear (Appendix D).

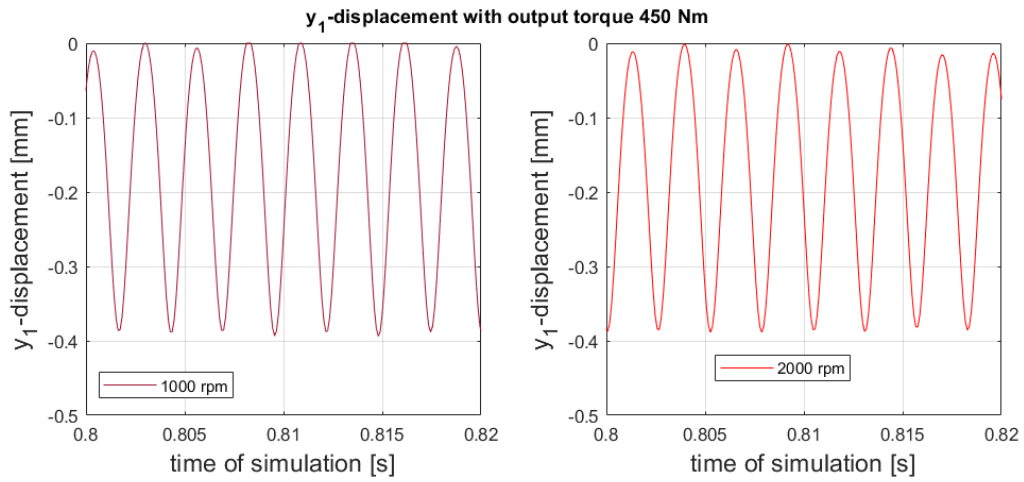


Figure 6.7: Simulations' results to evaluate the displacements y_1 with the non-linear model ($p = 2,35$) at two different speed with $k_{cy} = 1,5 \cdot 10^{10} \frac{N}{m^{2,35}}$

Chapter 7

Conclusions

The main conclusions - drawn from a critical analysis of the experimental data and simulations from non-linear stiffness model - are:

1. The efficiency of cycloid drive rises with the load. For small loads it is almost linear and increases very fast, but for the higher loads the efficiency curve bends and growth slower. It has been proven that this shape of efficiency curve can be simulated by introducing a non-linear stiffness to the model.
2. Sophisticated models that include all the dynamic elastic effects on the cycloidal plate can be found in the literature ([2]). These models need several adjustable parameters and large time for computation. This work proposed a new approach to describe the cycloid efficiency curve where the elastic effects is involved only between input shaft and cycloidal disc. The presented model shows a good fitting of the experimentation;
3. The proposed equation can be used to simulate the cycloid drive efficiency in drive trains with reasonable computational costs.
4. Input speed has a negligible impact on the efficiency - as the experimentation and simulations show-. In fact, it is clear that -in deformations' phenomena- the main dependence is on the normal load than on the sliding velocity.

All in all, this work shows -firstly- that a model with rigid bodies is not able to suit the experimentation and that elastic dynamic effects influence efficiency. This effects have a similar dependence as Hertz theory shows. However, in order to have a better model, a deep investigation on all the contacts acting in the gearbox reducer should be performed. This effects do not depend on the number of disks of the gearbox, but could make the efficiency raise up for high values of load.

In general, by observing the efficiency data, we discover the existence of two regions:

1. A first region for smaller output load values, where the variation in efficiency is considerable, the aforesaid elastic effects are very relevant and the non-linear stiffness model can explain successfully the dynamic behaviour;
2. A second region for higher output load values, where increasing the external load does not involve important variations on the efficiency that saturates to a constant value. In this field the rigid bodies model can satisfactorily describe the physical reality and allows to optimize the machine's parameters with reasonable computational cost.

This thesis has focused on the dynamic behavior of the machine because of its influence on efficiency. Firstly, we have analyzed the basic equations from kinematics and dynamics, later we have payed attention to the experimentation, later we have modified the basic model- calling other dynamic effects- in order to carry out the best fitting model for the cycloidal reducers. The overall work can be considered original because the attention has been also focused on the computational cost for the model proposed in order to have a good compromise between computational feasibility and capacity to describe the physical reality.

Appendix A

Kennedy theorem

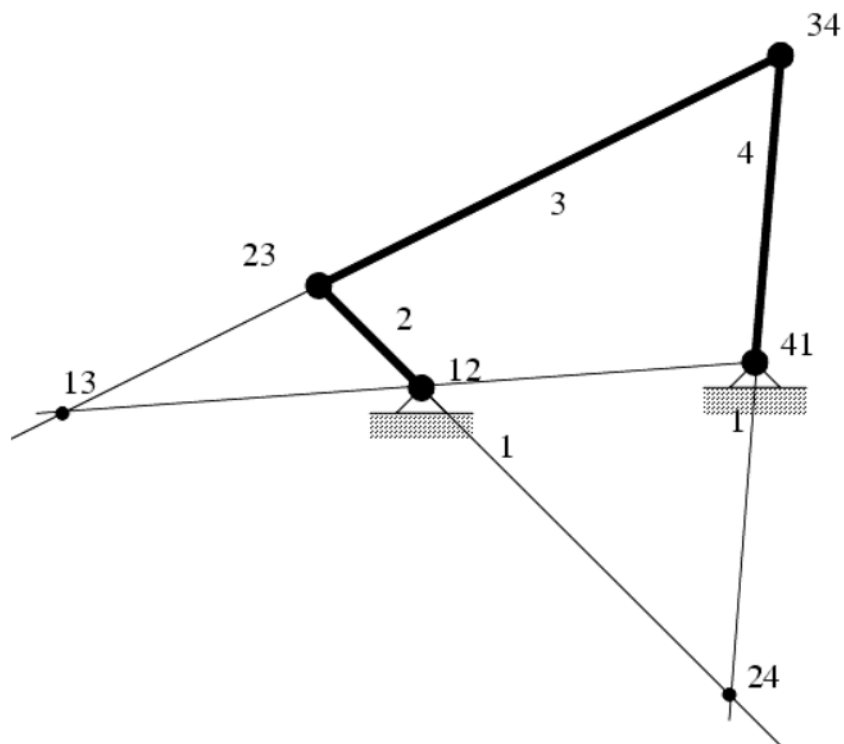


Figure A.1: Illustration for explanation of Kennedy theorem

The Kennedy's theorem states that the three instant centres of velocity (IVC) shared by three rigid bodies in relative planar motion to another (whether or not connected), all lie on the same straight line. A concrete and intuitive example is going to be

introduced. Figure A.1 shows a four-bar linkage where we can individuate three different moving bodies 2,3 and 4; and the fixed part, or better the frame 1. Then,

- 12 is the instantaneous centre of rotation of the motion of 2 related to 1;
- 41 is the instantaneous centre of rotation of the motion of 4 related to 1;
- 13 is the instantaneous centre of rotation of the motion of 3 related to 1;

Appendix B

General models for kinetic friction

During the computational and modelling work, one of the first decision was to individuate the more coherent and physical meaningful model for friction. As It is well-known, we have three different kind of friction interactions and in the rigid bodies model- the starting and the basic model- friction has been interpreted as the Colombian model affirms. Anyway, several approaches have been taken into account before choosing the Colombian model. For these reasons, we are going to introduced the simpler models for friction - the most common ones in scientific literature- that we have discussed about at length. Because we have solved the equations in steady state, the most of interest is for model of dynamic friction without being interested -for that applications- in static effect of first parting:

1. The first model considered is the Colombian one. In agreement with this, for two dry solid surfaces sliding against one another, the magnitude of the kinetic friction exerted through the surface is independent of the magnitude of the slipping velocity of the surfaces against each other. The kinetic friction coefficient is introduced as a constant depending on the kind of material of the sliding surfaces, on the roughness of them and on other secondary factors. In this model, if F_N is the normal force pressing the surfaces and μ is the experimental and constant kinematic friction coefficient, we can write the kinetic friction F_C as follows:

$$\vec{F}_C = -F_N \mu \frac{\vec{V}_s}{\|\vec{V}_s\|} \quad (\text{B.1})$$

Where \vec{V}_s is the sliding velocity. Though it greatly over simplifies the frictional phenomena it is widely used in the engineering world, when dynamic effects are not concerned. Also, the Coulomb model is a common piece of all more developed models.

2. The second most common model for friction is the damping friction model. In this case the friction has a linear dependency on the sliding speed. It is strictly

recommended to model -in a sample way- the kinetic residence of bodies moving on fluid or to quantify friction between lubricated slipping surfaces. The damping friction F_V could be evaluated as follows:

$$\vec{F}_V = -\beta \vec{V}_s \quad (\text{B.2})$$

Where β is the damping coefficient.

Finally- having introduced the Colombian model and the viscous one- It is meaningful presenting the Stribeck curve. The Stribeck curve is a more advanced model of friction as a function of velocity. Although it is still valid only in steady state, it includes the model of Coulomb and viscous friction as built-in elements. The Stribeck curve has been verified by comparing published results in tribology (figure B.1).

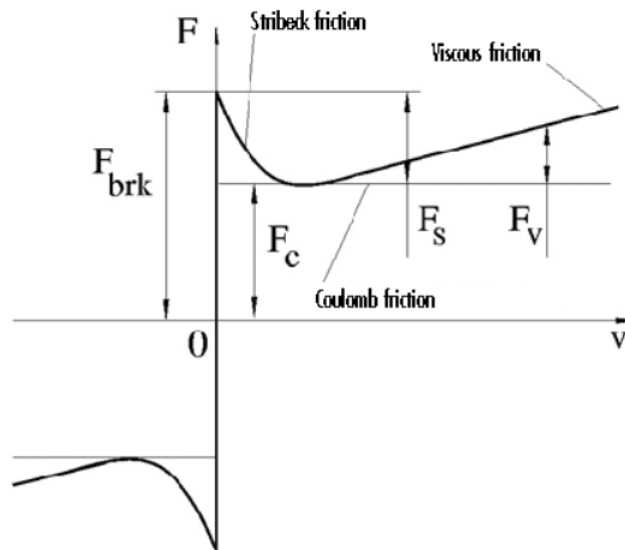


Figure B.1: Stribeck curve

Appendix C

Reference to Hertz theory of contact and Palmgren formula

Classical contact mechanics is most notably associated with H. Hertz. In 1882, Hertz solved the contact problem of two elastic bodies with curved surfaces. This still-relevant classical solution provides a foundation for modern problems in contact mechanics. For example, in mechanical engineering and tribology, Hertzian contact stress is a description of the stress within mating parts. The Hertzian contact stress usually refers to the stress close to the area of contact between two spheres of different radius. In the particular case of analysis, we have two cylinders of reduced axial length and with parallel axes: one in coupling with its external surface, the other one with its internal surface. However, we will make a summary of all the most used cases known in the literature. This is helpful to justify the experimental shape value of the coefficient p carried out by the computational work in order to get overlapping between experimentation and theoretical prevision. Therefore we are planning to make a complete review of the most common cases of contact bodies studied with Hertz theory, specifying only the final relation between the normal force F_N of contact and the depth of penetration (d) of one body (1) on an other one(2):

1. Contact between a sphere and a half-space:

$$F_N(d) = \left(\frac{16E^*R}{9} \right)^{3/2} d^{3/2} \quad (\text{C.1})$$

Where: R is the radius of the sphere, E^* could be determined as follows, reminding that ν is the Poisson coefficient and E is the Young coefficient:

$$E^* = \frac{1 - \nu_1^2}{E_1} + \frac{1 - \nu_2^2}{E_2} \quad (\text{C.2})$$

2. Contact between two spheres:

$$F_N(d) = \left(\frac{16E^*R}{9} \right)^{3/2} d^{3/2} \quad (\text{C.3})$$

Where:

$$\frac{1}{R} = \frac{1}{R_1} + \frac{1}{R_2} \quad (\text{C.4})$$

3. Contact between two cylinders with parallel endless axes:

$$F_N(d) = \left(\frac{\pi}{4} E^* L \right) d \quad (\text{C.5})$$

Where L is the length of the cylinder that makes negligible the radius of the cylinders.

Furthermore, we can add an experimental formula obtained by Palmgren for cylinders not infinitely long compared to the radial dimensions but with external coupling and parallel axes:

$$F_N(d) = 8,075 \cdot 10^4 \frac{N}{m^2} L^{8/9} d^{10/9} \quad (\text{C.6})$$

We are not in any of the cases listed, because we have two cylinders in coupling with a very reduced coupling length compared to the radial dimensions. This appendix is born to give us the idea of the typical values of the stiffness coefficient and the non-linear exponent: a sort of idea of the magnitude order of quantities that will be found through the computational work.

Table C.1: Stiffness coefficient and exponent of non-linearity in the general theoretical cases proposed

General case	Stiffness coefficient k_{cy}	Exponent of non-linearity p
Sphere and a half-space and two spheres	$\left(\frac{16E^*R}{9} \right)^{3/2}$	3/2
Two cylinders with parallel endless axes	$\left(\frac{\pi}{4} E^* L \right)$	1
Cylinders not infinitely long with parallel axes (Palmgren formula)	$8,075 \cdot 10^4 \frac{N}{m^2} L^{8/9} d^{10/9}$	10/9

Appendix D

Basic phenomenology of simple non-linear spring-mass system

In this appendix we want to lay the foundations of the basic dynamic laws applied to mass system with non-linear spring.

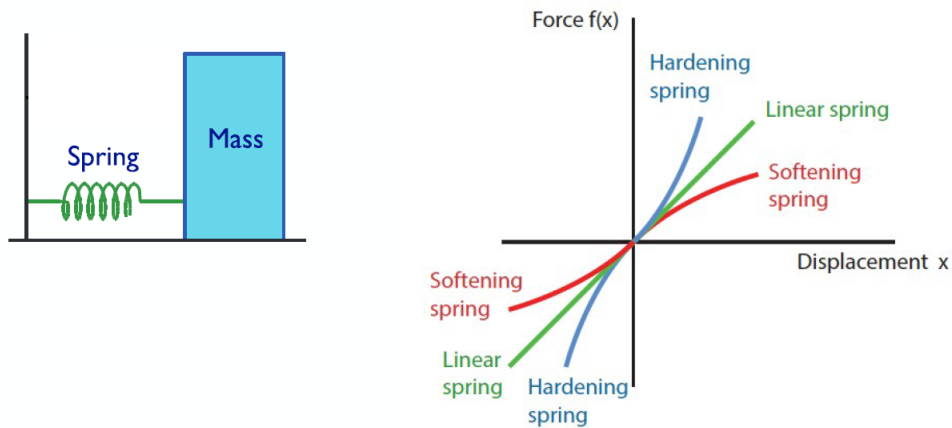


Figure D.1: Simple non-linear spring-mass system

By applying the main dynamic principle to the mass-spring system when also a sinusoidal force takes action, we are going to have:

$$m\ddot{x} + k_{cy}x^p = F(t) = F_0 \sin(\omega t) \quad (\text{D.1})$$

To avoid numerical problem with the exponentiation, we will rewrite the equation in the following way:

$$m\ddot{x} + k_{cy}|x|^{p-1} x = F(t) = F_0 \sin(\omega t) \quad (\text{D.2})$$

If we posed $k_{cy} = 10$, $F_0 = 100\text{ N}$ and $\omega = 10\text{ rad/s}$, we would obtain the following responses by varying the exponent of non linearity p (figure D.2).

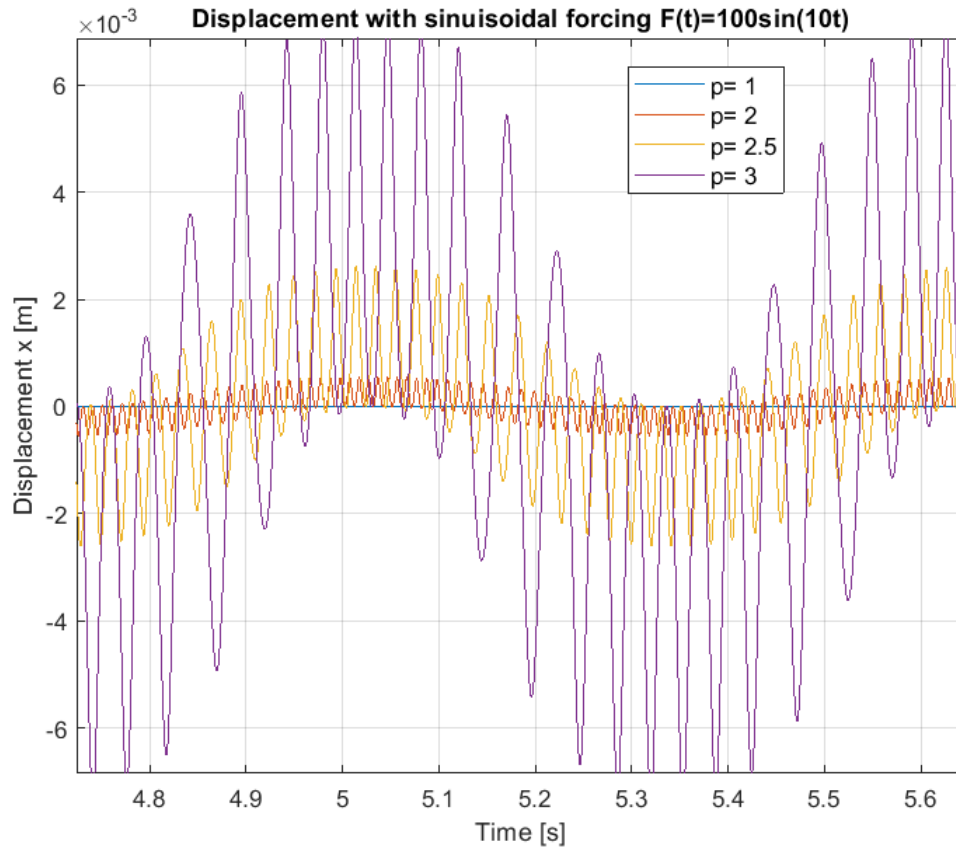


Figure D.2: Non-linear spring-mass system: sinusoidal forcing

Appendix E

Introduction to Simulink to resolve the main dynamic equation of non linear stiffness model

In the main equation, it is introduced also the damping effect only because adding this kind of friction does not complicated so much both the model and the numerical scheme to solve the differential equation. The main dynamic equation is:

$$m_{cy}\ddot{y}_1 + k_{cy}y_1|y_1|^{p-1} \left(1 - e^{-\frac{\sum_i C_{Y_i}}{\sum_i M_{C_i}}}\right) + c_{cy}\dot{y}_1 \left(1 - e^{-\frac{\sum_i C_{Y_i}}{\sum_i M_{C_i}}}\right) - m_{cy}\omega_0^2 y_1 = F(t) \quad (\text{E.1})$$

$$F(t) = K_s \mu_s \sum_j S_{X_j} - K_s \sum_j M_{S_j} \frac{\sum_i C_{Y_i}}{\sum_i M_{C_i}} \quad (\text{E.2})$$

To make the mathematical and numerical procedure more linked to the physical meanings we are going to introduce this quantities related to the kind of acting force:

1. Elastic force:

$$F_{el}(y_1) = k_{cy}y_1|y_1|^{p-1} \left(1 - e^{-\frac{\sum_i C_{Y_i}}{\sum_i M_{C_i}}}\right) \quad (\text{E.3})$$

2. Damping force:

$$F_{dam}(y_1) = c_{cy}\dot{y}_1 \left(1 - e^{-\frac{\sum_i C_{Y_i}}{\sum_i M_{C_i}}}\right) \quad (\text{E.4})$$

3. Inertial force:

$$F_{in}(y_1) = -m_{cy}\omega_0^2 y_1 \quad (\text{E.5})$$

4. Forcing:

$$F_0 = F(t) = K_s \mu_s \sum_j S_{X_j} - K_s \sum_j M_{S_j} \frac{\sum_i C_{Y_i}}{\sum_i M_{C_i}} \quad (\text{E.6})$$

Then we are going to get:

$$m_{cy}\ddot{y}_1 + F_{el}(y_1) + F_{dam}(y_1) + F_{in}(y_1) = F_0 \quad (E.7)$$

$$\ddot{y}_1 = \frac{-F_{el}(y_1) - F_{dam}(y_1) - F_{in}(y_1) + F_0}{m_{cy}} \quad (E.8)$$

The solution in time is obtained through Simulink which employs methods of time solution of the type of ode45 or more sophisticated. The solver allows automatic or manual selection of the method of solution in time and the time discretization interval. The working interface is of the type of block diagrams. Simulink, developed by MathWorks, is a graphical programming environment for modeling, simulating and analyzing multidomain dynamical systems. Its primary interface is a graphical block diagramming tool and a customizable set of block libraries. It offers tight integration with the rest of the Matlab environment and can either drive Matlab or be scripted from it.

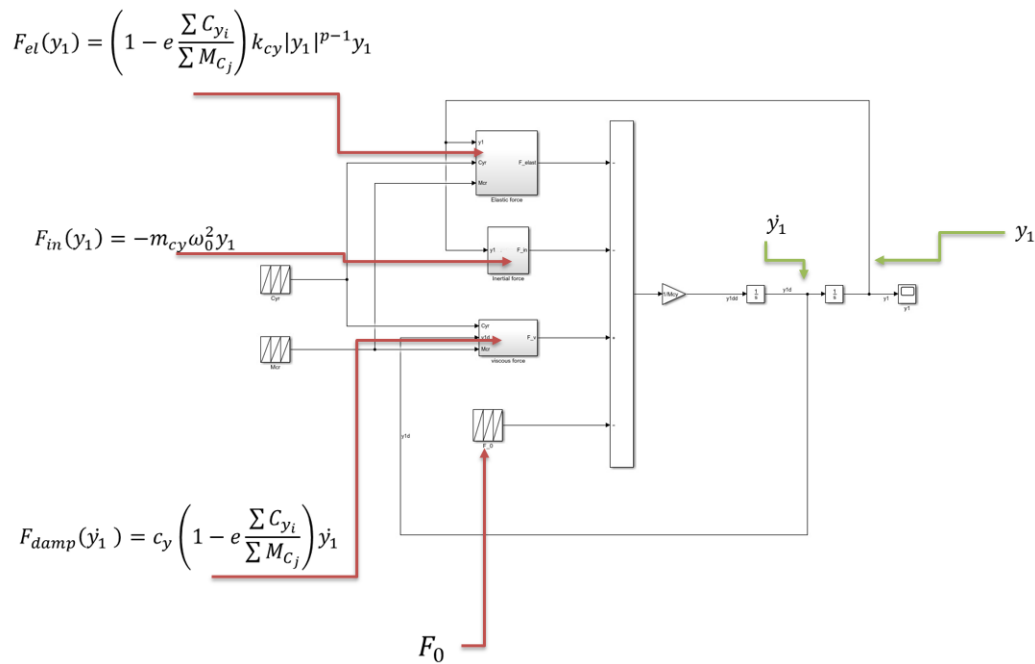


Figure E.1: Simulink blocks

Bibliography

- [1] T. Mackic, M. Blagojevic, Z. Babic, N. Kostic: Influence of design parameters on cyclo drive efficiency. *Journal of the Balkan Tribological Association* Vol. 19 (2013)
- [2] M. Blagojevic, V. Nikolić-Stanojevic, N. Marjanović, L. Veljovic: Analysis of Cycloid Drive Dynamic Behavior, *Scientific Technical Review* (2009)
- [3] Jean-Luc Dion, Nicolas Peyret: Study report on the analytic dynamical modeling of cycloidal reducers, Technical article, Laboratoire QUARTZ, Saint Ouen (Paris), France (2013)
- [4] O. Alipiev: Geometry and forming of epicycloidal and hypocycloidal toothed wheels in modified cyclo-Transmission, Ph.D. thesis, Ph.D. Dissertation, Ruse (1988)
- [5] B. M. Borislavov, I. Borisov, P. Vilislav: Design of a planetary-cyclo-drive speed reducer cycloid stage, geometry, element analyses, Technical Rapport, Linnaeus University (2012)
- [6] J. Uicker, G. Pennock, J. Shigley: *Theory of machines and mechanisms- fourth edition*, Oxford University Press (2010)
- [7] J.-H. Shin, S.-M. Kwon: Influence of the friction on the cycloidal speed reducer efficiency, *Mechanism and machine theory* 41 (2006)
- [8] M. Blagojevic, N. Kocic, M. and Marjanovic, B. Stojanovic, Z. Dordevic, L. Ivanovic, N. Marjanovic: Influence of the friction on the cycloidal speed reducer efficiency, *Journal of the Balkan Tribological Association* 18 (2012)
- [9] W. Shuyan, T. Guizhong, J. Xujun: Estimation of sliding loss in a cycloid gear pair, *International journal of advancements in computing technology* (2012)
- [10] Y.-W. Hwang, C.-F. Hsieh: Geometry design and analysis for trochoidal type speed reducers with conjugate envelopes, *Transactions of the CSME/ SCGM* 30 (2006)
- [11] Sandeep V. Thube, Todd R. Bobak: The dynamic simulation and analysis of a cycloidal speed reducer, Paper Number: DETC2011-48494, Washington, DC, USA (2011)
- [12] Chmurawa M.: Obiegowe przekładnie cykloidalne z modyfikacją ząbienia *Zeszyty Naukowe Politechniki Śląskiej, Mechanika*, z 140, Gliwice 2002
- [13] Schempf H.: Comparative design, modeling and control analysis of robotic

- transmissions, doctoral dissertation, Massachusetts Institute of Technology, Cambridge (1990)
- [14] Larsson E., Persson J.: Optimising a cyclo drive, Lund University and Borg Warner (2013)
- [15] Motion Control Drives: Fine Cyclo®F2C-C series, Sumitomo Drive Technologies. Catalogue 991137-F2003E-1
- [16] Zah M., Lates D., Csibi V.: thermal calculation for planetary cycloidal Gears with Bolts. *acta universitatis sapientiae electrical and Mechanical Engineering* (2012)
- [17] Nabtesco Motion Control, INC. planetary Vs cycloidal, Technical Catalogue (2018)
- [18] Twinspin Catalogue Spinea .pdf (High precision reduction gears) seventeenthBednarczyk S.: Określenie geometrii koła zebatego w obiegowej przekładni cykloidalnej. *Zeszyty Naukowe Politechniki Śląskiej, Transport*, z.82, s.29-39, Gliwice (2014)
- [19] Stryczek J.: Koła zebate maszyn hydraulicznych. *Oficyna Wydawnicza Politechniki Wrocławskiej*, Wrocław (2007)